Investigation on the Thermoelectric and Structural Properties of Cobalt-Antimony based Skutterudites and Modifications with Indium and Rare-Earth Elements

Dissertation

von
Andreas John Sesselmann
Augsburg
16. Juli 2012

Contents

Chapter 1

Introduction

Materials science nowadays investigates on the relationship between the structure of materials at atomic or molecular scales and their macroscopic properties. Furthermore it plays a key role for the upcoming challenges in terms of energy efficiency and mitigation of global warming. Thermoelectric generators (TEGs) are a promising technology to use heat and to convert it into electricity - in the ideal case, TEGs will be quite, robust, scalable, *efficient* and autarkic.

This thesis investigates on the thermoelectric (TE) material skutterudite. This type of material is found to be one of the most promising novel thermoelectric materials in the last two decades. Especially cobalt antimony based skutterudites, which can be modified by rare earths (RE), elements from the boron group and other electropositive species, are expected to be used in prospective thermoelectric generator modules for high temperature purposes.

This Manuscript comprises five chapters: (I) Introduction, (II) Skutterudite Materials, (III) Experimental Methods, (IV) Results and Discussion and (V) Summary. Chapter (I) introduces the basic knowledge about the thermoelectric effects, the Hall effect, the figure of merit Z and the applied theoretical models in this thesis (i.e. the single parabolic band and the Debye model). Furthermore the applicability of thermoelectric generators or Peltier coolers is briefly covered and recent concepts for novel thermoelectric materials are presented, which are in the focus of the scientific community.

The skutterudite material class is described in the following chapter. The crystal structure, possible compositions, transport properties, and further general information about the skutterudite material is given to the reader.

In the second half of chapter (II) the research on skutterudite materials (with a thermoelectric context) of the last fifteen years will be reviewed. A multiplicity of important scientific papers are discussed and referred in the bibliography of this work.

The chapter (III) includes the description of devices, which were necessary for the synthesis and processing of the material, and several measuring instruments that are partly home-built and not commercially available. In the first section the entire preparation steps of the skutterudite material are described, which comprise induction melting, annealing and sintering of the material - in the majority of cases under inert conditions. In the following the methods and instruments for characterization of the (high temperature)[1] transport properties are presented, which are in detail the electrical and thermal conductivity, the (local) Seebeck coefficient and the Hall mobility/coefficient. In the last two sections the powder diffraction method and the main operation modes of a scanning/transmission electron microscopy are briefly introduced.

The main results of this work are shown in chapter (IV). Main focus lies on the structural and thermoelectric properties of the skutterudite material, which is followed in each section by a detailed discussion. The chemical composition in each section is different and the concentration of one or two elements is varied. The chemical compositions are as follows: $In_xCo_4Sb_{12}$, $Ce_xIn_xCo_4Sb_{12}$ and $Gd_xIn_xCo_4Sb_{12}$ (the x in the chemical composition denotes that this particular element is varied in its concentration).

The last chapter will summarize the main results and findings, which can be drawn from the experiments within this thesis.

1.1   Thermoelectric (TE) Effects and Hall Effect

A first description of a thermoelectric effect is found in the publication "Ueber die magnetische Polarisation der Metalle und Erze durch Temperatur-Differenz"[2] from Thomas Johann Seebeck in 1821 [1], which was later also named after him. He constructed a conductor loop which consisted of two

---

[1]i.e. $300\,\mathrm{K}$ to $700\,\mathrm{K}$

[2]engl.: Magnetic polarization of metals and minerals by temperature differences (The oral presentation was held already in 1821, which was then published in 1826)

different metals and applied a temperature difference at the two connection points. The induced current was visualized by using a magnetic needle, which responded to the created magnetic field. Today the Seebeck effect does not describe a magnetic phenomenon but a generated voltage potential[3] (synonymous with a generated electromotive force) induced by the temperature difference between the junctions of two different materials A and B, which are electrically connected. The voltage difference is called Seebeck voltage U_S, which is proportional to the temperature difference ΔT between the two connection points and the proportionality constant is called (differential) Seebeck coefficient S (in this case S_ab) or thermopower[4]:

$$U_\text{S}(T) = -S_\text{ab}(T)(T_\text{hot} - T_\text{cold}) \quad . \tag{1.1}$$

With a differential notation eq.(1.1) becomes:

$$U_\text{S}(T) = -\int_{T_\text{cold}}^{T_\text{hot}} S_\text{ab}(T)dT \quad . \tag{1.2}$$

According to *eq.*(1.1) the Seebeck coefficient is positive when the cold end of the conductor has a positive voltage difference and vice versa.

In 1834 Jean Charles Athanase Peltier observed the inverse effect [2]. He reported that at the junctions of two different metals, heat is dissipated at one of the two connection points and released at the other, when a current is supplied. This phenomenon is only dependent on the direction of the electric current and today known as the Peltier effect. Mathematically this can be described as follows:

$$\dot{Q} = \Pi_\text{ab}(T)I \quad , \tag{1.3}$$

where $\Pi_\text{ab}(T)$ is the (differential) Peltier coefficient, $\dot{Q}$ is the absorbed heat per unit time, and I is the electrical current.

The third thermoelectric effect was *predicted* by Lord Kelvin (William Thomson) in 1851 [3]. He described that for a single homogeneous conductor

---

[3]T. J. Seebeck thought it to be a thermo-magnetic effect, which was finally corrected by Lord Kelvin

[4]Seebeck coefficient and thermopower are used as synonyms in this work - α, which is frequently used as the thermopower variable, is referred to the thermal diffusivity in this work. The roman letter S is used here as variable for the Seebeck coefficient

with a temperature gradient, heat is transported when an electrical current is supplied. This can be expressed by the formula

$$\tau_{\mathrm{Th}} = \frac{\dot{Q}}{I \Delta T} \quad , \tag{1.4}$$

where τ_{Th} is the Thomson coefficient, $\dot{Q}$ is the absorbed heat per unit time, I is the electrical current and ΔT is the applied temperature difference in the homogeneous conductor. Thomson was able to demonstrate this effect in 1854 that besides the Peltier effect a further reversible thermal phenomenon must exist, which is today known as the *Thomson heat*. Furthermore his thermodynamical calculations were showing how the Peltier and the Seebeck coefficients are related to each other, and consequently is expressed in the first Thomson relation (also referred to as first Kelvin relation) [4]:

$$\Pi = ST \quad . \tag{1.5}$$

The Hall effect was discovered in the year 1879 by Edwin Herbert Hall [5] and denotes the response of charge carriers (i.e. an electric field) within a conductor due to a magnetic field $\vec{B}$, which is arranged nonparallel to the direction of a current density $\vec{j}$ (i.e. $\vec{j} \times \vec{B}$). The charge carriers experience a Lorentz force due to the perpendicular magnetic component and as a consequence are deflected from their original path and accumulate vertically to the direction of the electrical current. This accumulation of charge carriers causes a (small) voltage perpendicular to the direction of the electrical current and is denoted as the Hall voltage. The Hall effect is reversible and is only observed when a magnetic field is applied. In the simplest case the charge carriers create a Hall voltage U_{H} due to a perpendicular magnetic field B, which is given by

$$U_{\mathrm{H}} = \frac{-I \cdot B}{n_{\mathrm{H}} \cdot e \cdot d} \quad , \tag{1.6}$$

where I is the applied current, B the magnetic field, d the thickness of the specimen, e is the electron charge and n_{H} is the effective charge carrier density.[5] The Hall constant R_{H} is defined as

$$R_{\mathrm{H}} = \frac{E_y}{j_x \cdot B} = \frac{U_{\mathrm{H}} \cdot t}{I \cdot B} = -\frac{1}{n_{\mathrm{H}} \cdot e} \quad . \tag{1.7}$$

---

[5]In eq.(1.6) the electron charge e is regarded as positive and for this reason a minus sign is added.

E_y is the induced transversal electrical field and j_x is the direction of the current density (perpendicular to the magnetic field). Latter is defined as $j_x = ne^2\tau_{e/h}E_x/m$, where $\tau_{e/h}$ is the charge carrier relaxation time, E_x is the longitudinal electrical field and m the mass of the charge carrier.

For (thermoelectric) materials the type of charge carriers can be both, electrons and holes at the same time. As a consequence the charge carrier density becomes an *effective* charge carrier density, which is a superposition of minority and majority charge carrier densities. This is accordingly to the mass of the charge carriers m, which also becomes a superposition of two distinct charge carrier masses.[6]

Furthermore the Hall mobility μ_H of a particular material can be directly derived from the Hall constant R_H and the electrical conductivity σ:

$$\mu_H = |\sigma \cdot R_H| \quad . \tag{1.8}$$

1.2 Research in Thermoelectric Materials and Applications

The implementation of (one of) the thermoelectric effects for industrial applications required a long time after the discovery of the Seebeck effect. The first main field of application is the relative temperature measurement. The electromotive force generated by the temperature difference is almost linear for specific pairs of conductors within a certain temperature range. Thermometric use can be obtained by setting one junction to a known temperature (reference temperature) and the other junction is placed at the location to be measured (see fig.1.1). Consequently the generated Seebeck voltage of the pair of conductors (thermocouple) becomes a function of the temperature of the measuring junction. When the functional dependence is known the temperature at the measuring junction can be determined. Today the temperature measurement by thermocouples is a widely established and reliable method for almost every temperature range.

---

[6]This assumption is based on ideal materials with parabolic bands. The effective mass of a charge carrier is furthermore dependent on its energy and momentum relationship. To be more precise, it is: $m^* \propto \left[\frac{d^2E}{dk^2}\right]^{-1}$, where E is the energy of the charge carrier and k is the absolute wave vector.
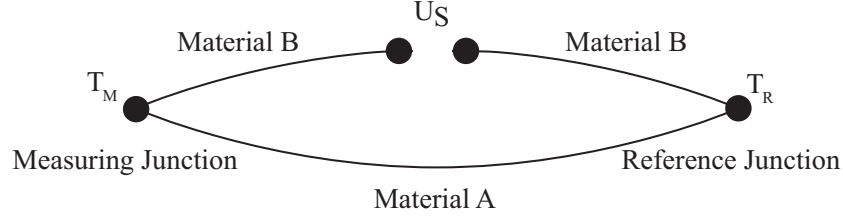
Figure 1.1: *Schematic drawing of a relative temperature measurement by a thermocouple. The reference junction is set to a known temperature T_R whereas the other junction is placed near the point of measuring at a temperature T_M. When a temperature difference between T_R and T_M exists, a voltage generated by the Seebeck effect can be observed at the point U_S.*

Peltier elements are another well-known application based on one of the thermoelectric effects. Mostly thermoelectric cooling is intended and consequently an electrical current is applied in these modules. These modules consist of several dozens to hundreds of thermocouples, which themselves are made of two different types of thermoelectric materials: n-type and p-type, which have electrons and holes as major charge carriers, respectively. The thermocouples are electrically connected in series and thermally connected in parallel and therefore can build up a cold and hot side on the two surfaces of the Peltier element, depending on the direction of the electrical current. In figure 1.2 a typical construction of a Peltier element is shown. A "Peltier element"[7] can also be used as a thermoelectric generator, when a heat flow is present. Then the reverse effect, i.e. the Seebeck effect, will generate a voltage and consequently converts a temperature difference into electrical energy. However the efficiency of thermoelectric modules and the operating temperature range were still limited, especially for higher temperatures than 473 K, which is the upper limit for bismuth telluride based thermoelectric modules. With the onset of space missions and the need of autarkic power generation, thermoelectric materials were investigated in-depth from the early 1960s on. Metals as thermoelectric materials were finally replaced by more efficient semiconductors, such like Bi_2Te_3 [6–9]. The research effort in thermoelectric generators and materials was mainly (quite independently)

---

[7]In the operation mode as thermoelectric generator, the module is actually not named Peltier element. The design of such a thermoelectric generator however is identical to a Peltier element.
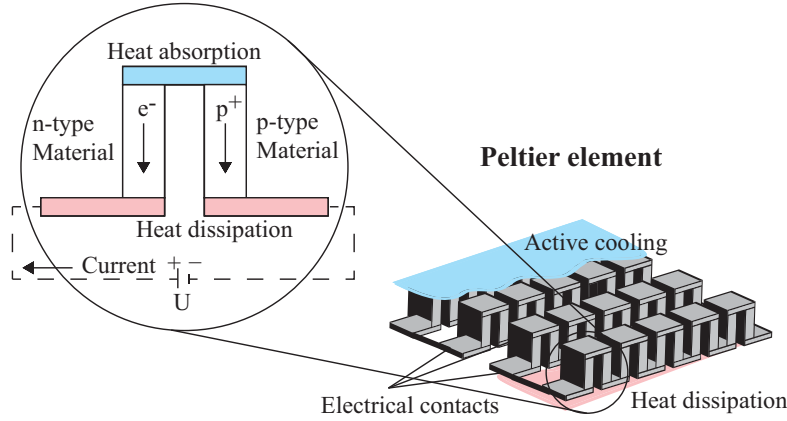
Figure 1.2: *Typical construction of a Peltier element/thermoelectric module (right) and an enlarged schematic of a thermocouple consisting of a n- and p-type thermoelectric material (left).*

put by the United States and the Soviet Union and lead to the first radioisotope thermoelectric generators (abbr.:RTG[8]) with a reasonable power output up to several hundred watts. The heat source is created by a material, which releases heat by radioactive decay (e.g. PuO_2 containing Pu^{238}) and the heat sink is created by heat radiation into the space. Famous examples, where RTGs were applied are the Voyager[9] or Cassini-Huygens[10] missions.

Today thermoelectric generation and refrigeration is used in a considerable scope of applications, its utilization however remains in niche markets, where high conversion efficiencies are not the main criterion. This trend is changing, which can be seen to the ongoing effort for optimization of thermoelectric materials, development of module technology comprising novel thermoelectric materials and new fields of application regarding waste heat recovery in terms of sustainable usage of (fossil) energy. Recent thermoelectric applications are found in waste heat recovery systems in the automotive industry [10] or industrial (combustion) facilities [11], Microgenerators/-refrigerators (e.g. Lab-on-a-Chip modules) [12], high efficiency power generation modules in autarkic space technology [13, p.515 ff.], cooling systems of

---

[8]**R**adioisotope **T**hermoelectric **G**enerator
[9]Voyager 1,2 missions (NASA, year 1977)
[10]Cassini-Huygens mission (NASA, year 1997)

electro-optic devices [14] and in major/small appliances (e.g. refrigerators, air conditioners) [15]. Along with the enhancement of the system efficiency and reliability, high interest lies in the optimization of thermoelectric materials, which forms almost the basic of all further requirements. The interested reader may consider following work of Riffat et al. [16], which is a noteworthy overview of recent and potential thermoelectric applications.

1.3   The Figure of Merit Z

First discussions on the efficiency of thermoelectric generators and refrigerators were made by Edmund Altenkirch[11] in the years 1909 and 1911 [18, 19], where he identified the requirements for high efficient thermoelectric materials for both applications, which are as follows:

- High thermoelectric coefficient (i.e. Seebeck/Peltier coefficient)

- High electrical conductivity (reduces Joule's heat)

- Low thermal conductivity (minimizes heat transfer losses)

The mathematical form of these requirements was formulated by Ioffe, who introduced the *figure of merit*[12] Z which is defined as [8]:

$$Z = \frac{S^2 \cdot \sigma}{\kappa} \quad , \tag{1.9}$$

where σ is the electrical conductivity, S the Seebeck coefficient and κ the thermal conductivity, respectively. Frequently the thermal conductivity is furthermore split into its two components:

$$\kappa = \kappa_{\mathrm{e}} + \kappa_{\mathrm{l}} \quad , \tag{1.10}$$

---

[11]Lord Raleigh discussed this issue already in year 1885 [17]. However his interpretation was not completely correct.

[12]In literature the capital Z is also referred to a "device"-Z and the lower case letter z to a "material"-Z [9]. This distinction is mainly motivated by the fact that a high efficient thermoelectric module is not solely dependent on a material with a high thermoelectric efficiency. For the device-Z more issues are considered than only the transport properties of the material. In this thesis "Z" is the material-Z and therefore refers to the transport properties of a thermoelectric material.

where κ_l is the lattice thermal conductivity and κ_e the electronic thermal conductivity, respectively. This is based on the fact that the lattice thermal conductivity is caused by lattice vibrations (phonons) and the electronic thermal conductivity by the charge carriers of the material. Z has the units of inverse Kelvin [K^{-1}]. For a more convenient handling the *dimensionless figure of merit ZT* was introduced, where the absolute temperature T is multiplied by Z. The maximum efficiency of power conversion with a thermoelectric material can be further expressed in terms of the Carnot efficiency[13] η_carnot and the dimensionless figure of merit ZT, which is as follows:

$$\eta_\mathrm{TE} = \eta_\mathrm{carnot} \cdot \frac{\sqrt{1 + Z((T_\mathrm{h} + T_\mathrm{c})/2)} - 1}{\sqrt{1 + Z((T_\mathrm{h} + T_\mathrm{c})/2)} + T_\mathrm{h}/T_\mathrm{c}} \quad . \tag{1.11}$$

Equation (1.11) shows clearly that the Carnot efficiency is reduced by the figure of merit, which is attributed to the entropy of the system. Furthermore the term $S^2 \cdot \sigma$ is frequently utilized with regard to thermoelectric cooling applications and is called *power factor*.[14] Good thermoelectric materials are considered as having a ZT of around one and above and a power factor of around $1 \times 10^{-3}\,\mathrm{W\,m^{-1}\,K^{-2}}$.

1.4 Single Parabolic Band and Debye Model

The characterization of thermoelectric materials involves in first order the measurement of the variables in equation (1.9), which are the temperature dependent values of S, σ and κ. This is reasonable, since the *efficiency* of the thermoelectric materials is a main criterion for the advancement of the research on thermoelectric materials. For a further understanding of the materials however a physical interpretation of the particular variables is necessary. This is complicated by the fact that S, σ and κ are interdependent on each other and are determined by several different physical/chemical phenomena.

Both, the single parabolic band model and the Debye approximation facilitate the interpretation of the measured transport properties of the skutterudite

---

[13]$\eta_\mathrm{carnot} = \frac{T_\mathrm{h} - T_\mathrm{c}}{T_\mathrm{h}}$, where T_h is the temperature of the heat reservoir and T_c is the temperature of the heat sink, respectively.

[14]The power factor is used within the calculation of the maximum power generation $p_\mathrm{max} = \frac{S^2 \cdot \sigma}{\Delta T^2 / (4L)}$.

material. The former is used to interpret the electronic characteristics of the skutterudites and its deviations from a metal with a single parabolic band structure. The other - the Debye approximation - makes an estimation about the weighing of different scattering types (e.g. phonon-phonon interactions or scattering at crystal defects) and consequently gives more insight into the lattice thermal conductivity of the material and help to further interpret possible deviations from this model (e.g. due to bipolar thermodiffusion).

In this chapter both models, the single parabolic band model and the Debye model, are introduced and briefly described. These models can be applied to a certain extent to the skutterudite material class. Further details will be discussed in upcoming sections (see ch.4).

1.4.1   Single Parabolic Band Model

The thermoelectric effects are *non-equilibrium* situations and consequently complicate an exact calculation of the macroscopic transport properties. Scientific papers from Thomson [3], Boltzmann [20] and Onsager [21] helped to overcome this problem by assuming certain boundary conditions and simplifications. With the work of Onsager this non-equilibrium situation can be regarded as a collection of local equilibria, which can be used to simplify the ansatz for the general Boltzmann transport equation, which has to be solved to derivate the macroscopic transport equations:

$$\dot{f}_k = \left.\dot{f}_k\right|_{\text{diff}} + \left.\dot{f}_k\right|_{\text{field}} + \left.\dot{f}_k\right|_{\text{scatt}} \quad . \tag{1.12}$$

In equation (1.12) f denotes a distribution function, $\dot{f}_k$ is the net rate of the change, with k being a general label for the states of the carriers, and $\left.\dot{f}_k\right|_x$ the particular distributions which may change per time and are caused by a certain physical mechanism ($x \,\hat{=}\,$diff (diffusion), $x \,\hat{=}\,$field (external field), $x \,\hat{=}\,$scatt (scattering)). The basic expression for the Seebeck coefficient from the linear response theory is

$$S = -L_{ET}/L_{EE} \quad \text{with} \quad \begin{array}{rcl} \vec{J} & = & L_{EE}\vec{E} + L_{ET}\vec{\nabla}T \\ \vec{U} & = & L_{TE}\vec{E} + L_{TT}\vec{\nabla}T \end{array} \quad , \tag{1.13}$$

where L_{ij} denotes the macroscopic transport coefficients, $\vec{J}$ is the electrical current density and $\vec{U}$ the heat current, $\vec{E}$ the electrical field and T the absolute temperature, respectively [22, p.270 ff.]. In the single parabolic

band model the Seebeck coefficient S at a constant temperature becomes then (see e.g. [23, p.36 ff.,p.61])

$$S = \pm \frac{k_B}{e} \left(\eta - \frac{r + \frac{5}{2}}{r + \frac{3}{2}} \cdot \frac{F_{r+\frac{3}{2}}(\eta)}{F_{r+\frac{1}{2}}(\eta)} \right) \quad , \tag{1.14}$$

where k_B is the Boltzmann constant, e the electronic charge, r is the scattering exponent[15], η the reduced Fermi energy ($\eta = E_F/(k_B \cdot T)$), and F the Fermi-Dirac integral ($F_j(x) = \frac{1}{\Gamma(j+1)} \int_0^\infty \frac{t^j}{\exp(t-x)+1} \, dt$, with $\Gamma(j+1) = j\Gamma(j)$, $\Gamma(1) = 1$, $\Gamma(1/2) = \sqrt{\pi}$; $\Gamma(n) = (n-1)!$). For temperatures beyond the Debye temperature Θ_D acoustic scattering was assumed for the calculation, which is in terms of the scattering exponent $r = -1/2$.

Furthermore the carrier concentration n_{boltz} can be determined and is mathematically derived from the Boltzmann transport equation as follows (Fistul formalism [24]):

$$n_{boltz} = 2 \left(\frac{2\pi m^* k_B T}{h^2} \right)^{3/2} \cdot F_{\frac{1}{2}}(\eta) \quad , \tag{1.15}$$

with h being the Planck constant, T the absolute temperature and m^* the density of states effective mass.[16] The density of states effective mass m^* can be determined by adjusting it to the measured data in a S-n diagram[17]. The fitted value of m^* denotes the density of states effective mass for a single parabolic band. In a more complex band structure, where several bands at one point in the reciprocal space may exist (i.e. non-parabolic), the fitted value of m^* is a mean value of several effective masses and additionally with different weighting. Nevertheless, with this procedure, m^* can be easily approximated and the band degeneracy can be directly identified, when the measured values of the Seebeck coefficient and the carrier concentration systematically deviate from the model.

For separation of the lattice and the electronic thermal conductivity (see eq.(1.10)) the Wiedemann Franz law (see eq.(1.23)) was applied and the

---

[15]r depends on the type of scattering and is defined here as: neutral impurities ($r = 0$), ionized impurities ($r = 3/2$) and acoustic scattering ($r = -1/2$).

[16]In other derivations the prefactor of the Fermi-Dirac integral is occasionally implemented in eq.(1.15) and consequently yields to a (slightly) different notation of n_{boltz}:

$n_{boltz} = \frac{4}{\sqrt{\pi}} \left(\frac{2\pi m^* k_B T}{h^2} \right)^{3/2} \cdot F_{\frac{1}{2}}(\eta)$ with $F_j(x) = \int_0^\infty \frac{t^j}{\exp(t-x)+1} \, dt$.

[17]This diagram is also named "Pisarenko" plot.

Lorenz number was estimated as a function of temperature from the measured S data assuming the single parabolic band model and exceptionally the acoustic phonon scattering. The calculation of the Lorenz number is often necessary for thermoelectric materials since the value for a metal ($L_0 = 2.45 \times 10^{-8}\,\mathrm{V^2\,K^{-2}}$) frequently overestimates the electronic thermal conductivity in this treated temperature region. This leads to an underestimated lattice thermal conductivity, which then apparently cannot be further reduced due to its supposed low value. The Lorenz number in the single parabolic band model (see e.g. [25, p.51],[26, p.138]) is found to be

$$L_0 = \left(\frac{k_{\mathrm{B}}}{e}\right)^2 \left(\frac{3F_0(\eta)F_2(\eta) - 4F_1(\eta)^2}{F_0(\eta)^2}\right) \quad . \tag{1.16}$$

The presented model of course does not comprise every physical aspect of the investigated material. Its limits are visible most notably for intrinsic semiconductor behavior and in the case of bipolar thermodiffusion. First is explainable by the excitation of intrinsic electrons, which at a particular temperature are located in the conduction band and consequently shift the electrical conductivity, thermal conductivity (due to the heat conduction by the extra electrons) and the Seebeck coefficient (where the imbalance of the electronic charge due to a temperature difference evens out to a certain extent). Second, the bipolar thermodiffusion effect occurs commonly in small bandgap semiconductors [27, 28] and is most significant, when more than one type of charge carriers are present. A more detailed description can be found, e.g. in [28, p.112] and [23, p.44].

1.4.2   Debye Model

The calculation of the lattice thermal conductivity is carried out to draw conclusions about the particular scattering mechanisms, which are taking place at the projected temperature between 300 and 700 K in the skutterudite material. In the Debye model [29] all branches of the vibrational spectrum are replaced by three branches with the identical dispersion relation:

$$\omega = c \cdot k \quad , \tag{1.17}$$

with ω being the angular frequency, c the speed of light and k the wave vector. With this "crude approximation(s)" [30, p.458] a simplification of the Boltzmann equation can be attained, without knowing the exact phonon

spectra of the material. Thus the phonon relaxation time τ_{ph}, which consists of several scattering types, can be approximated and compared to the experimental data. In this model the lattice thermal conductivity κ_{l} is derived from the thermal conductivity data $\kappa(T)$ by application of the Wiedemann-Franz law (see eq.(1.23)) and the calculated Lorenz number L_0 (see eq.(1.16)). In the following the derivation of the lattice thermal conductivity is briefly summarized and the main assumptions of this model are presented.

The thermal conductivity κ is mathematically described in the kinetic theory as follows

$$\kappa = \frac{1}{3}C \cdot v \cdot l \quad . \tag{1.18}$$

C is the specific heat capacity, v the mean velocity of the particles (phonons) and l is the mean free path between two scattering events. Equation (1.18) is phenomenological a good description of the thermal conductivity. However a mathematical treatment of the lattice thermal conductivity κ_{l}, which is a non-equilibrium transport parameter, has to consider the microscopic response by the crystal lattice due to heat conduction, i.e. to obtain a solution of the Boltzmann transport equation with reasonable assumptions. The linearized Boltzmann equation can be written as

$$\frac{f_{\mathrm{ph}} - f_{\mathrm{ph}}^0}{\tau_{\mathrm{ph}}} = \vec{v}_{\mathrm{g}} \cdot \vec{\nabla}T \frac{\partial f_{\mathrm{ph}}^0}{\partial T} \quad , \tag{1.19}$$

where f_{ph} is the phonon distribution function, f_{ph}^0 the local equilibrium distribution and $\vec{v}_{\mathrm{g}}$ is the phonon group velocity. It is an assumption of the linearized Boltzmann equation to distinguish between a local equilibrium distribution f_{ph}^0 and a (general) distribution function f_{ph}, i.e. the system will experience a local distribution, which tends to return to the (general) distribution function. Furthermore the Bose-Einstein distribution is valid here, since the involved particles are phonons. In the diffusion term of the Boltzmann equation (right side of equation (1.19)) a temperature gradient is present, which represents (a steady state) temperature field in the specimen.

When the equation (1.19) is solved[18] κ_l can be expressed as follows:

$$\kappa_l = -\frac{\left|\dot{\vec{Q}}\right|}{\left|\vec{\nabla}T\right|} = \frac{1}{2\pi^2 v}\int\limits_0^{\omega_D} \hbar\omega^3 \tau_{\mathrm{ph}}(\omega)\frac{\hbar\omega/k_{\mathrm{B}}T^2 \cdot e^{\hbar\omega/k_{\mathrm{B}}T}}{\left(e^{\hbar\omega/k_{\mathrm{B}}T}-1\right)^2}\cdot d\omega \quad , \qquad (1.20)$$

with $\left|\dot{\vec{Q}}\right|$ being the heat flux, ω_D denotes the Debye frequency ($\omega_{\mathrm{D}} = k_{\mathrm{B}}\Theta_{\mathrm{D}}/\hbar$), v is the average phonon velocity (simplification by the Debye theory) and for f_{ph}^0 the phonon distribution function is inserted ($f_{\mathrm{ph}}^0 = 1/(\exp[\hbar\omega/k_{\mathrm{B}}T]-1)$). When $\hbar\omega/k_{\mathrm{B}}T$ is substituted by x and the Debye temperature Θ_{D} is entered in equation (1.20), it gives the Debye approximation, which is applied in this work to compare it to the experimental data:

$$\kappa_l = \frac{k_{\mathrm{B}}}{2\pi^2 v}\left(\frac{k_{\mathrm{B}}T}{\hbar}\right)^3 \int\limits_0^{\Theta_{\mathrm{D}}/T} \tau_{\mathrm{ph}}\cdot\frac{x^4 e^x}{(e^x-1)^2}\cdot dx \quad . \qquad (1.21)$$

Equation (1.21) is clearly dependent on the phonon relaxation time τ_{ph}, which is governed by the Matthiessen rule [32, 33] and the different scattering mechanisms. Consequently the inverse phonon relaxation time can be approximated by the expression:

$$\tau_{\mathrm{ph}}^{-1} = \frac{v}{L} + A\omega^4 + B\omega^2 T\, e^{-\Theta_{\mathrm{D}}/3T} + \frac{C\omega^2}{(\omega_0^2-\omega^2)^2} \quad , \qquad (1.22)$$

with ω_0 being the resonance frequency of the filler element (discussed later), L is the average grain size, and the coefficients A, B, C are the fitting parameters. The terms on the right side of equation (1.22) represents the boundary and point defect scattering, phonon-phonon Umklapp processes and the phonon resonant scattering contribution, respectively. Boundary scattering is dominating in the low temperature regime, whereas Umklapp scattering is strongly present at higher temperatures. Point defect scattering is important for the intermediate temperature range and the phonon resonant scattering is an approach to include the characteristic of the skutterudite material.

---

[18]The calculation can be read in detail e.g. in [31] (in *german*).

1.5 Concepts for Novel Thermoelectric Materials

One of the recent concepts for novel thermoelectric materials was formulated by Slack, who successfully initiated a new research on novel thermoelectric materials [13]. In his work he highlighted five major points, which are important for efficient thermoelectric materials:

1. Reduction of the lattice thermal conductivity κ_l

2. High carrier mobility μ (for both n- and p-type materials)

3. The density of states effective mass m^* should be equal to the free electron mass m_0

4. The bandgap energy E_g should be equal or higher than $0.25\,\mathrm{eV}$ (see [34])

5. μ, κ_l and m^* are independent of the charge carrier concentration n, and κ_l and m^* are independent of temperature T

Point (1) refers to the fact that the electronic thermal conductivity κ_e is strongly correlated to the electrical conductivity of the material. This is described in the Wiedemann-Franz law, where the electronic thermal conductivity is related to the electrical conductivity:

$$\kappa_e = L_0 \cdot \sigma \cdot T \quad .$$

(1.23)

L_0 is the Lorenz number, which is in the range of $10^{-8}\,\mathrm{V^2\,K^{-2}}$. In consideration of an enhanced ZT the electronic part is an inevitable contribution to the overall thermal conductivity. Consequently the reduction of the lattice thermal conductivity is the only possible way to optimize the thermal conductivity without deteriorating the electrical conductivity. Thus it is of interest, what is the possibly lowest lattice thermal conductivity. Slack calculated the minimum thermal conductivity for several compounds [35]. These values are comprehensibly very close to that of amorphous materials, e.g. the minimum thermal conductivity κ_{min} of $CoSb_3$ is $\kappa_{min} = 0.37\,\mathrm{W\,m^{-1}\,K^{-1}}$ [36]. Point (2) considers the charge carrier mobility μ, which is proportional to

the electrical conductivity σ and inversely proportional to the charge carrier density n. This can be expressed as follows:

$$\sigma = n \cdot e \cdot \mu \quad , \tag{1.24}$$

where n is the charge carrier density, e the electron charge and μ the charge carrier mobility. It has to be noted that the equation (1.24) accounts for one type of charge carriers, i.e. n- or p-type. In total it is assumed that a high charge carrier mobility is most desirable and can be expressed in terms of a good thermoelectric material as the weighed mobility U [8, 34, 37]. Accordingly the weighed mobility U is defined as:

$$U = \mu \cdot \left(\frac{m^*}{m_0}\right)^{3/2} \quad . \tag{1.25}$$

Equation (1.25) already explains point (3), which proclaims a balanced ratio of the density of states effective mass m^* and the free electron mass m_0. Point (4) is mainly based on calculations, which were carried out by Mahan [34]. He found that the best semiconductor for large figure of merit should be 10 $k_\mathrm{B}T$, where k_B is the Boltzmann constant. At room temperature it gives a value of $0.25\,\mathrm{eV}$. Lower values tend to a decrease of the absolute Seebeck coefficient and a rise of the thermal conductivity at higher temperatures due to bipolar thermodiffusion. Point (5) denotes that the parameters of the figure of merit are interdependent and of different weight. For this reason decoupling of parameters and optimization processes would be desirable. Optimization is needed e.g. for the doping concentration and as a consequence for the charge carrier density. Latter increases indeed the electrical conductivity, however it deteriorates the absolute Seebeck coefficient value and the carrier mobility. Slack furthermore pointed out that metals, even semi-metals do not tend to have large Seebeck coefficients. Therefore small bandgap semiconductors seem to be ideal, because those comprise a reasonable Seebeck coefficient and at the same time a good carrier mobility and low thermal resistivity. The bandgap can be also regarded as a result of the "character" of the bonding which also provides further information of the material, e.g. for large bandgaps ionic bonding can be assumed (and therefore high κ_l), whereas for smaller bandgaps of semiconductors more covalent bonding is expected.

Slack formulated his concept in form of a key term (*"Phonon Glass Electron Crystal"*)[19], which concisely encompasses the five assumptions. This concept pushed forward the discovery of new thermoelectric materials, such like cage compounds, where a decoupling of thermal and electrical properties is possible to a certain extent. Nevertheless recent publications also tend to deviate from this path and e.g. search for strong dependencies between the density of states effective mass and the charge carrier density at different temperatures [38] or attenuate the concept, like in the case of rattling in skutterudites [39].

A widespread field of new thermoelectric compounds and especially its synthesis was disclosed by studies of *low-dimensional material systems*. Early works of Hicks and Dresselhaus showed that with the use of quantum wells the power factor should be significantly increased [40]. This was one of the starting points[20] to investigate on superlattices, quantum wires, quantum dots and nanostructuring of thermoelectric materials in general, in respect of an increased ZT. A considerable improvement of the figure of merit was demonstrated in diverse material systems, e.g. Bi_2Te/Sb_2Se, $PbTe/PbTeSe$, $SiGeC/Si$, $GaAs/AlGaAs$ and $InGaAs/AlInGaAs$ [42–49]. This enhancement was obviously achieved by a controlled structuring of the material and to a smaller extent by the chemical composition of the compound itself. Even silicon, which possesses a low figure of merit, exhibits improved thermoelectric properties by a specific structuring of the material [50, 51]. Based on the experiments of low dimensional thermoelectric materials it was assumed that bulk nanocomposites should also help to further reduce the thermal conductivity and on the other side retain the electrical properties of the material [52, p.203-259]. Works of Poudeu and Kanatzidis showed that pervasive nano-sized precipitates can lead to a vast improvement in bulk materials [53, 54]. These precipitates are formed due to coulomb interactions of ions or thermodynamic reasons and are believed to be stable even at higher temperatures. Nanostructuring by harsh methods such like planetary ball milling or spin-melting revealed that these approaches can lead to an enhanced figure of merit under certain circumstances [55]. However grain growth or densification of the nano-powders may occur and for this reason short-term compaction of these materials are mostly preferred (e.g. spark plasma sintering, current assisted sintering). For further detailed information the reader may

---

[19]abbr.:PGEC
[20]see also [41]

consider following recent review articles about investigations on low dimensional systems and other nanostructuring approaches [54–58].

Chapter 2

Skutterudite Materials

The origin of the name skutterudite derives from its place of finding, namely the cobalt mines in Skutterud (Norway), where the naturally occurring mineral $CoAs_3$ was firstly discovered and described [59, 60].[1] The general formula of skutterudites is TPn_3 (or more convenient: T_4Pn_{12}), where T is a transition metal and Pn is a pnicogen atom. It comprises a cubic structure with 32 atoms and corresponds to the space group $Im\overline{3}$ (No.204), where the transition metals occupy the $8c$-sites $(1/4, 1/4, 1/4)$ and the pnicogen atoms the $24g$-sites (0, y, z), respectively [61]. The pnicogen atoms form a rectangle (four-membered ring) and enclose the transition metal in an octahedral coordination. Oftedal assumed that this pnicogen rectangle is strongly constrained, i.e. $y + z = 0.5$, which is apparently not the case in practice and shows therefore a little rectangular distortion [62, chapt.33]. Furthermore Jeitschko et al. have shown that the skutterudite structure can be modified by insertion of maximal two additional atoms, which fill the $2a$ vacant sites (0,0,0) of the unit cell and occupy a body-centered position in the cubic structure [63] (see fig.2.1). There is a huge variety of elements, especially

---

[1]It should be noted that K.F. Boebert (director of the cobalt mine in Skuterud in the early 19th century) stated in his work that he was assumably the first person who discovered the skutterudite material and started to call attention to it [59, p.221].

rare earths, which can be taken as a "filling" atom. Constraints for the selection are mainly the atom/ion radii and the electronegativity of the relevant element. First is based on the fact that the vacant site of the skutterudite structure comprises a limited space and second the (weak) interaction with the local electronic environment (i.e. with the pnicogen atoms) has to be considered, so that predominantly the filling atom possesses an electronegativity significantly lower than the Pn-atom [64].

Skutterudites, based on transition metals from the group 9 (including cobalt), can be diamagnetic semiconductors, which applies e.g. for $CoSb_3$. Its lattice constant at room temperature ranges from about $7.7\,\text{Å}$ for CoP_3 to $9.3\,\text{Å}$ for $IrSb_3$ [62]. $CoSb_3$ has a lattice constant of $9.0385\,\text{Å}$ [62]. Other transitional metals (e.g. from group 10) can lead to a metallic behavior of the skutterudite compound with paramagnetic properties [65].

2.1 Thermoelectric Properties

The thermoelectric properties of skutterudites were firstly examined by Dudkin et al.[2] more than 50 years ago [69]. It was found that $CoSb_3$ features in fact a large Seebeck coefficient, though comprises a relatively high thermal conductivity, which made it apparently less interesting as a thermoelectric material. An important step forward was made by Slack in the 1990s, who proclaimed the concept of a phonon-glass electron-crystal (see sec.1.5) for novel thermoelectric materials, which induced a search for new materials, such as cage compounds (e.g. Clathrates, Skutterudites). First investigations on the transport properties, carried out by Morelli et al. showed that filled skutterudite $CeFe_4Sb_{12}$ possesses a vastly reduced lattice thermal conductivity and at the same time a high electrical conductivity, ensuing to an enhanced ZT of 0.125 at room temperature [70]. For high temperatures the ZT for this material system ($CeFe_{4-x}Co_xSb_{12}$) reaches up to about 0.9 at $800\,\text{K}$ [71]. In this vein, a more or less systematic search on different filler and/or pnicogen and transition metal elements started and resulted in a huge diversity of single filled skutterudites with highly optimized thermoelectric

---

[2]Seebeck's work [1] refers to a term 'weisser Speiskobalt', which is sporadicly believed to be a skutterudite compound [67]. Gustav Rose, who discovered many minerals, including the perovskites ($CaTiO_3$), suggests that it refers to a mineral called Cloanthite ($NiAs_2$) [68, p.51 ff.]. This leads to the assumption that Seebeck did not investigate on a skutterudite mineral in his original work.
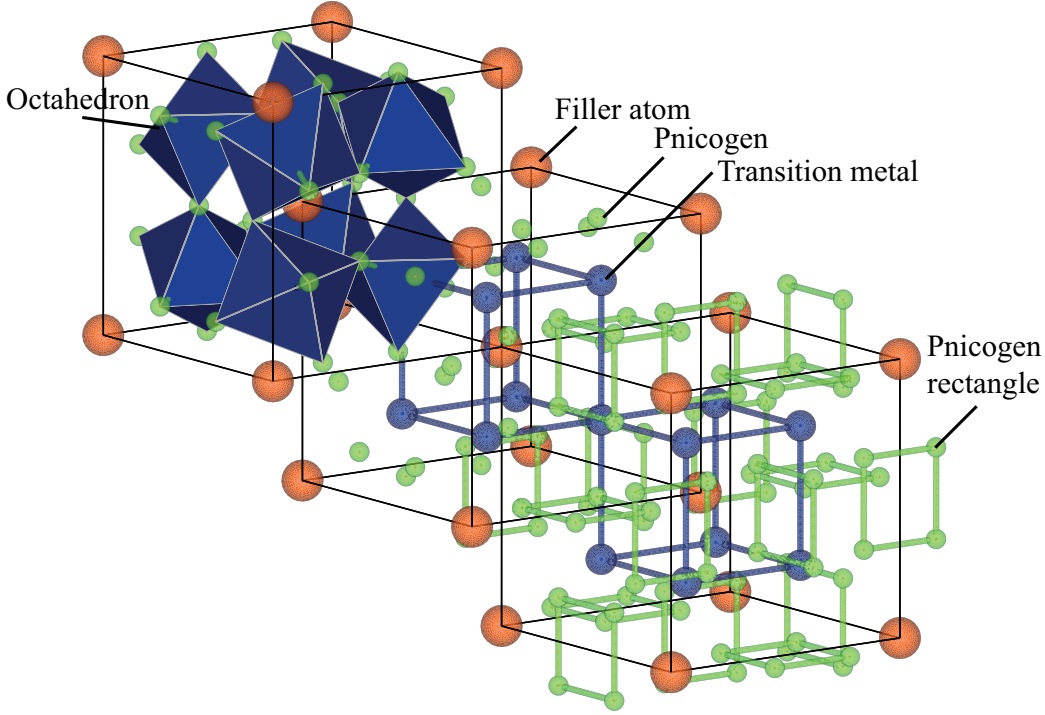
Figure 2.1: *Schematic of a filled skutterudite crystal structure (transition metal T=blue, pnicogen Pn=green, filler atom R=orange). The unit cell at the top left shows the octahedra, which are formed by the pnicogen atoms and surround the transition metal. The unit cell at the bottom right shows the pnicogen rectangles and the cubes, which are formed by the transition metal. The schematic was made by the program VESTA [66].*

properties [23, 39, 62, 65, 72–78].

The ultimate cause of the improved thermoelectric properties for single filled skutterudites is due to a sensitive interaction between the filler atom and the host lattice. This phenomenon can be visualized e.g. by inelastic neutron scattering, where an additional mode in filled skutterudites can be observed for low phonon energies [79]. Koza et al. furthermore showed that this interaction is not primarily reducing the phonon mean free path (which was firstly believed), but the group velocity of the phonons [39]. Thereby the lattice thermal conductivity can be vastly reduced.

A further advancement was the insertion of two or more different filler elements in the skutterudite structure, which was expected to create extra

vibrational phonon modes, which would scatter the phonons at different frequencies leading to a further reduction of the thermal conductivity [80, 81]. Thus this enhancement of the thermal resistivity is caused by a drastic change of the phonon spectra at lower energies (where heat conduction is most prominent), but on the other side the electronic properties of the compound was more or less retained [82]. Nevertheless the beneficial effect of the individual fillers is hardly traceable by handling of more than two different elements, which enables hundreds/thousands of possibly stable compositions and opens up a large parameter space.

2.2 Recent Progresses in Research of Skutterudite Thermoelectric Materials

Skutterudites have attracted much attention as promising thermoelectric materials for the recent two decades. This development was strongly promoted by a concept of Slack (see sec.1.5). According to Slack, a good thermoelectric material possess a large unit cell, heavy constituent atoms, low differences in electronegativity of the constituent atoms and large carrier mobility. These requirements are fairly satisfied for the skutterudites.

In 1993 Caillat first announced that binary skutterudites are having the "potential to overcome the ZT limit of 1" [83]. However it was not the binary skutterudites that exhibit the high thermoelectric figure of merit. The skutterudite crystal structure offers a large icosahedral void, which can be occupied by foreign elements. This "filling" leads to a vastly reduced thermal conductivity of the material without deteriorating the electrical conductivity and the Seebeck coefficient with regard to the thermoelectric efficiency.

These filler elements can be lanthanides, actinides, alkaline (earths), and certain elements from the boron and carbon group. Noteworthy is the fact that possible filler elements can be expanded by applying high pressure during the synthesis, which was revealed e.g. for iodine in $RhSb_3$ [84] or several elements in RuP_3 [85].

First filled skutterudites ($LaFe_4P_{12}$) were synthesized and structurally characterized by Jeitschko et al. in 1977 [63]. Polycrystalline $CeFe_{4-x}Co_xSb_{12}$ and $LaFe_{4-x}Co_xSb_{12}$ material (with $0 < x < 4$) were the first filled skutterudites, which were characterized in terms of thermoelectric properties by Sales et al. in 1996 [71]. The following year Singh et al. presented the first

calculated thermoelectric properties of lanthanum filled skutterudites from first principles with a local-density approximation [86]. In the year 1997 a first attempt to explain the effectiveness of the filler elements with regard to the lattice thermal conductivity was done by Sales et al. [87]. According to the paper the large atomic displacement parameter of the void filling elements is believed to describe an independent Einstein oscillation and was subsequently denoted as "rattling" in this context.[3]

This oscillation of the filler element is capable of scattering the heat carrying phonons efficiently, which is reflected in a considerable reduction of the thermal conductivity (q.v. [79, 89]). Furthermore it was observed also by Meisner that partial void filling with relatively low fractions of the filler element have already a major influence on the thermal conductivity [90]. Nolas et al. described in his review article [91] this phenomenon and excluded mass fluctuation scattering as only source of the observed thermal conductivity reduction referring to the formalism of Callaway [92]/Abeles [93] and denoted it as an "interesting approach for further optimization of the transport properties for thermoelectric applications".

After a decade it became apparent that mainly two compounds are in the focus for thermoelectric applications: $CoSb_3$ and $FeSb_3$. The compound $FeSb_3$ is metastable and can be synthesized by substitution of Co in the host compound $CoSb_3$. From elementary constituents un-doped $FeSb_3$ can only be prepared as thin film with sophisticated molecular beam epitaxy devices [94–96]. This p-type compound is capable of reasonable ZT values for high temperatures between $300 - 700\,K$ when it is stabilized and optimized in terms of thermoelectric efficiency by filling/doping elements [97].

In 2004 Toprak et al. revealed a positive impact of nanostructuring of $CoSb_3$ material on the thermal resistivity. Wet chemical synthesis was applied in this study to fabricate skutterudite nanoparticles in a very controlled way [98]. Comparable results were observed with $CoSb_3$ nanocomposites, which also reduce the thermal conductivity significantly [99]. Double and multifilling of the skutterudites was approached by several groups and led to extraordinary ZT values particularly for n-type material and after 2010 even for p-type compounds [75, 80, 100–102]. It is assumed that due to several specifiable Einstein oscillations of the different filling species the efficiency of phonon scattering is strongly enhanced.

Early attempts to interpret the mechanisms of filling were made by Shi et al.,

---

[3]see also [88]

who investigated on the filling fraction limit for these intrinsic voids in the skutterudite crystal [64]. The maximum filling fraction is according to the study determined by the valence state, electronegativity and the formation enthalpy of secondary phases (e.g. $CoSb_2$, ISb_2) of the specific element I. Calculations showed that solely considering the formation enthalpy of filled skutterudites itself is insufficient to explain the experimentally obtain results and mostly predict a total filling fraction of all voids - which is not the case. This approach to estimate the filling fraction is apparently valid for most dual-element filling, i.e. the fraction limit of a dual-element filling is composed of the particular single element fraction limits [103]. Fraction limits of multiple filling (three or more) elements is based on its diversity and complexity not yet systematically analyzed [104].

Moreover Shi et al. proclaimed a rule of thumb for suitable filling atoms [64]: Firstly the (ionic) atomic radius of the filling element should be close to the space provided by the icosahedral void, because it will not enter the vacant lattice position if the ion/atom is too large. In the opposite case it does diffuse out, because the element does not bond sufficiently with the surrounding environment. Secondly the electron negativity of the filling atom plays a crucial role, which is due to the indispensable bonding to the Sb (or more general the pnicogen) atoms. It was suggested that heavy elements from the noble gas group (e.g. Xe) would be the most beneficial filling element in terms of thermoelectric efficiency [65, p. 152 ff.]. However attempts resulted in the fact that such filled skutterudites cannot be synthesized.

Filling of the skutterudite material does influence the thermal and the electrical conductivity. For this reason the filling elements can enhance the power factor $\sigma \cdot S^2$ dramatically, i.e. its doping effect contributes to an optimization of the charge carrier density in respect of the thermoelectric efficiency. Filling elements typically provide one (e.g. Tl^{1+}) to three electrons (e.g. Ce^{3+}) to the skutterudite structure, which means a heavily doped semiconductor with electrons as its major charge carriers (i.e. n-type) is easily accessible. Filler elements do not always act as donors and it was shown by Fukuoka et al. that iodine can be inserted as a filling anion in $RhSb_3$ by applying high pressure during the synthesis [84]. However there are only very few examples reported, where the filling element act as electron acceptor.

For p-type material charge compensation has to be considered. This is predominantly done by substitution of Co with Fe in the $CoSb_3$ material, which acts as a dopant for the intermetallic site ($8c$ Wyckoff position) and creates one hole per atom, because of the electron deficiency of Fe in comparison

to Co. On account of this, a thermoelectric ideal composition out of several filler elements and iron in $CoSb_3$ is supposed to be more difficult to produce, because the additional electrons from the filling element add up to the minority charge carriers, decreases the effective mobility and as a consequence counteracts to some extent to an optimized power factor.

The primary macroscopic effect of filling the void in the skutterudite crystal is the enhancement of the thermal resistivity. An insight into the main scattering mechanisms with simple models was done e.g. by Nolas et al. in 2006 [105]. Therein the lattice thermal conductivity data from low to high temperatures of different skutterudite materials, i.e. unfilled $CoSb_3$, Yb/La filled skutterudites and tin doped and filled skutterudites were analyzed. At low temperatures, boundary scattering is - as was expected - the main scattering mechanism for pure $CoSb_3$ material, which is superimposed at higher temperature by point and boundary scattering. At high temperatures ($\gg 300\,$K) Umklapp scattering is the dominating scattering mechanism. For the filled skutterudites the intermediate temperature (above room temperature), where the thermoelectric figure of merit is highest, is of main interest. In this region an additional term, the resonance scattering contribution, is introduced, which fits with the experimental data. It is notable that Umklapp scattering is not a major concern for the unfilled and filled skutterudites, which is based on the fact that in the intermediate temperature, where the resonant scattering is most efficient, Umklapp scattering is of less importance [105]. Point defect scattering is contributed to the order-disorder state at the void lattice site ($2a$ position). Alloy scattering from Sn atoms was discussed and highlighted as potential scattering mechanism, which already showed a vast reduction in the lattice thermal conductivity for unfilled skutterudite material.

Kim et al. showed in his recent calculations with $Ba_xCo_4P_{12}$ skutterudite material that the low thermal conductivity can be described with point-defect scattering by the Ba atom for the composition with $x = 0$–0.25 [36]. For higher filling fractions ($x = 0.25$–0.5), where secondary phases are expected the calculated interfacial scattering matches fairly with the experimental data, which shows a minimum in the lattice thermal conductivity in the regime with a secondary phase. Accordingly this is apparently dominated by a significant reduction of the long-range acoustic phonon transport.

The mechanism of the observed Einstein oscillation by the filler element in the skutterudite material was described in more detail by Koza et al., which revealed a well-defined phase relation of the host lattice and the filler atom

[39]. Electron spin resonance measurements of $Ce_{1-x}Yb_xFe_4P_{12}$ material furthermore suggest that the Yb^{3+} ion is spending more time at off-center than on on-center positions in the oversize cage, depending on the given temperature [106]. The paradigm of the PGEC concept is therefore not fully applicable on the filled skutterudite material system, which was renamed by Koza et al. to "Phonon Crystal Electron Crystal", because of the distinct correlation of the host skutterudite lattice with the filler atom.

Matsuhira et al. showed that the estimated Debye temperatures of skutterudite compounds are mainly dependent on the nature of the pnicogen elements ($24g$ Wyckoff position) and the Einstein temperature to a certain extent correlates to the energy of the low energy optical mode that are caused by the filler atoms [107]. The fact that the pnicogen rings are primarily responsible for thermal conductivity of the skutterudite material can be read e.g. in [65, p.167 ff.].

The skutterudite material shows high figure of merit at intermediate temperatures. Nevertheless for industrial applications the mechanical properties, thermal stability, oxidation resistance and possible large-scale production are of eminent importance. Several groups investigated on these issues and found very appealing mechanical properties [108, 109]. Thermal cycling was found to be partly problematic and attempts with aerogel were carried out at the Jet Propulsion Laboratory to suppress the Sb loss of the skutterudite material [110]. Furthermore it was found that the oxidation resistance of pure $CoSb_3$ material seems to be stable at least below $673\,K$ and slowly decompose in vacuum or under inert conditions at higher temperatures [111]. For filled skutterudites the oxidation-sensitivity might be increased at higher temperatures, however studies on this and especially on large scale production issues are only sparsely reported. Melt-spinning techniques were successfully applied and show enhanced thermoelectric efficiency due to the high grain boundary density and subsequently low thermal conductivities [112–115]. New synthesis methods for skutterudite compounds are still under investigation and already showed advances in terms of processing durations of skutterudites. [116].

Indium as filler atom plays a peculiar role in the $CoSb_3$ skutterudite material. It was indeed found to have very promising thermoelectric properties, which are comparable to the "traditional" filler elements [117]. However

it is debated whether In can access permanently the void interstitial in the skutterudite crystal lattice, because indium possesses significantly different properties than other typical filler elements, such as rare earth elements [64]. Furthermore InSb as secondary phase is believed to enhance the thermoelectric properties, when it is abundant as nanosized precipitates in the skutterudite bulk material [118]. Whether indium can access the icosahedral void or exclusively functions as nanosized InSb precipitates is still under current investigation and as a consequence the interest on indium filled skutterudites is still lively [119–121].

Chapter 3

Experimental Methods

The experimental methods used in this thesis comprise different instruments and devices. The skutterudite material is first synthesized and subsequently compacted. In between and especially after the compacting of the material the thermoelectric properties were determined (i.e. κ,σ,S). This was mostly done as a function of temperature ranging from about $300\,\text{K}$ to $700\,\text{K}$. Furthermore an analysis of the microstructure was carried out as well as structural properties of the skutterudite material. These measurements were typically done at room temperature and/or low temperatures. This chapter will provide information how the skutterudite material was synthesized, compacted and prepared for the particular measurements. Additionally brief introductions are given for thermoelectric characterization methods (at elevated temperatures), powder diffraction and electron microscopy.

3.1 Synthesis and Compacting

Skutterudites cannot be directly grown from the melt, because the intermetallic phase suffers a peritectic decomposition at $1147\,\text{K}$ for pure $CoSb_3$ (see fig.3.1). Still, there are various methods to synthesize a skutterudite material from elementary constituents: melt-quench-annealing, mechanical alloying, solvothermal reaction, high pressure synthesis and recently microwave synthesis [116]. In this work the skutterudite material was obtained by a melt-quench-annealing approach. As a consequence of the relatively low density of the material and crystallographic defects after the annealing step, the skutterudite material was compacted with a short-term sintering press.
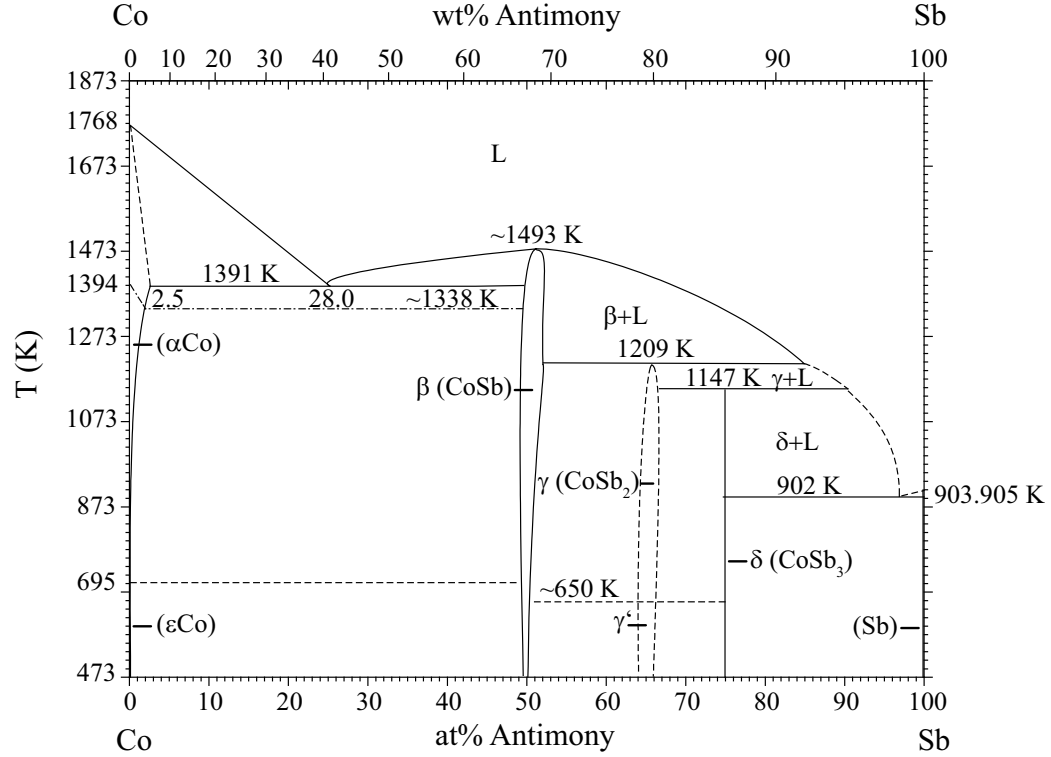
Figure 3.1: *Binary phase diagram of Co and Sb (after [122] and references therein).*

The synthesis starts with the selection of the constituents. These were chosen in form of lumps, pellets or flakes to avoid oxidation of the material. Especially for rare earth elements the work under inert atmosphere is of importance - and thus was done within a glove box system.

The elementary constituents were first placed in a silica quartz tube and then closed with a glass valve under argon atmosphere. This was done by an arrangement of a glass valve, a manufactured laboratory glassware, membrane pump and an argon gas cylinder. The evacuated quartz ampule is then sealed with an oxygen/propane burner.

The sealed quartz ampule is then placed within an induction coil and is held by a cord made out of silica glass. The melting process of the constituents was supported by small vibrations to further homogenize the material. Additionally the ampule itself was manually turned over several times. This

was followed by quenching the ampule in water.

Subsequently the ampule is sealed in another quartz tube, which protects the synthesized material from being oxidized in case of cracks/fissures in the first ampule. Latter is frequently observed due to an incorporation of strain during the quenching and a considerable thermal expansion of the skutterudite material during the annealing period.[1] The ampules are placed within a conventional muffle type furnace and were long term annealed (typically one week).

After the annealing process the material was pulverized and placed in a graphite die. The sintering press is a current assisted device, which heats the graphite die and the skutterudite material by application of a high direct current and thus heats up the material by Joule's heat. In parallel, a pressure in the range of 5×10^1 MPa was applied to densify the material. This whole sintering process typically takes 30 minutes in order to get a high density skutterudite pellet. The typical diameter of the round shaped sample was 15 mm with a thickness of around 4 mm.

Sample Preparation for Thermoelectric and Structural Characterization

The determination of the dimensionless figure of merit ZT involves several measurements. Furthermore the structural characterization of the material demands an additional amount of samples of the same (as-cast) material. In this part the sample preparation for different measurements and the probe geometry is described (see fig.3.2).

The skutterudite material in this thesis is synthesized by melting the constituent elements followed by an annealing step. After the heat treatment of the material, it is removed from the silica glass (see therefore sec.3.1). In most cases, the material fills-out the inner shape of the quartz ampule, during the melting step in the synthesis process. The cylindrical as-cast material, which is typically around 10 g is then cut into different slices, which is used for analysis by electron microscopy, local Seebeck coefficient and heat capacity measurements. A considerable amount is ground in a mortar with a pestle made out of agate. The powder is used for the powder diffraction mea-

---

[1] With this technique most of the skutterudite material will be retained. In case of pulverization of the material in order to place it in a new quartz ampule, this may not be assured. Furthermore the diffusion length of a bulk material is comparably high and will therefore benefit to the crystallization process.

surement and additionally for transmission electron microscopy. The main fraction of the powder is sintered in a short-term sintering device (see therefore sec.3.1). The pellet is then cut into two smaller pellets with reduced thickness (around 2 mm) from which one is used for measuring the density of the sample and the temperature dependent diffusivity of the sample (used to determine - together with the heat capacity - the thermal conductivity of the sample). The other circular shaped pellet is employed to prepare two further bar shaped specimens, which is in one case used for a temperature dependent Seebeck coefficient measurement and in the other for a temperature dependent electrical conductivity measurement. Main advantage is that the temperature dependent measurements can be carried out without thermal cycling of the specimens (an alternative are simultaneous S-σ-(κ)-measuring instruments). One bar shaped specimen is typically used to additionally determine the room temperature Seebeck coefficient (an averaged value from the local Seebeck coefficient values) as the temperature dependent Seebeck coefficient measurement uses a passive way of cooling and therefore attains values only above room temperature (see sec.3.2.2). Furthermore one of the bar shaped specimens is used to measure the Hall coefficient and its electrical conductivity at room temperature.[2] In the Hall measurement the thickness is proportional to the Hall constant and therefore small thicknesses are desirable. For this reason the bar shaped sample is additionally cut in the horizontal plane to obtain two further samples with a thickness of about 0.6 mm. The Hall specimens are typically prone to breaking, so it is ideal to have a backup specimen in case of damage. The specifics of every specimen can be viewed in figure 3.2.

3.2   Electrical and Thermal Characterization

The measurements of the macroscopic transport properties (i.e. κ,σ,S) at temperatures in the range between 300 K and 700 K are in parts carried out in purpose-built instruments, which were constructed in-house at DLR. These measuring instruments were specifically designed to minimize the effect of possible measurement uncertainties due to heat radiation and degradation/oxidation of the probe head material, samples and chemical reactions

---

[2] A high temperature Hall-$S(T)$-$\sigma(T)$-measurement device is currently in the stage of development and uses a circular sample geometry.
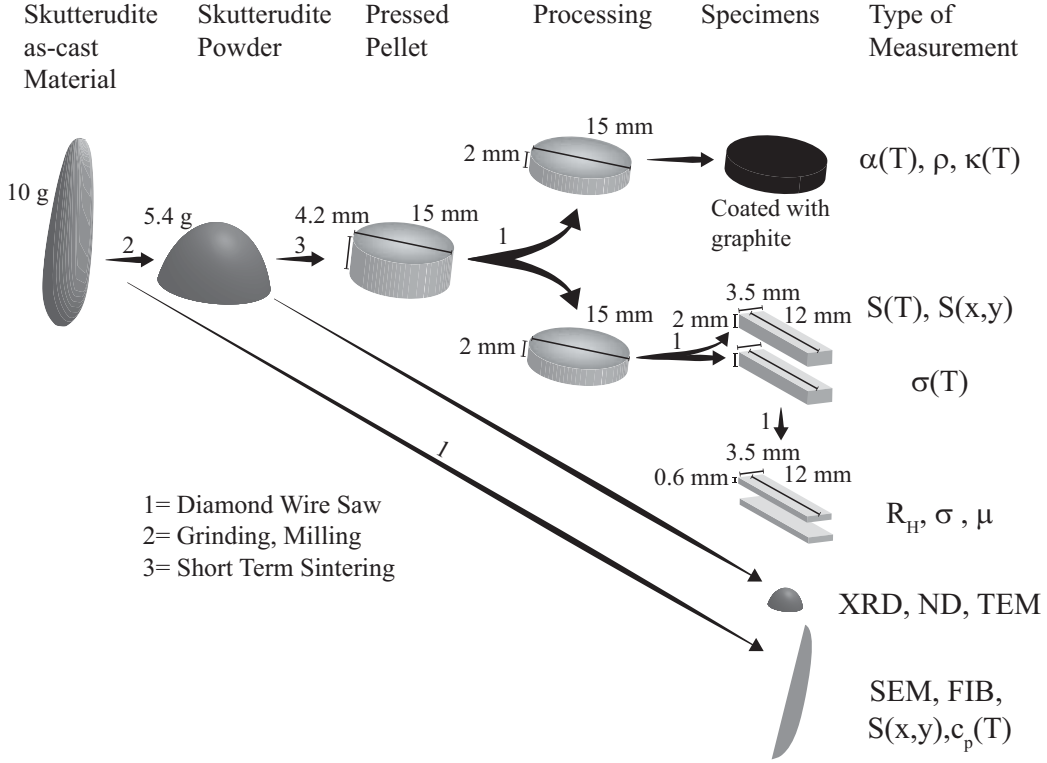
Figure 3.2: *Schematic drawing of the sample preparation beginning from the as-cast skutterudite material to the particular type of measurement. The acronyms and parameters denote following measurements: $\alpha(T) \widehat{=}$ temperature dependent diffusivity, $\rho \widehat{=}$ density at room temperature, $\kappa(T) \widehat{=}$ calculated thermal conductivity from $\alpha(T), \rho$ and c_p, $S(T) \widehat{=}$ temperature dependent Seebeck coefficient, $S(x,y) \widehat{=}$ local measurement of the Seebeck coefficient, $\sigma(T) \widehat{=}$ temperature dependent electrical conductivity, $R_H \widehat{=}$ Hall coefficient at room temperature, $\sigma \widehat{=}$ electrical conductivity at room temperature, $\mu \widehat{=}$ effective mobility calculated from R_H and σ, $PXRD \widehat{=}$ powder X-ray diffraction, $ND \widehat{=}$ neutron powder diffraction, $TEM \widehat{=}$ transmission electron microscopy, $SEM \widehat{=}$ scanning electron microscopy, $FIB \widehat{=}$ focused ion beam (as sample preparation for TEM),$c_p(T) \widehat{=}$ temperature dependent heat capacity.*

between them. The measurement of the thermal diffusivity at high temperatures is carried out by a commercial laser flash apparatus, which determines together with the density and heat capacity measurement the thermal conductivity. The local Seebeck coefficient measurement and the Hall measurement setup are also home-built devices. In this section these instruments are introduced and subsequently described.

3.2.1   Electrical Conductivity

The measurement of the electrical conductivity/electrical resistivity is carried out by a 4-point probe method, i.e. the current is applied to the sample by wires different from the wires used for sensing the voltage. The four-terminal sensing eliminates contributions from the impedance of the wiring and (small) contact resistances and is therefore a frequently used method to determine the electrical conductivity [62, ch.23].
Inaccuracies may occur by a direct current 4-point measurement of thermoelectric materials. This is caused by the thermoelectric materials themselves, which typically possess a high Peltier coefficient and as a consequence create an additional Seebeck voltage due to the induced temperature gradient along the sample. For this reason an alternating current is used, which is chosen in the range of few Hz to avoid capacitive and inductive effects.
The current contacts of the boron nitride probe head are Pt-wires welded to Inconel[3] blocks. The pins for voltage sensing are made of tungsten and have an interspace distance of around 3 mm. The contacts can be in both cases pressured on the sample either by a tungsten spring (current contacts) or by a tungsten screw (voltage probe tips). The sample temperature is recorded by a Pt-Pt/Rh thermocouple, which is located at the specimen mounting. The sample has a bar shaped geometry and has a typical size of $12 \, \text{mm} \times 3.5 \, \text{mm} \times 2 \, \text{mm}$.
The probe head is inserted in the quartz tube placed in a tube furnace and the measurement can be carried out under inert atmosphere or vacuum. The temperature of the tube furnace is adjusted by a PID controller and the measurement is done by a precision digital multimeter in combination with a frequency generator. The electrical conductivity is calculated from the

---

[3]Austenitic nickel-chromium-based superalloy

measured resistance R of the specimen according to:

$$\sigma = \frac{l}{A} \cdot \frac{1}{R} \quad , \tag{3.1}$$

where l denotes the interspace of the tungsten pins and A the sample cross section of the specimen.

3.2.2 Temperature dependent Seebeck Coefficient

The Seebeck coefficient measurement is carried out by a 2-point probe method. The specimen is heated up to the projected temperature and an additional small temperature gradient (few Kelvin) is applied during the measurement of the Seebeck voltage. Since the Seebeck coefficient measurement comprises a temperature sensing (at the two connection points) and a concomitant voltage measurement, both have to be carried out simultaneously - or more precisely, within a period of time, where the condition is at equilibrium.
The probe head consists of boron nitride with two carbon parts, which are located at the beginning and the end of the sample mounting. The graphite part of the end has a conical surface which is thermally connected to a complementary carbon rod. This construction is intended to establish the steady state temperature gradient of the probe head and as a consequence of the specimen itself. The measuring wires are thermocouples, which can do both, the electrical and the thermal measurement. The thermocouples are pressed on the sample by tungsten springs and the sample itself is fixed by a boron nitride bar. The tube furnace is identical to the furnace used in the electrical conductivity measurement, however a thermal gradient within the probe head is obtained by a thermal coupling of the carbon rod to the surrounding temperature outside the tube furnace (see fig.3.3).
 The geometry of the specimen is similar to that of the electrical conductivity measurement, but preferably thin samples are used due to a possible thermal gradient in flatwise plane.[4]
The measurement is carried out in sequence, beginning with the temperature measurements of the different thermocouples, followed by the voltage sensing and then the temperature measurement is repeated. Thus the temperatures before and after the voltage sensing can be used to evaluate the mean value. The Seebeck coefficient is then determined by the ratio of the

---

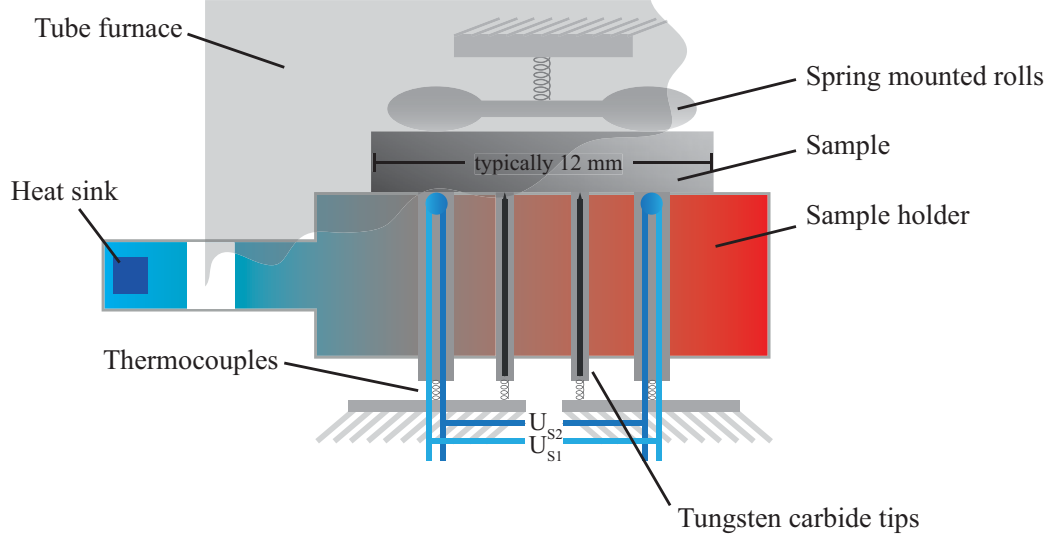[4] "thin" means a typical thickness of the specimen of several millimeters.

Figure 3.3: *Schematic drawing of the Seebeck coefficient measurement instrument. In eq.(3.2) the denoted Seebeck voltage U_S can be assigned to both displayed voltages in the schematic, i.e. U_S1 or U_S2.*

measured Seebeck voltage U_S and the temperature difference of the two averaged temperatures:

$$ S = \frac{U_\mathrm{S}}{[(T_{1-\mathrm{before}} + T_{1-\mathrm{after}})/2] - [(T_{2-\mathrm{before}} + T_{2-\mathrm{after}})/2]} = \frac{U_\mathrm{S}}{\Delta T_{1,2}} \quad . \quad (3.2) $$

$T_{1-\mathrm{before}}$ is the temperature value at point 1 prior to the voltage sensing and $T_{1-\mathrm{after}}$ denotes the temperature measurement after the voltage sensing. The measurement at point 2 on the sample is accordingly. The averaged temperature difference is described as $\Delta T_{1,2}$. The temperature difference is typically a few Kelvins and lessens when the inside temperature of the tube furnace possesses a value near room temperature by reason of the passive cooling. Mostly the Seebeck coefficient measurement is done in the cooling down period to exclude noise, which may come from the heater, the thyristor or the temperature controller. All these devices are shut down in the cooling down period.

For several temperature dependent Seebeck coefficient measurements a different home-built instrument was utilized (indicated in the particular diagrams), which is based on a different method, more comparable to the local Seebeck coefficient measurement (see following section). The instrument features an active heater for the small temperature gradient and thus different temperature gradients can be established. The Seebeck coefficient S of the sample is determined by

$$S = \frac{-U_{S1}}{T_2 - T_1} + S_1(T) \quad , \tag{3.3}$$

where U_{S1} is the Seebeck voltage measured with one wire of the thermocouple, T_1 and T_2 are the temperatures at the particular connection points of the specimen and S_1 is the temperature dependent Seebeck coefficient of the wire material. Furthermore the Seebeck voltage U_{S2} of the specimen using the other wire of the thermocouple is recorded. This leads to a more accurate determination of the Seebeck coefficient, since the inaccuracy of the thermocouples and the dark electromotive force[5] can consequently be deducted:

$$S = \frac{-\left[S_1(T) - S_2(T)\right]}{1 - (dU_{S1}/dU_{S2})} + S_2(T) \quad . \tag{3.4}$$

The derivative of the measured Seebeck voltages dU_{S1}/dU_{S2} in eq.(3.4) is determined by a linear regression. Furthermore S_2 is the temperature dependent Seebeck coefficient of the other wire material.

3.2.3   Local Seebeck Coefficient

The scanning Seebeck coefficient microprobe can locally measure the Seebeck coefficient of a (thermoelectric) material by application of a heated tip, which scans the surface of the material in a raster pattern. It allows one to obtain information about the homogeneity of the material in regard to the Seebeck coefficient. The instrument is indeed a home-build instrument, but is nowadays commercially available [123].
The Seebeck coefficient microprobe consists of a *x-y-z* positioning stage, a sample holder and a probe head. For the measurement a precision digital multimeter is used, which process the data from the thermocouple wires. The

---

[5]i.e. an unwanted leak voltage

probe head comprises a custom-made heated tip, which is able to press onto the material's surface with an adjustable force. When the heated tip touches the surface a local heating in the vicinity of the tip occurs and a temperature gradient establishes. At the two wires (Cu-Cu, CuNi-CuNi), which are both electrically and thermally connected to the probe tip and the specimen, different voltages U_0 and U_1 are measured yielding the Seebeck coefficient of the sample S_{sample} according to the equations

$$
\begin{aligned}
U_0 &= (S_{\text{sample}} - S_{\text{Cu}}) \cdot (T_1 - T_0) & (3.5) \\
U_1 &= (S_{\text{sample}} - S_{\text{CuNi}}) \cdot (T_1 - T_0) & , & (3.6)
\end{aligned}
$$

which can be combined to the expression

$$
S_{\text{sample}} = \frac{U_0}{U_1 - U_0} \cdot (S_{\text{Cu}} - S_{\text{CuNi}}) + S_{\text{Cu}} \quad . \tag{3.7}
$$

T_1 is the temperature at the probe tip and T_0 is measured on the sample with a significant distance to the probe tip. Latter is realized either by a welded contact between the thermocouple and the sample, or a thermocouple, which is located in the sample holder and for this reason has a good electrical and thermal contact to the specimen. S_{Cu} and S_{CuNi} denote the literature values of the Seebeck coefficient of copper and copper-nickel. The measurement is typically carried out in a raster scan of an user-defined geometry (several millimeters) at room temperature in air.

3.2.4   Hall Coefficient and Hall Mobility

The Hall coefficient and the Hall mobility of the samples are measured with a 6-point probe method at room temperature. In figure 3.4 it is shown that from point contact 1 to 2 the current is impressed into the bulk sample and the Hall voltage U_{H} is measured by using the point contact 3-5 and 4-6, respectively. Furthermore the point contacts are used to measure the electrical resistivity by the 4-point probe method, i.e. contact point 1 and 2 are used for imprinting the current and the point contacts 3-4 and 5-6, respectively, are used to measure the electrical resistivity on two different points. Perpendicular to the sample an electromagnet is installed, which can create a magnetic field up to $0.9\,\text{T}$. The Hall effect induces a small voltage, which has to be determined by a precision digital multimeter. For this reason a

Lock-In amplifier is used to imprint an AC current (19.1 Hz, 2 V), to detect the Hall voltage and to avoid generation of Peltier heat[6]. The strength of the magnetic field was recorded by a teslameter. The instrument is capable of measuring the Hall voltage and the electrical resistivity from about 10 K to room temperature, due to a resistive heater near the sample mounting in combination with a closed cycle helium cooled cryostat. For the typical measurement the different magnetic field strengths and the corresponding Hall voltage are recorded. The sample thickness is determined by a caliper and the distances between the point contacts are measured by a light microscope. The current, which is impressed in the sample, is constant. For this reason one can derive the Hall constant R_H from a linear regression of the U_H-B diagram (Hall voltage U_H versus magnetic field strength B) according to

$$R_H = \frac{M \cdot d}{I} \quad , \tag{3.8}$$

where M is the slope of the linear regression in the U_H-B diagram and d the thickness of the specimen. In the measurement the current I does not change significantly and is for this reason as before mentioned regarded as a constant value. The effective charge carrier density n_H is then determined by equation (1.7). For the evaluation of the Hall mobility μ_H the Hall constant R_H has to be multiplied with the corresponding electrical conductivity σ (see eq.(1.8)).

3.2.5 Thermal Conductivity

The thermal conductivity κ is obtained in this work by the measurement of the density ρ, the heat capacity c_V and the thermal diffusivity α of the sample, according to

$$\kappa = \rho \cdot c_p \cdot \alpha \quad . \tag{3.9}$$

It is notable that the heat capacity at constant pressure c_p is almost identical with the heat capacity at constant volume c_V for solid state materials and is for this reason assumed to be equal.
Diffusivity measurements in this work are carried out by a commercial laser

---

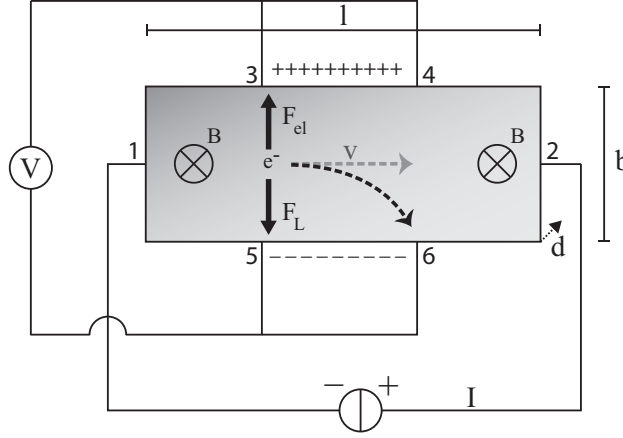[6]see sec.3.2.2 for further explanation about the Peltier heat

Figure 3.4: *Schematic drawing of the 6-point Hall measurement setup, showing the forces F_{el}, F_L and velocity v of the charge carrier (here: electron), which are induced in the sample by a magnetic field B. The parameters l,b and d denote the particular dimensions of the sample (length, width and thickness, respectively) and the numbering specifies the particular electrical contacts of the sample with the setup [124]*

flash analyzer. Here the sample is placed in the sample holder, which is enclosed in a vertical tube furnace under inert atmosphere. The sample will be heated to the particular temperature and is subsequently illuminated by a pulsed infrared laser. The controlled laser shots establish a small temperature increase due to the additional heat, which is recorded at the backside of the specimen by an infrared sensor as a function of time. The thermal diffusivity α is then evaluated by the time dependent temperature change $\partial T/\partial t$, according to [125]

$$\frac{\partial T}{\partial t} = \alpha \nabla^2 T \quad . \tag{3.10}$$

For the measurement it can be assumed that the heat pulse is instantaneous, located at one point and behaves adiabatic in terms of the temperature rise. Then the evaluation of the thermal diffusivity yields to [126]

$$\alpha = \frac{1.38 \cdot L^2}{\pi \cdot t_{1/2}} \quad , \tag{3.11}$$

where L is the uniform thickness in 10^{-2} m and $t_{1/2}$ is the time required for

the back surface of the specimen to reach half of the maximum temperature rise.

The density of the material is measured in this work by the Archimedes method. This simple technique comprise the determination of the weight in air and in water. Thus the volume of the specimen V_s can be calculated as follows due to the displaced water:

$$V_s = \frac{m_s - m_w}{\rho_w} \quad .$$

(3.12)

In equation (3.12) m_s is the mass of the specimen, m_w is the weight of the specimen under water and ρ_w is the density of water. The density of the specimen ρ can then be calculated by the ratio of the mass and the volume of the sample ($\rho = m_s/V_s$). This measurement is done at room temperature. The changes of the density as a function of the temperature is small and for this reason ρ is kept constant. The calculated values of the thermal conductivity will be therefore overestimated because the density commonly descends with increasing temperature.

The heat capacity measurement was carried out in a differential scanning calorimeter. An extensive study of the heat capacity on skutterudites was carried out by Stiewe et al. [127], which showed almost constant heat capacity values for the skutterudite compound as a function of temperature. Above all, the sample preparation for measurements with the differential scanning calorimeter is critical and can lead to significant deviations. As a consequence the heat capacity value c_p was assumed to be constant and was set equal to the value of $0.23 \, \mathrm{J \, g^{-1} \, K^{-1}}$, which is also the value derived from the work in [127].[7]

3.3 Powder Diffraction

In this thesis powder diffraction measurements have been carried out to determine the phases and the structural properties of the skutterudite powder. In this section a brief introduction is given to the measurement principle,

---

[7]An calculation according to the Dulong-Petit law outputs a value, which is almost identical to the value of $0.23 \, \mathrm{J \, g^{-1} \, K^{-1}}$: $c_n = 3R \approx 24.9 \, \mathrm{J \, mol^{-1} \, K^{-1}} \rightarrow c_n/M_{\mathrm{CoSb_3}} \cdot 4 = 0.235 \, \mathrm{J \, g^{-1} \, K^{-1}}$ with $M_{\mathrm{CoSb_3}} = 424 \, \mathrm{g \, mol^{-1}}$ being the molar mass of $CoSb_3$, c_n is the molar heat capacity according to Dulong-Petit, R the universal gas constant and the factor 4 due to four involved atoms in the compound.

which can be applied for both, X-ray and neutron powder diffraction.

When a visible beam is normally scattered at the surface of any material, optical diffraction occurs, which can be regarded as a daily experience. In the case the beam consists of particles with a wavelength equal or less in comparison to interatomic distances (typically in the order of 10^{-10} m) strong deflection of the incident beam occurs. This effect was explained by W.L. Bragg and his father, who proclaimed that the particles of the incident beam are systematically scattered at the lattice planes of the crystal. As a consequence the crystal structure (or type of Bravais lattices) can be determined by analyzing the incident and the reflecting beam. When the condition is met that the angle of the incident beam is equal to the angle of the reflecting beam then *Bragg's law* applies:

$$n_{\mathrm{bragg}} \cdot \lambda = 2d_{\mathrm{bragg}} \cdot \sin \Theta \quad , \qquad (3.13)$$

n_{bragg} is an integer, λ the wavelength of the incident beam, d_{bragg} is the spacing between the planes of the crystal and Θ is the angle between the incident beam and the particular plane.[8] There are several different types of measuring devices that use the diffraction method to determine the crystal structure of a material. Nevertheless the Bragg-Brentano and Debye-Scherrer geometries are most common for *powder* diffraction measurements, where in principle all possible Θ angles are recorded simultaneously (reflection, transmission) and the wavelength of the incident beam is fixed (e.g. $\mathrm{Cu}_{\mathrm{K}\alpha}$, with $\lambda = 1.5405$ Å). To capture the reflecting/transmitted beams a special photographic film was used, which encircled the sample in a certain distance. For measurements nowadays the photographic film is replaced by electronic detectors, which run a circular path from the perspective of the sample. For neutron powder diffraction a further method is frequently used, which is called the *time-of-flight* (TOF) measurement. In this case the wavelengths of the incident neutrons are known[9] and scatter at the powder sample. The sample itself is surrounded by fixed neutron detectors, which record the reflecting beam. This is alike to the early Debye-Scherrer method with a photographic film, however at the fixed detectors the measurement is time resolved, and an extra diffraction pattern can be recorded at every detector itself (fixed Θ, varying λ). For further information about powder X-

---

[8]In the neutron powder diffraction pattern d_{bragg} is equal to the expression d-Spacing.

[9]The neutrons with different wavelength possess different velocities and are therefore separated by the time/duration of flight.

ray diffraction it is referred to a textbook [128]. For more informations about time-of-flight neutron powder diffraction the interested reader may consider following website [129].

3.4 Electron Microscopy

Electron microscopy analysis was carried out to obtain high resolution images of the material and as a consequence characterize its microstructure. Furthermore energy dispersive X-ray measurements were carried out to determine the chemical composition of the material and the precipitates. This established measurement technique is written similarly condensed like in sec.3.3. Optical microscopy uses light and a system of lenses to enlarge a particular object to a certain degree. However the order of magnification in light microscopy can only be achieved to a certain extent due to a physical limit of the resolving capacity using visible light. The resolving capacity is proportional to the wavelength of the applied beam and therefore it is necessary to use light with a shorter wavelength in order to get higher magnification levels. Another approach is to use electrons instead of electromagnetic waves, which can have a thousandfold smaller wavelength than visible light. As lenses, electrical and magnetic fields are being used to manipulate the path of the electrons. These findings led to the construction of an *electron* microscope in the 1930s, which in principle does not differ from a conventional light microscope. Two parallel developments in the field of electron microscopy were followed. One type directs the electron beam entirely through the thin specimen, transmits it, is then subsequently magnified and captured by a fluorescent screen/detector - a so-called *transmission electron microscope*. The other type uses a focused electron beam, which scans the surface of the specimen in a raster pattern. Two main physical effects occur at this moment. The focused electron beam is partly backscattered and can be subsequently captured by a detector (backscattering mode). Another effect is that the incident electron beam creates secondary electrons[10] in the material itself, which can to a small extent leave the material's surface. These secondary electrons can then be captured by applying an electrical field and a detector (secondary electron mode). The second type of electron microscopes is called *scanning electron microscope.*
An electron beam of high energy mostly causes a X-ray excitation in the

---

[10]By definition all electrons which possess an energy equal or less than $50\,\text{eV}$.

material. Each element has an unique atomic structure and therefore has its own characteristic X-ray fingerprint. Latter is cause by excitation of electrons in an inner shell by the electron beam. Thus the created hole in the inner shell can be occupied by another electron, which is coming from a higher-energy shell. The difference in energy is then either transferred to another electron (Auger electron) or it can be released as an electromagnetic wave (characteristic X-ray). For this reason it is possible to determine the chemical composition of the specimen by evaluating the X-rays created within a considerable volume of the specimen.

Further literature about electron microscopy can be found e.g. in following textbooks [130, 131].

Chapter 4

Results and Discussion

4.1 Sample Preparation of Indium and Rare-Earth (Gd,Ce) filled Skutterudites

The basic composition $CoSb_3$ is an intermetallic compound with a peritectic point at $1147\,K$ (see fig.3.1). Thus the skutterudite compound would dissociate in thermal equilibrium at $1147\,K$ from $CoSb_3$ into $CoSb_2$ and elementary antimony (solid $\rightleftharpoons$ solid+liquid). When the compound is synthesized from a melt, two further regions above this peritectic point have to be considered. Between $1147\,K$ and $1209\,K$ there is the $\gamma+L$ region and furthermore at higher temperatures from $1209\,K$ to about $1338\,K$ the $\beta+L$ region is present. As a consequence this temperature range from the liquid phase L to the peritectic point has to be transcended quickly, which is mostly realized by quenching the melt to room temperature. However this harsh treatment prevents the formation of a reasonable crystalline product. A subsequent annealing has to be carried out to obtain a crystalline skutterudite structure. The annealing temperature thereby has to be significantly below the peritectic point and the duration should be chosen in such a way that the diffusion/crystallization process can almost entirely be carried out.

At the beginning highly purified (elementary) constituents are inductively melted within an evacuated silica tube. The high purity of the elements is actually not mandatory for highly doped semiconductors, where the main influence will be dominated by the primary doping element(s) - the impurities would act as minority carriers in the material. Here it was chosen so that even lower doped/filled samples can be synthesized and hence the thermo-

electric properties can be determined. The presence of water inside the silica glass itself and oxygen inside the silica tube has to be avoided, because of potential oxidation of the skutterudite material or possibly more important the oxidation of elementary constituents. For this reason the quartz ampule was fabricated by first heating up the entire silica tube with a burner and subsequently fixing a silica joint at the end of the quartz tube. With this procedure most of the moisture within the silica tube disappears. When the quartz ampule is filled by the constituents it is flushed with argon before it is evacuated and sealed. This removes most of the oxygen, which is present in the ambient air. Skutterudite material containing rare earth elements requires working entirely in inert atmosphere, because of the pyrophoricity and the susceptibility to oxygen of rare-earth elements.

The material is then melted by induction at $1423\,\mathrm{K}$ for around $1.5\,\mathrm{h}$ to provide a homogenized melt. Synthesis experiments with a rocking furnace showed comparable results, when the rocking speed and the tilt angle of the furnace is optimized. This homogenization is specifically important for doped and filled skutterudite compounds, where constituents can have a proportion of weight equal to one atomic percent or less.

After the melting process the ampule is quenched in water, which rapidly cools down the material. At the same time a thermal stress is introduced into the quartz material, which makes the silica glass sensitive for further thermal or mechanical treatments. Furthermore rare earth elements react exothermally with elementary antimony and form intermediate compounds in the ampule before it is completely dissolved in the melt. From this chemical reaction the silica ampule suffers even more, which is observable at the inner wall of the quartz material. The exothermal reaction can be prevented inside the quartz ampule by an additional intermediate step, which comprises arc melting of elemental cobalt and the corresponding rare earth element. This precursor material can be put together with indium and antimony and can be processed as mentioned before. Experiments have shown that these additional steps may have a detrimental effect on the resulting skutterudite material (discussed in sec.4.3.3). The small ampule was furthermore encased in another bigger ampule under vacuum conditions and was subsequently sealed. In case of damage of the silica glass during the annealing treatment the material is protected from oxygen.

The annealing was carried out in a conventional furnace at typically $973\,\mathrm{K}$ or $1073\,\mathrm{K}$ (see therefore the experimental details in the particular sections) for $168\,\mathrm{h}$, which entailed mostly a highly crystalline skutterudite material with

comparably big grain sizes. The chosen heating and cooling rate was typically $2\,\mathrm{K\,min^{-1}}$. In parts the cooling period was replaced by an additional quenching step.

For the compaction with a current-assisted sintering device, adequate parameters had to be found, i.e. the sintering temperature, holding period, heating/cooling rate, applied pressure and prior grain size of the skutterudite powder. The chamber of the sintering device was evacuated and was additionally flushed with argon to minimize the oxygen content. The heating rate was about $1\,\mathrm{K\,s^{-1}}$ from $393\,\mathrm{K}$ to the target temperature of about $903\,\mathrm{K}$ with a holding period of around $0.5\,\mathrm{h}$. The cooling period is of major importance in regard to crack formation within the sample and as a consequence pressure-less cooling in an argon atmosphere was mostly preferred. The applied pressure during the sintering process was slowly raised from $18\,\mathrm{MPa}$ to $54\,\mathrm{MPa}$ and retained up to the beginning of the cooling step. The skutterudite was mostly finely ground by mortar and pestle.

4.2 Indium filled Cobalt-Antimony Skutterudites

Indium filled skutterudites have potential thermoelectric properties from around $300\,\mathrm{K}$ until $700\,\mathrm{K}$. Nevertheless the peculiar role of indium in the skutterudite structure is not yet fully understood, because it is doubted whether indium can occupy the void lattice site of the skutterudite structure. The investigation of In:CoSb₃ material will focus on the thermoelectric properties, structural changes in relation to the filling fraction and the secondary phases, which can possibly form at higher additions of indium.

4.2.1 Experimental Details

The polycrystalline $\mathrm{In}_x\mathrm{Co}_4\mathrm{Sb}_{12}$ ($x =$0.05, 0.1, 0.15 and 0.2) specimens were synthesized by induction melting followed by thermal annealing. Stoichiometric amounts of indium, antimony and cobalt with a degree of purity of at least $99.99+\%$ were loaded in silica tubes and sealed under vacuum/argon conditions at a pressure of about $10^{-3}\,\mathrm{mbar}$. The raw material was melted for $1.5\,\mathrm{h}$ at $1423\,\mathrm{K}$ in an induction furnace, which causes a 'stirring' effect of the cobalt pellet and therefore benefits to a mixing of the melt. Furthermore manual tilting and rocking of the silica tube was necessary for an ideal

homogenization. Annealing was carried out in a programmable furnace at 1073 K for 168 h with a heating and cooling rate of about $2\,\mathrm{K\,min^{-1}}$. Crystallographic and microstructure analysis of the as-cast material was carried out by powder X-ray diffraction using $\mathrm{Cu_{K\alpha}}$ radiation ($\lambda = 1.5406\,\text{Å}$) from $2\theta = 10 - 80$ with a step size of $0.02\,\mathrm{deg}$ and a scan rate of $500\,\mathrm{s\,deg^{-1}}$ and SEM together with EDX was applied on embedded as-cast specimens. Further investigations with a transmission electron microscope were performed on specific samples, which were either prepared by an focused ion beam (FIB), or by a conventional powder preparation. The spatial distribution of the Seebeck coefficient $S(x,y)$ on a large area of the sample ingot (typically $1\,\mathrm{mm}\times 7\,\mathrm{mm}$) was determined at room temperature by a home-built Potential & Seebeck Microprobe (PSM) [123]. For characterization of the temperature dependent Seebeck coefficient S, electrical conductivity σ, thermal diffusivity α and room temperature Hall coefficient $\mathrm{R_H}$, densification of the ingot material was carried out. This was achieved by a current assisted short-term sintering of the skutterudite powder in a graphite die at typically 900 K and 50 MPa for 0.5 h. Measurements of high-temperature Seebeck coefficient S and electrical conductivity σ were performed using temperature differential and 4-point probe methods. The thermal conductivity κ was calculated from the thermal diffusivity α measured by a laser flash analyzer, specific heat[1] c_p and density ρ using the relationship $\kappa = \alpha \cdot c_\mathrm{p} \cdot \rho$. The density was measured by the Archimedes method at room temperature. The TE properties at high temperatures were measured typically in the range from 300 K to 700 K.

4.2.2   Results

This section comprises the results from phase and structural analysis of the as-cast material and in the following the Seebeck coefficient, electrical and thermal conductivity data as a function of temperature. Hall measurements and neutron powder diffraction data of the skutterudite material are presented in the end of this section.

Figure 4.1 shows the powder X-ray diffraction pattern of indium filled skutterudite samples with different indium concentrations after the annealing step. It is clearly visible that all shown samples form almost a pure skutterudite phase (see fig.4.1). The natural skutterudite compound $\mathrm{CoSb_3}$

---

[1]c_p is used instead of c_v due to the almost identical values for solid state materials.

exhibits a body-centered cubic symmetry and belongs to the space group $Im\overline{3}$ (No.204, cubic). The typical lattice parameter of phase-pure $CoSb_3$ material is around $a = 9.0385\,\text{Å}$, has a theoretical density of $\rho = 7.631\,\text{g cm}^{-3}$ and comprise a molecular weight of $424.18\,\text{g mol}^{-1}$ with a corresponding volume of $V = 738.40\,\text{Å}^3$ (see JCPDS No. 78-0976). The indium filled skutterudite samples show high crystallinity and a considerable expansion of the lattice parameter in regard to pure $CoSb_3$. From Rietveld refinement the estimated lattice parameter of $In_{0.05}Co_4Sb_{12}$ is $a = 9.041\,\text{Å}$ and increases with indium filling fraction up to $a = 9.048\,\text{Å}$ in the case of the composition $In_{0.2}Co_4Sb_{12}$. In the region of low 2θ in figure 4.1 a broad signal may be detected in several diffraction patterns, which originates from the almost non-diffracting silicon substrate. Impurity phases such as InSb, Sb, and $CoSb_2$ appear only for highest filling fraction of $x = 0.2$ with a proportion between 1% to around 3%. InSb is an intermetallic compound exhibiting a face-centered cubic crystal symmetry ($F\overline{4}3m$, No.216). The lattice constant of InSb is typically $a = 6.4782\,\text{Å}$ and it is the only binary compound of indium and antimony (see JCPDS No. 06-0208). Elementary antimony has a rhombohedral crystal structure ($R\overline{3}m$, No.166) with typical lattice parameters of $a = 4.3007\,\text{Å}$ and $c = 11.222\,\text{Å}$, respectively (JCPDS No. 85-1324). Further possible impurity phases are CoSb and $CoSb_2$, whereas only the latter is observed in the PXRD pattern of the $In_{0.2}Co_4Sb_{12}$ compound. $CoSb_2$ is monoclinic and possesses the space group P21/c (No.14, JCPDS No. 29-0126). Elementary Co and In was not found in the diffraction patterns.

In the SEM images the skutterudite material show large grains with sizes up to several hundred micrometers in diameter (fig.4.2). Furthermore the as-cast skutterudite material exhibit pores, and consequently possesses only a low density ($< 90\%$ of the theoretical density) and has to be consequently further processed/compacted. In the case of the as-cast material with highest filling in the series of indium filled samples ($x = 0.2$) secondary phases, such like InSb, Sb and $CoSb_2$, appear. A more detailed investigation results that these precipitates possess a substructure, where secondary material is surrounded by another material. EDX measurements suggest that these spherical precipitates consist of elementary Sb, which are enclosed by another InSb phase (see fig.4.3). Experiments on higher filling fractions of indium ($x > 0.2$) was carried out by Mallik et al. [132], which show a decomposition of the skutterudite material, with large amounts of secondary material.

In figure 4.4 TEM and SAED images of the FIB samples with the composition $In_{0.05}Co_4Sb_{12}$ and $In_{0.2}Co_4Sb_{12}$ are displayed, respectively. It can

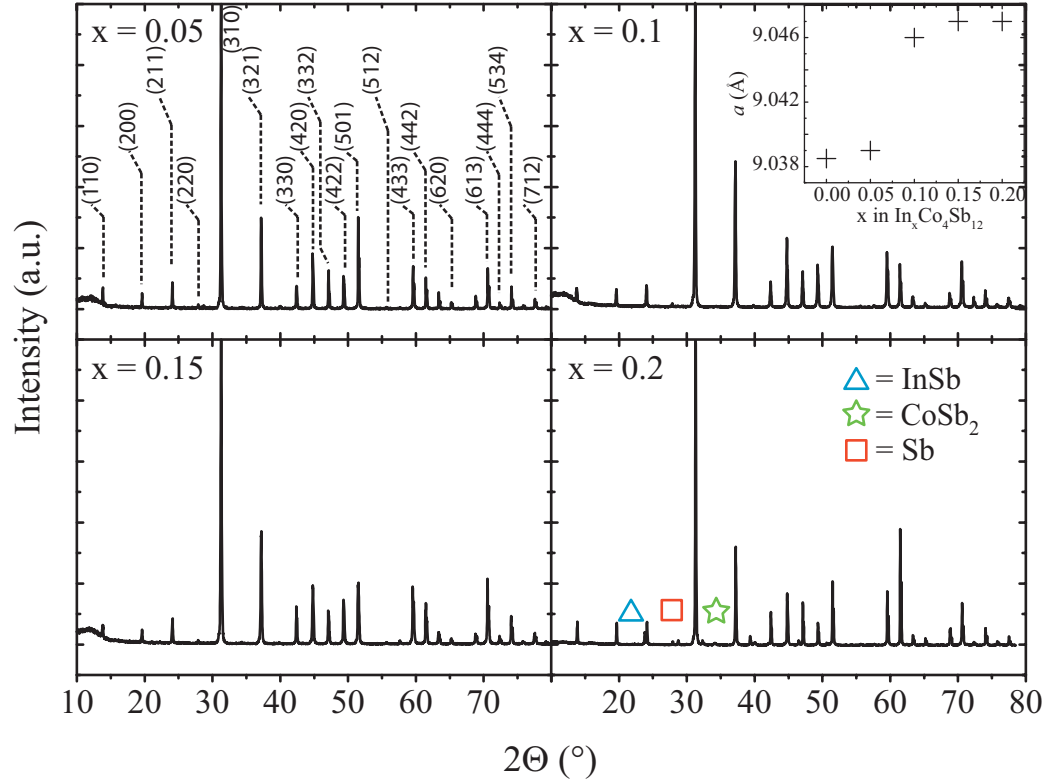Figure 4.1: *Powder X-ray diffraction pattern of as-cast $In_xCo_4Sb_{12}$ skutterudite material (with $x = 0.05, 0.1, 0.15$ and 0.2), prepared by induction melting and subsequent annealing. The numbers in brackets denote the hkl lattice planes of the skutterudite phase and the symbols show traces of the impurity phases. In the inset diagram the corresponding lattice parameter a is depicted.*

be clearly seen that both images show rod-like patterns, which at first view appears to be inherent nanostructures of the material.

It should be noted this result was also observed in another study, where Mallik et al. (DLR) investigated on skutterudite material with additions of indium far above the filling fraction limit of the skutterudite material [132]. Several Scanning Transmission Electron Microscopy (STEM) measurements were carried out to obtain a high resolution image of these structures (fig.4.5).
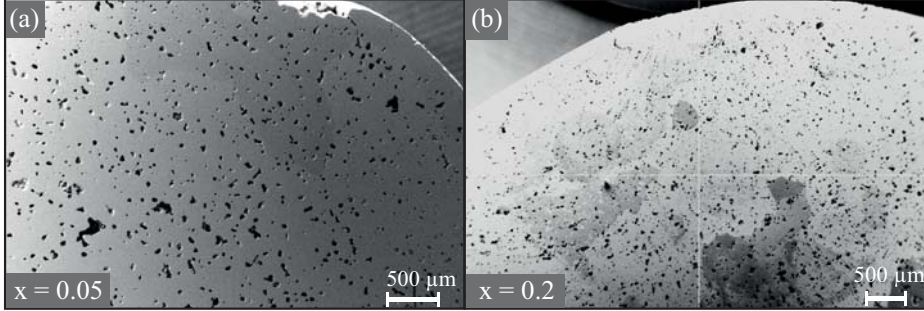
Figure 4.2: *Images from Scanning Electron Microscopy showing the surface of as-cast skutterudite material (In$_x$Co$_4$Sb$_{12}$). All images feature pores, under which image (a) exhibit large grain sizes and image (b) show inhomogeneities indicating several impurity phases within the as-cast material with an indium filling fraction of $x = 0.02$. Both images were taken in the electron backscattering mode.*

Further analysis with EDX (mapping) however did not lead to a reasonable answer with respect to the chemical composition and the underlying mechanism how these structures form. This issue was mainly clarified by using a different preparation method for the skutterudite material, since it is known that the gallium ions, which are employed in the focused ion beam method, may have an influence on the sample. For this reason other specimens were prepared by a conventional powder preparation, which comprises a finely ground material placed on a copper grid. This method did not show any of these rod-like structures, leading to the conclusion that these artifacts are due to the ion beam itself. It can be speculated that this might have to do with the indium content in the skutterudite material by reason of a higher density of rods with the amount of dissolved indium.

TEM-EDX measurements on the specimens were carried out and can be seen in figure 4.6, which were focused on the objective evidence of indium in the skutterudite matrix. The TEM-EDX measurements were carried out in a phase pure skutterudite region, which was ensured by electron diffraction of the investigated area (see fig.4.6). It can be seen that for different sample preparations and with different filling fraction an indium signal is detectable. It is notable that with higher indium fraction a higher indium signal is obtained, even though impurity phases are already formed in the In$_{0.2}$Co$_4$Sb$_{12}$ sample.

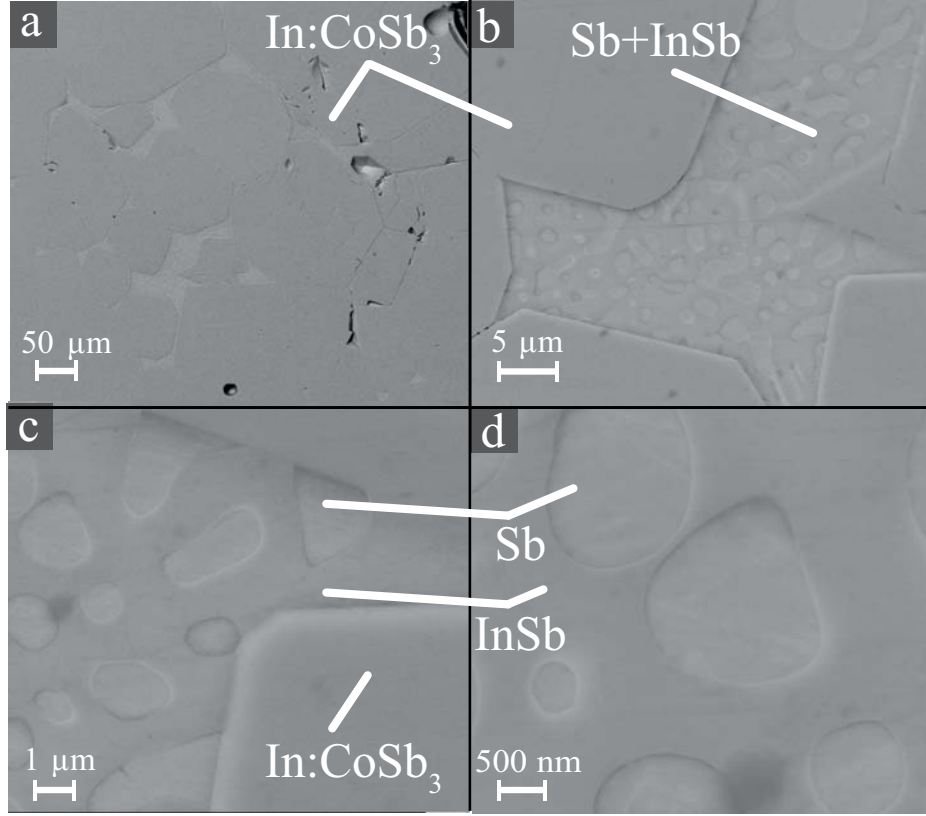Figure 4.3: *Images from Scanning Electron Microscopy showing the precipitates found in the* $In_{0.2}Co_4Sb_{12}$ *as-cast skutterudite material. It is visible that the secondary material exhibits a substructure, which indicates InSb and elementary Sb.*

Figure 4.8 shows the spatial distribution of the Seebeck coefficient S along the ingot samples with different filling fractions ($x = 0.05, 0.1, 0.15$ and 0.2). Typically an area of $7\,\text{mm}$ in length and $1\,\text{mm}$ in width was measured on a cross-section of the ingot samples. All samples show n-type behavior (i.e. a negative sign of the Seebeck coefficient) at room temperature. The distribution of S values can be accessed by the histogram of the local Seebeck coefficient data (see fig.4.8). The room temperature Seebeck coefficient, which is obtained by a Gaussian fit of the $S(x, y)$ histogram, is influenced by the addition of indium beginning from $S_{0.05} = -226\,\mu\text{V K}^{-1}$ for the lowest addition ($x = 0.05$), $S_{0.1} = -180\,\mu\text{V K}^{-1}$ for $x = 0.1$, $S_{0.15} = -169\,\mu\text{V K}^{-1}$ for
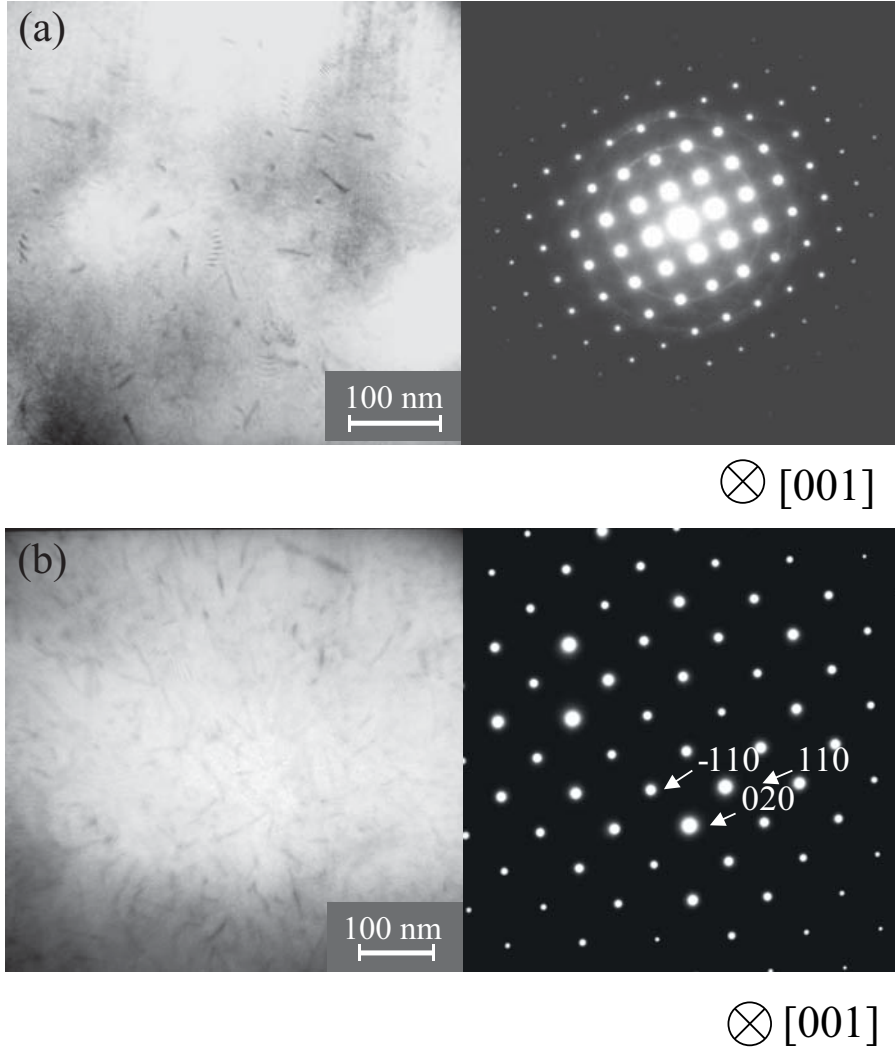
Figure 4.4: *TEM Images and electron diffraction patterns of indium filled skutterudites with different filling fraction of indium (FIB lamellae samples). The images (a) and (b) show the* $In_{0.05}Co_4Sb_{12}$ *and* $In_{0.2}Co_4Sb_{12}$ *as-cast material with the corresponding small angle electron diffraction (SAED) pattern, respectively.*
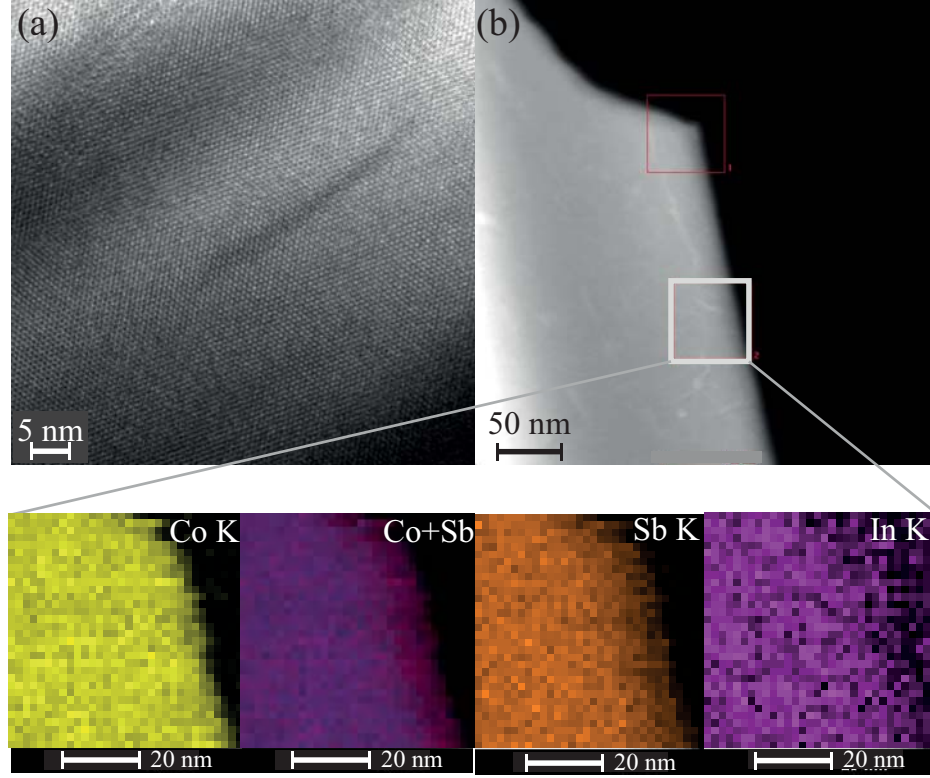
Figure 4.5: *TEM images of skutterudite material with additions of indium far above the filling fraction limit of 1.36 at. Left image (a) is showing a high resolution image of the as-cast material exhibiting a rod-like structure within the specimen. Right image (b) is showing a high resolution TEM image with the corresponding EDX mapping data (bottom figures) showing the K-line intensities of Co, Sb, In and a superposition of Co and Sb, respectively.*

$x = 0.15$ and $S_{0.2} = -162\,\mu V\,K^{-1}$ for the highest indium fraction ($x = 0.2$), which reveals a lowering of the Seebeck coefficient with increasing filling fraction in absolute numbers. It should be noted that the area of ingot samples feature pores and consequently local differences of the material's density, which may have an influence on the lateral Seebeck coefficient measurement, as every measured point on the surface of the ingot sample has not the identical mechanical stability, and therefore could lead to small deviations of the measured local Seebeck coefficient.

The skutterudite material with different indium content was short-term

compacted and the high temperature thermoelectric properties were subsequently characterized. The obtained samples had a high density of at least 98%. Figure 4.9 shows the Seebeck coefficient S as a function of temperature within the range of 350 K to 700 K. The data show that all specimens exhibit n-type behavior, i.e. the negative sign of the Seebeck coefficient indicate that electrons are the major charge carriers. All skutterudite samples possess high Seebeck coefficients ($> |-100 \, \mu V \, K^{-1}|$) and increase linearly with ascending temperature. The absolute Seebeck coefficient as a function of the indium concentration x increases by trend up to a value of $x = 0.15$ and descreases again for the sample with highest indium content in this series ($x = 0.2$). The skutterudite specimens with $x = 0.1$ and 0.15 show an almost equivalent slope of the graph with a constant difference ΔS of about $20 \, \mu V \, K^{-1}$. The skutterudite sample with highest content of indium ($x = 0.2$) crosses the two data sets of the specimens with $x = 0.1$ and 0.15 at different temperatures (400 K and 675 K, respectively). The behavior of the lowest indium filled material in this series ($x = 0.05$) is significantly different. It exhibits the highest Seebeck coefficient in absolute numbers ($S_{\max} = -320 \, \mu V \, K^{-1}$) and has an inflection point at about 550 K. For higher temperatures the absolute Seebeck coefficient of this sample strongly descends.

Figure 4.9 shows the temperature dependence of the electrical conductivity σ of all compacted In:CoSb$_3$ samples. All specimens show a decrease of the electrical conductivity with increasing temperature. Furthermore it is observed that the electrical conductivity σ is by trend increasing with the amount of indium in the skutterudite material and is highest for the sample with $x = 0.15$, reaching about $950 \, S \, cm^{-1}$ at 350 K and lowest for In$_{0.05}$Co$_4$Sb$_{12}$ with about $200 \, S \, cm^{-1}$ at 550 K. For the composition with $x = 0.2$ the electrical conductivity decreases again and drops about 15% in comparison to the In$_{0.15}$Co$_4$Sb$_{12}$ specimen. The sample with $x = 0.05$ possesses a minimum of σ at 550 K and is therefore analog to the behavior shown in the $S(T)$ diagram.

The thermal conductivity κ as a function of temperature of the short-term sintered In:CoSb$_3$ samples can be seen in figure 4.9. The addition of indium leads to a dramatic reduction of the thermal conductivity in comparison to binary CoSb$_3$ skutterudite, which possesses a value of $11 \, W \, m^{-1} \, K^{-1}$ at room temperature [134]. The thermal resistivity increases with the amount of indium in the skutterudite material beginning from $x = 0.05$ to 0.2. It is notable that a significant suppression of the thermal conductivity is already obtained with an indium addition of $x = 0.1$, with a value of about $3 \, W \, m^{-1} \, K^{-1}$ at 500 K. The lowest value for the total thermal conductivity
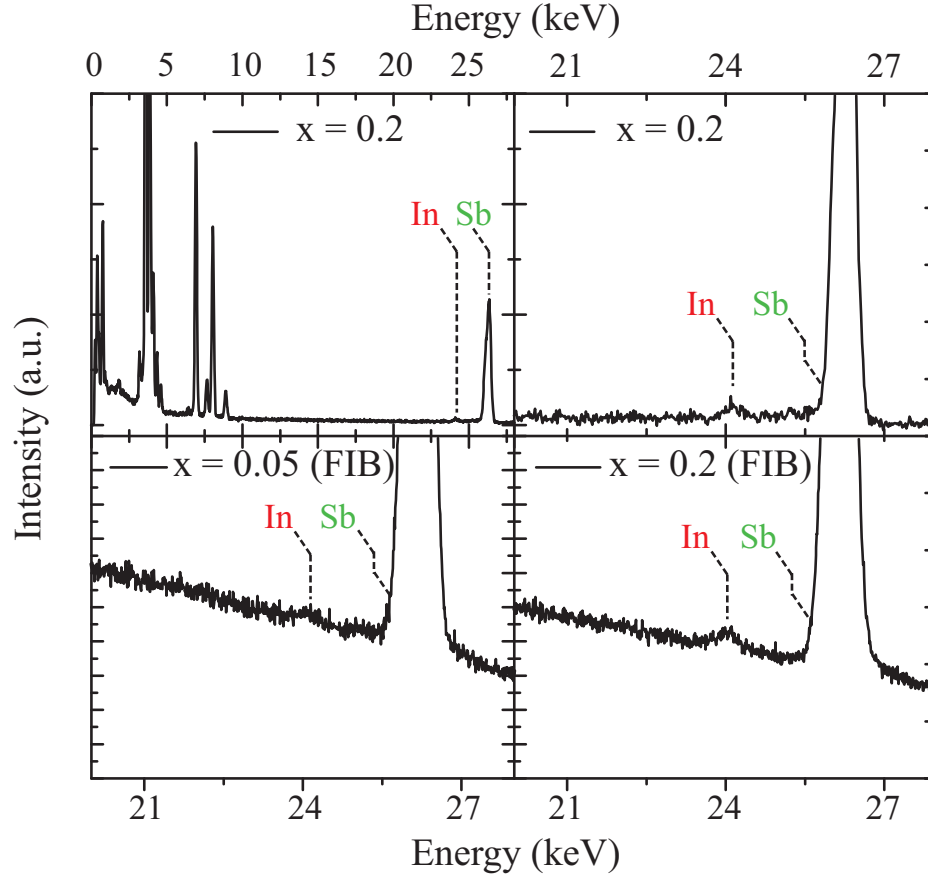
Figure 4.6: *EDX measurement of the skutterudite as-cast material. The measurement was carried out at a phase-pure region to exclude signals of impurity phases. Diagrams (a) and (b) show a TEM-EDX measurement of finely ground skutterudite powder with a composition of $In_{0.2}Co_4Sb_{12}$ with a different energy range ((a) full range, (b) region of interest). The diagrams (c) and (d) are TEM-EDX measurement of a FIB lamellae with varying indium concentration ($In_xCo_4Sb_{12}$). The signals and the corresponding elements of the particular elements are denoted within the diagram (antimony and indium).*
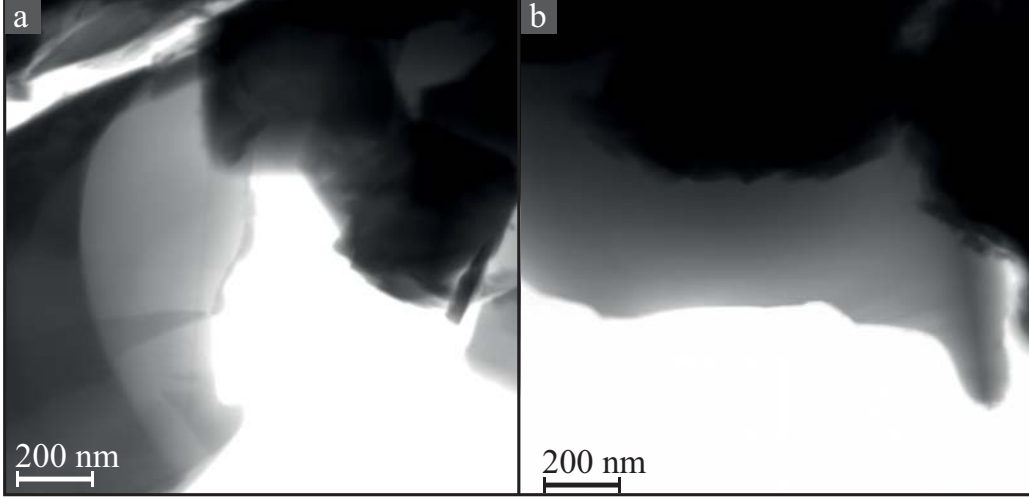
Figure 4.7: *TEM Images of indium filled skutterudites with different filling fraction of indium (ground material). The images (a) and (b) show both* $In_{0.2}Co_4Sb_{12}$ *as-cast material prepared by different synthesis parameters (details can be found in [133]) and latter is termed as "quenched" in this work.*

is obtained with highest indium addition ($x = 0.2$), however in this case, the contribution of the electronic part of the thermal conductivity has to be considered (see sec.4.2.3). The $In_{0.05}Co_4Sb_{12}$ sample exhibits a flattening starting from about $500\,\mathrm{K}$ followed by an increase of thermal conductivity above $550\,\mathrm{K}$, which coincides with its characteristics of the temperature dependent Seebeck coefficient S and electrical conductivity σ data.

Hall measurements of the compacted samples were carried out at $270\,\mathrm{K}$ and are denoted in table 4.1. The table 4.1 shows that the effective charge carrier density n_H, the Hall mobility μ_H and the corresponding electrical conductivity σ at this temperature. The data shows that with ascending indium fraction of the skutterudite material the effective charge carrier density beginning from $n_H = 1.5 \times 10^{19}\,\mathrm{cm}^{-3}$ for $x = 0.05$ up to a value of $n_H = 9.1 \times 10^{19}\,\mathrm{cm}^{-3}$ with $x = 0.2$ is steadily increasing. The Hall mobility μ_H of the skutterudite samples is inversely proportional and consequently highest for an indium fraction with $x = 0.05$ $\mu_H = 245\,\mathrm{cm^2\,V^{-1}\,s^{-1}}$ and lowest for $x = 0.2$ with a Hall mobility of $\mu_H = 81\,\mathrm{cm^2\,V^{-1}\,s^{-1}}$. As already denoted in the temperature dependent σ measurement the $In_{0.2}Co_4Sb_{12}$ material does not have the highest σ value, but is lower than the $In_{0.15}Co_4Sb_{12}$
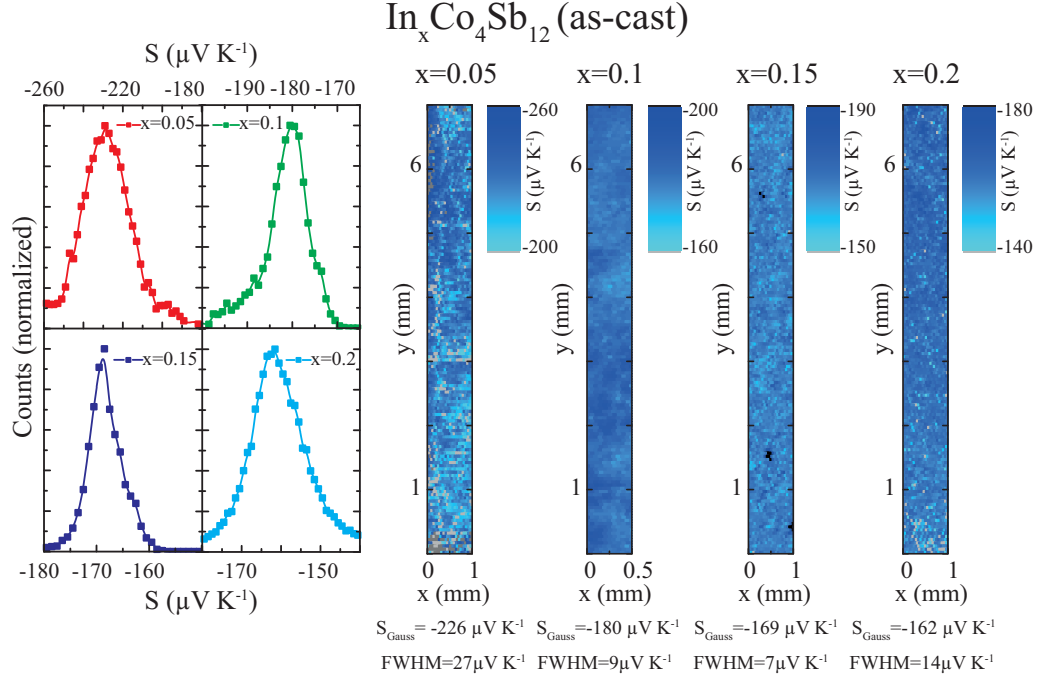
Figure 4.8: *Diagram of the local Seebeck coefficient $S(x, y)$ measurements of the as-cast $In_x Co_4 Sb_{12}$ skutterudite material (with $x = 0.05, 0.1, 0.15$ and 0.2), prepared by induction melting and subsequent annealing. The left figure shows the distribution of the Seebeck coefficient values along the particular skutterudite material (histogram). The right illustration shows the local Seebeck coefficient data in x and y direction of the particular skutterudite material. The full width half maximum (FWHM) values are denoted below as well as the maximum S values, which were obtained by a Gaussian fit of the histogram data points.*

specimen. This means that the further reduction of the Hall mobility in the sample with $x = 0.2$ may not be completely attributed to the effective charge carrier density, as this is continuously increasing with the amount of indium.

The calculated temperature dependent thermoelectric figure of merit ZT for compacted In:CoSb$_3$ material is shown in figure 4.9. It is observed that the sample with $x = 0.05$ has the lowest ZT of all, having a maximum $ZT_{max} = 0.3$ at $550\,\mathrm{K}$. Highest $ZT_{max} = 0.78$ at $675\,\mathrm{K}$ of all In:CoSb$_3$ specimens is obtained for the compacted $In_{0.15}Co_4Sb_{12}$ material due to a higher electrical conductivity and a moderate Seebeck coefficient in comparison to

	$n_{\mathrm{H}}(10^{19}\,\mathrm{cm}^{-3})$	$\mu_{\mathrm{H}}(\mathrm{cm}^2\,\mathrm{V}^{-1}\,\mathrm{s}^{-1})$	$\sigma(\mathrm{S}\,\mathrm{cm}^{-1})$
In$_{0.05}$Co$_4$Sb$_{12}$			
x=0.05	1.5	235	575
x=0.1	5.2	125	1034
x=0.15	7.7	113	1380
x=0.2	9.1	81	1175

Table 4.1: *Results from Hall and electrical conductivity measurements of the compacted* In$_x$Co$_4$Sb$_{12}$ *material with* x =0.05, 0.1, 0.15 *and* 0.2 *at* 270 K *showing the effective charge carrier density* n_{H}, *the Hall mobility* μ_{H} *and the electrical conductivity* σ, *respectively.*

the In$_{0.2}$Co$_4$Sb$_{12}$ sample. However all samples apart from the short-term sintered sample with lowest indium fraction ($x = 0.05$) show a considerable ZT in the range from 450 K to 700 K beginning from $ZT = 0.5$ to value of about $ZT = 0.8$. The errors in the measurement is based on the correspondent measurement accuracy, which is assumed as follows: $\Delta S = 2\,\mu\mathrm{V}\,\mathrm{K}^{-1}$, $\Delta\sigma = 2\,\mathrm{S}\,\mathrm{cm}^{-1}$, $\Delta T = 0.2\,\mathrm{K}$ and $\Delta\kappa = 0.2\,\mathrm{W}\,\mathrm{m}^{-1}\,\mathrm{K}^{-1}$.

Neutron powder diffraction measurements of the In:CoSb$_3$ Skutterudite material

The neutron powder diffraction data of In$_{0.05}$Co$_4$Sb$_{12}$ and In$_{0.2}$Co$_4$Sb$_{12}$ was recorded at four different temperatures (12 K, 50 K, 150 K and 300 K). The pattern of the powder diffraction measurement can be seen in figure 4.10, figure 4.11 and the Rietveld refinement results are shown in table 4.2 and furthermore in figure 4.12.

The powder diffraction data (see fig.4.10) shows that both specimens exhibit high crystallinity with an almost pure skutterudite phase. Secondary phases are visible for the low indium filled sample (CoSb$_2$) and high filled sample (Sb, InSb) however the fraction is below 1% and do not show any additional reflections at higher orders in the diffraction pattern. For the evaluation of the data the FULLPROF program was used (see e.g. [135, 136] and references therein), which handles time-of-flight neutron powder diffraction data in the J. Hodges formulation. In this formulation the peak shape function is a convolution of a pseudo-Voigt function with a pair of back-to-back exponen-
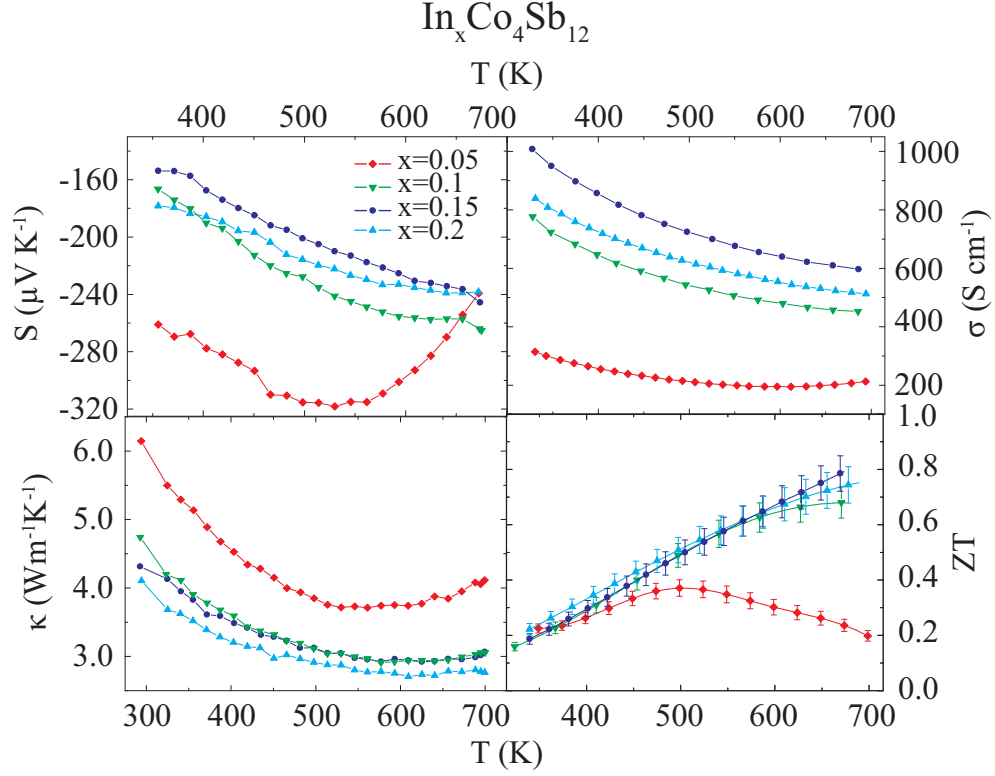
Figure 4.9: *Temperature dependent thermoelectric properties of short-term sintered* $In_xCo_4Sb_{12}$ *skutterudite specimens with* $x = 0.05, 0.1, 0.15$ *and* 0.2. *The diagrams show the Seebeck coefficient S (top left), the electrical conductivity* σ *(top right), thermal conductivity* κ *(bottom left) and the dimensionless figure of merit ZT (bottom right) as a function of temperature in the range of* $350\,K$ *to* $700\,K$. *The error is considered to be around* 8% *and is based on a calculation of errors of the particular measuring instruments:* $\Delta S = 2\,\mu V\,K^{-1}$, $\Delta\sigma = 2\,S\,cm^{-1}$, $\Delta T = 0.2\,K$, $\Delta\kappa = 0.2\,W\,m^{-1}\,K^{-1}$.

tials (see details in the FULLPROF TOF manual)[2]. The evaluation of the temperature dependent data was started by refining the background parameters (6-coefficient polynomial function), the zero shift, the scale factor, the absorption correction parameters, the cell parameters of $CoSb_3$, the parameters of the peak shape function, the fractional coordinates of the antimony

---

[2]The parameter NPROF=10 was set in the evaluation.

atom in CoSb$_3$, the occupation of Sb, Co and In (depending on its multiplicity and the maximum starting composition)[3] and the thermal parameters of Sb, Co and In. This was first applied to the data, which was recorded at the lowest temperature (here 12 K). The evaluation of data recorded at higher temperatures was done stepwise, i.e. the results from the previous measurement (i.e. data recorded at lower T) were taken as a basis for the next evaluation.

The results in figure 4.12 show that the lattice parameter a of the skutterudite phase increases with ascending temperature, which expresses the relative thermal expansion[4] of the skutterudite crystal and with regard to the absolute value it describes the filling fraction in the skutterudite host lattice by indium (the higher the lattice parameter the more indium is inserted in the crystal). The refined positions of the antimony atom are almost identical for both specimens and the positions do not change significantly as a function of temperature. The Oftedal relation [61] is almost fulfilled and the specimens possess all values little below Sb$_y$+Sb$_z$=0.5, where Sb$_y$ is the y position and the Sb$_z$ the z position of the antimony in the skutterudite crystal, respectively. These values are frequently found in other filled skutterudites [138]. The refined occupancies show that in both specimens the particular $2a$ positions are not fully occupied and below the starting composition and as a consequence indicate that the indium did not fully dissolve in the skutterudite phase. Most notably this is the case for the In$_{0.05}$Co$_4$Sb$_{12}$ specimen, which possesses an occupancy of around 1 at% instead of a value of 5 at% (the starting composition).

The thermal parameters[5] of Co and Sb are significantly increasing with temperature. This behavior is seen in both specimens, with almost identical values. The thermal parameter B$_{iso}$ of the $2a$ position is also shown in figure 4.12. In the evaluation of the lowest filled skutterudite sample a distinct value of the thermal parameter at the $2a$ position was not quantifiable, i.e. the uncertainty was much higher than the refined value. However the high

---

[3]The indium starting composition in the synthesis was set to the particular occupancy of indium in the $2a$ position in CoSb$_3$.

[4]This thermal expansion only denote the expansion of the lattice distances and can be different to the thermal expansion determined by a dilatometer (see e.g. [137]).

[5]The thermal parameter in this thesis refers to the B$_{iso}$ and U$_{iso}$, respectively. The B$_{iso}$ is the thermal parameter in the units [Å^2] which is refined in the program FULLPROF. The (isotropic) atomic displacement parameter (ADP) has the same units and can be derived from the B$_{iso}$ by multiplication of a factor (U$_{iso}$=B$_{iso}$/($8\pi^2$)) [139].

	$In_{0.05}Co_4Sb_{12}$	$In_{0.2}Co_4Sb_{12}$
R_P (%)	2.90	2.96
R_{WP} (%)	2.57	2.61
R_{exp} (%)	1.29	1.31
χ^2	3.96	3.97
a (Å)	9.04185(1)	9.04816(1)
$U_{iso}(In)$ (Å^2)	0	0.016(3)
$U_{iso}(Co)$ (Å^2)	0.0038(1)	0.0040(1)
$U_{iso}(Sb)$ (Å^2)	0.00561(4)	0.00566(4)
$y(Sb)$	0.33495(5)	0.33517(6)
$z(Sb)$	0.15781(4)	0.15789(5)
Occ.(In) (%)	1	13
$\alpha_{150K-300K}$ (10^{-6} K^{-1})	8.3	8.4

Table 4.2: *Results from the Rietveld refinement of the time-of-flight neutron powder diffraction measurements (*$In_{0.05}Co_4Sb_{12}$* and *$In_{0.2}Co_4Sb_{12}$*) at room temperature - the R-factors are taken from the measurement at the lowest temperature. The occupancy of Co, Sb and In was refined for the* 12 K *data and subsequently fixed for the refinement of the remaining data set (the data recorded at* 50 K, 150 K *and* 300 K*). The calculation of the R-factors can be seen in the FULLPROF manual [140, p.44]. The data was evaluated by the FULLPROF program.* $\alpha_{150K-300K}$ *is the linear thermal expansion evaluated from the lattice parameter at* 150 K *and* 300 K, *respectively, after [141]. The uncertainty is denoted as follows: e.g.* 0.33495(5) = 0.33495 ± 0.00005.

filled skutterudite sample shows a dramatic increase of the thermal parameter at the 2a position in the skutterudite crystal, which represents a verifiable thermal motion of the indium atom at the 2a position.

4.2.3   Discussion

Indium filled skutterudites show potential thermoelectric properties between 300 K to 700 K. It is clearly observable that the addition of indium increases the thermoelectric efficiency (i.e. ZT) of the CoSb$_3$ material, from about $ZT_{max} = 0.35$ at 500 K for the $In_{0.05}Co_4Sb_{12}$ skutterudite sample up
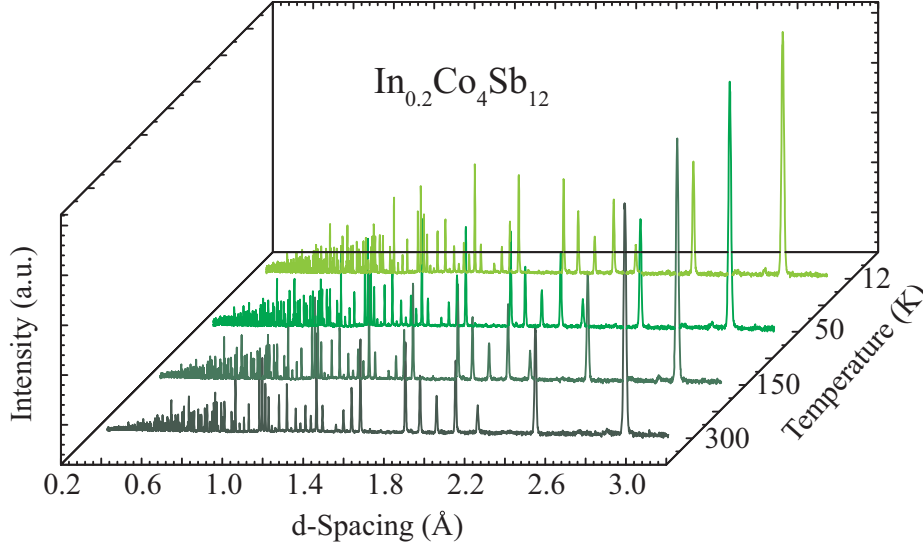
Figure 4.10: *Time-of-flight neutron powder diffraction data of the* In$_{0.2}$Co$_4$Sb$_{12}$ *specimen as a function of d-spacing in [Å] at different temperatures* 12 K, 50 K, 150 K *and* 300 K.

to $ZT_{max} = 0.75$ at 700 K for the skutterudite specimen with high indium fraction (In$_{0.2}$Co$_4$Sb$_{12}$).

For the In$_{0.2}$Co$_4$Sb$_{12}$ skutterudite composition 20% of the interstitial voids should be occupied.[6] Much higher additions of indium in the skutterudite material are to date not reported yet, because it is empirically revealed that a filling fraction limit far below the total number of void lattice sites in the skutterudite crystal exists, which is in the case for indium in CoSb$_3$ about 22% [117]. Higher indium filling fractions favor the formation of impurity phases, like InSb and leads to a highly inhomogenous material.

The Synthesis of indium filled skutterudites is very sensitive and can result in a macroscopic variation of the Seebeck coefficient across the synthesized as-cast material. This is mainly caused by formation of stable secondary phases and low portions of the constituents, which complicates a homogeneous distribution of $S(x, y)$. Furthermore the low solubility limit of about

---

[6]When it is assumed that indium occupies exclusively the 2a void lattice site.
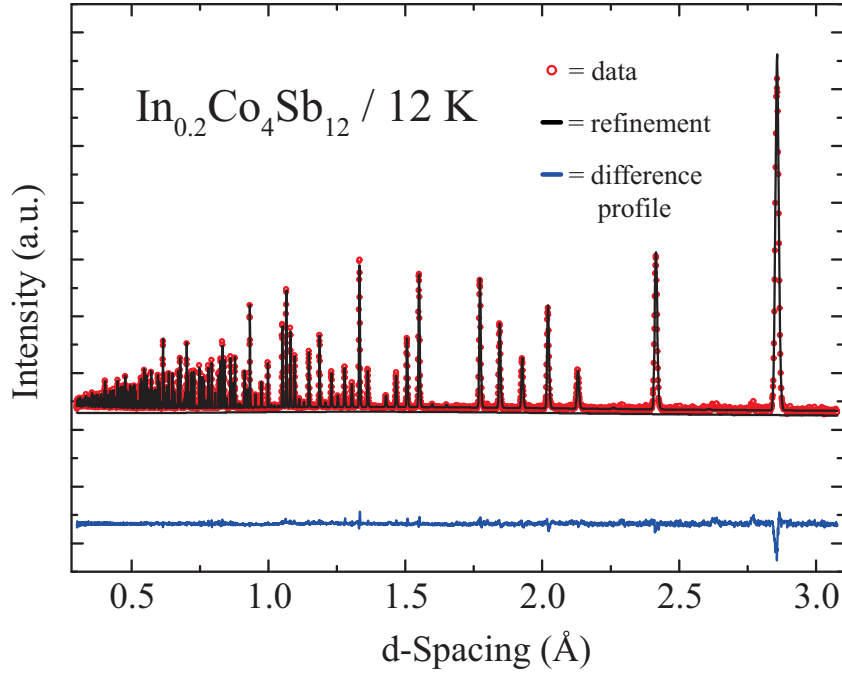
Figure 4.11: *Data and Rietveld refinement of the time-of-flight neutron pow-der diffraction data of* $In_{0.2}Co_4Sb_{12}$ *at* $12\,K$. *The difference profile is shown below the data points (blue solid line).*

1.36 at% indium[7] in the skutterudite phase can lead to local accumulation of indium and hence a formation of impurity phases, which on the other side lead to a considerable reduction of the effective filling fraction in the whole skutterudite material. As a consequence it was necessary to obtain an almost homogenous material out of the synthesis and to avoid severe gradients or macroscopic inhomogeneities of the Seebeck coefficient across the examined material, which could lead to a distortion of the measurement results.

PXRD and SEM analysis showed that except for the sample with highest indium filling fraction no impurity phases were detected. The $In_{0.2}Co_4Sb_{12}$ specimen showed a small amount of secondary phases, so that it can be spec-

---

[7]In [117] the reportes filling fraction limit is reported to be 22% of all available $2a$ Wyckoff positions in the skutterudite unit cell: $1.36\,at\% = 100\,at\% \cdot 0.22/(0.22 + 4 + 12)$
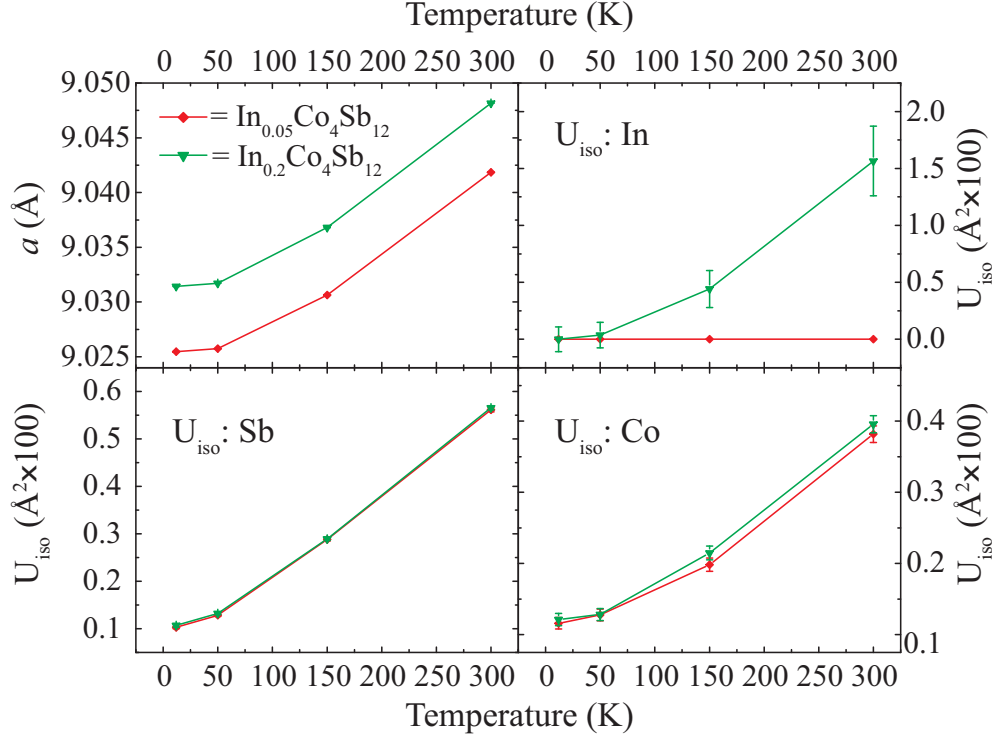
Figure 4.12: *Results from the Rietveld refinement of the temperature dependent time-of-flight neutron powder diffraction measurement of single indium filled skutterudites (*In$_{0.05}$Co$_4$Sb$_{12}$ *and* In$_{0.2}$Co$_4$Sb$_{12}$*). Top left diagram shows the temperature dependent lattice parameter a. Top right, bottom left and bottom right diagrams display the atomic displacement parameter U$_{iso}$ of the particular elements as a function of temperature.*

ulated that a formation of the phases InSb, Sb, and CoSb$_2$ can already start prior to an indium addition of 1.36 at% with this synthesis method.

A local Seebeck coefficient measurement can also be used to identify inhomogeneities and gradients in the material. The Seebeck coefficient is sensitive to different phases (materials possess an unique Seebeck coefficient due to differences in the band structures, doping level, etc.) and to the charge carrier density (see eq.(4.1) and eq.(4.2)) and can therefore visualize the influence of secondary material on the matrix phase and/or macroscopic differences in the doping level. Latter is mostly caused by insufficient intermixture during the
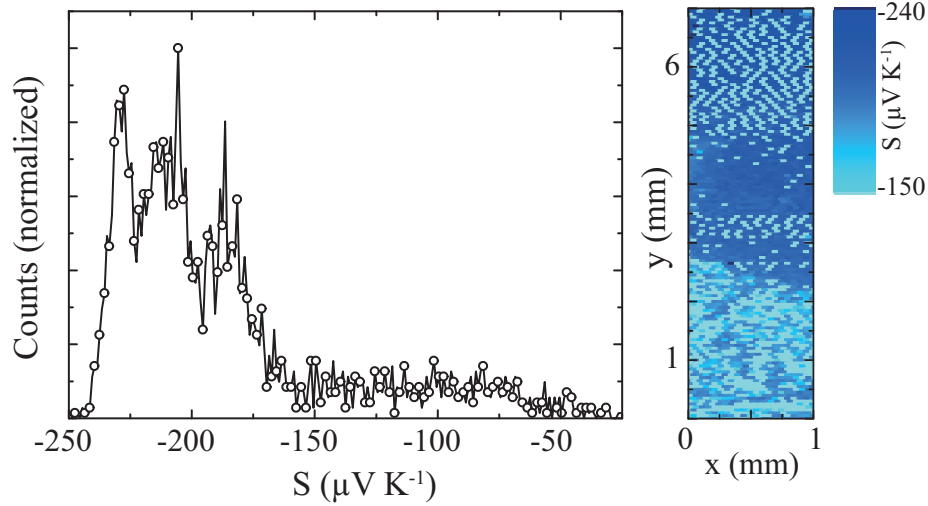
Figure 4.13: *Measurement of the local Seebeck coefficient $S(x,y)$ with the corresponding distribution of the particular Seebeck coefficients (histogram) show macroscopic inhomogeneities due to insufficient mixing within the synthesis process*

melting process. The sensitivity increases for lower doped semiconductors and is in many cases superior to EDX measurements of the doping element concentration (see e.g. [142]). First attempts of the synthesis procedure showed that there can be huge differences in the local Seebeck coefficient values within the skutterudite material, which display different compositional phases and a multiplicity of doping levels (see fig.4.13).[8]

The full width half maximum of the $S(x,y)$ data provides information about the phase homogeneity in the skutterudite material. The distribution of the Seebeck coefficient is narrower for a heavily doped semiconductor[9] than for lower doped samples - preconditioned that no severe macroscopic inhomogeneities are present. The microstructure is also determined by the resolving capacity of the $S(x,y)$-measuring instrument. The step width of the measurement was typically set to 50 µm, and thus resolves structures above this

---

[8]To differentiate between these two effects further complementary measurements have to be carried out (e.g. PXRD, SEM, EDX/WDX).

[9]i.e. n is in the range of $10^{19} \, \mathrm{cm}^{-3}$

value.

All examined In:CoSb$_3$ as-cast samples possess an almost homogeneous distribution of the $S(x, y)$ values across the as-cast ingots (see fig.4.8). The descending absolute Seebeck coefficient values of the as-cast material beginning from In$_{0.05}$Co$_4$Sb$_{12}$ up to In$_{0.2}$Co$_4$Sb$_{12}$ indicates that indium was incorporated to an ascending level from low to high indium addition into the material. However the corresponding short-term compacted skutterudite samples show a slightly different trend (see fig.4.9). In the $S(T)$ data set the highest absolute Seebeck coefficient value was obtained for the In$_{0.15}$Co$_4$Sb$_{12}$ specimen and not for the highest indium filled sample within this series ($x = 0.2$). Two effects should be considered here: (I) It can be an effect of the instruments and the subsequent evaluation. The histograms of the local Seebeck measurements possess a small asymmetry towards lower absolute S values and consequently a Gaussian fit may overestimate the Seebeck coefficient value. Furthermore the temperature dependent Seebeck coefficient measurements provides only S values above room temperature and therefore a direct comparison of the two values is not possible. Moreover the temperature dependent $S(T)$ measurement instrument records an effective Seebeck coefficient, i.e. an integrative value of the compacted sample and as a consequence may be different to a value obtained by a Gaussian fit of a topological Seebeck coefficient measurement $S(x, y)$. (II) It can be speculated that due to the sintering process the Seebeck coefficient has been (apparently) changed. The as-cast material does not exhibit a 100% relative density and features pores and other mechanical irregularities. Especially the local Seebeck coefficient measurement can be influenced by the constitution of the surface (areas of lower density, pores, etc.). However the material may be changed during the sintering process and the compaction can be regarded as an additional heat treatment, which will have an impact on the thermoelectric properties of the skutterudite material (e.g. possible evaporation of secondary phases).

In consideration of these two main points it can be concluded that especially the occurrence of elementary Sb in the as-cast material has an influence of the compacted sample, since its melting temperature is around the applied sintering temperatures. Nevertheless the effect of the elementary Sb may not be too strong, since it can be assumed there is indeed a uncertainty in measurement, due to the pores and the lower density in the as-cast material.

Structural and Thermoelectric Properties: The evaluation from the Rietveld refinement of the PXRD data shows that the incorporation of indium causes an increase of the lattice parameter in comparison to pure $CoSb_3$ having a lattice parameter of $a = 9.0385\,\text{Å}$ at room temperature. When the interstitial void is filled the inserted atom will interact with its surrounding/cage, which consists primarily of pnicogen atoms (here: Sb). According to literature the expansion of the lattice parameter a occurs for all filling elements, and is based on the ion radius and valence state of the particular filler element [65]. A strong variation is e.g. observed with Ce ($Ce_xCo_4Sb_{12}$), where an expansion of a can be around 0.2 % with a filling fraction of 0.6 at%. In the opposite case e.g. Nd (believed to be Nd^{3+}) exhibits a minor change of the lattice parameter a below 0.04% with a relatively high filling fraction of about 1.8 at% [143]. In this work the evaluation of a shows that the indium filling causes an increase of a about 0.08% with a filling fraction around 1.2 at% and therefore appears to have a considerable lower impact on the lattice parameter than the elements with a high positive charge (e.g. Ce^{3+}) and can be compared to those with a lower valence state. In^{3+} in an eight-fold configuration possesses an ion radius of $r_{In} = 1.06\,\text{Å}$ [144], which is relatively small in comparison to other filler elements, such as Ba^{2+} ($r_{Ba} = 1.56\,\text{Å}$ in eight-fold configuration [144]) or Yb^{2+} ($r_{Ba} = 1.28\,\text{Å}$ in eight-fold configuration [144]). Especially the fact that the Gd^{3+} ion is not considered to be a filler element in $CoSb_3$ due to its small ion radius ($r_{Gd} = 1.19\,\text{Å}$ in eight-fold configuration [144]) makes an In^{3+} ion less probable. The experimental radius of In^{1+} in eight-fold configuration, which is assumably much larger than In^{3+}, is not reported in literature. Latter may be a cause of the rarity of such an oxidation state of indium.

The results from the temperature dependent thermoelectric properties measurement (i.e. κ, σ, S) depict a clear trend of the different $In:CoSb_3$ compounds. The thermal conductivity κ, which is a major parameter especially in the material class of the skutterudites, shows a considerable decrease of the thermal conductivity with ascending indium addition. The thermal conductivity κ of pure $CoSb_3$ is about $11\,\text{W}\,\text{m}^{-1}\,\text{K}^{-1}$ at room temperature [134] and is reduced by half with an indium addition of about 0.3 at% ($x = 0.05$) ($In_{0.05}Co_4Sb_{12}$). The thermal resistivity is highest when the reported filling fraction limit for indium is attained, however already lower portions of indium result in a vastly enhanced thermoelectric figure of merit in this intermediate temperature between 350 K and 700 K.

For a more accurate description of the beneficial effect of the increased ther-

mal resistivity in terms of the thermoelectric efficiency ZT, an analysis of the lattice thermal conductivity κ_l is more convenient, because the electronic part is an inevitable contribution of a high electrical conductivity of the bulk material (see section 1.3). The electronic thermal conductivity κ_e is described by the Wiedemann-Franz law which proclaims that the electronic thermal conductivity is proportional to the electric conductivity σ and absolute temperature T, respectively (see eq.(1.23)). The Lorenz number is equal to $L_0 = 2.45 \times 10^{-8}\,\mathrm{V^2\,K^{-2}}$ for a metal. The Lorenz number however overestimates the electronic thermal conductivity of optimized thermoelectric materials in many cases [28]. Therefore a more appropriate calculation of the Lorenz number was applied (see sec.1.4).

Figure 4.14 shows the Lorenz number of the In:CoSb$_3$ specimens, based on calculations of a single parabolic band model. All values are lower than $2.45 \times 10^{-8}\,\mathrm{V^2\,K^{-2}}$ which means that an additional fraction is attributed to the lattice thermal conductivity of the skutterudite samples (see fig.4.15), in comparison to a constant Lorenz number of $2.45 \times 10^{-8}\,\mathrm{V^2\,K^{-2}}$. For the lowest indium filled CoSb$_3$ sample an increase of the Lorenz number at about $600\,\mathrm{K}$ is visible and can be most probably attributed to bipolar thermodiffusion. This behavior is similarly observed in the corresponding temperature dependent thermal conductivity data, because the bipolar thermodiffusion transfers heat due to a recombination of the electron hole pairs particularly at the cold end. This effect is dominantly observed for small gap semiconductors, such as InSb or CoSb$_3$ [28].

The lattice thermal conductivity data shows that the lowest value of all In:CoSb$_3$ samples reaches about $2.1\,\mathrm{W\,m^{-1}\,K^{-1}}$ at $700\,\mathrm{K}$, which is attained for the highest indium filled sample with a composition of In$_{0.2}$Co$_4$Sb$_{12}$. This supports the fact that the impurity phases in the highest filled skutterudite sample contributes positively to an increased thermal resistivity. The In$_{0.15}$Co$_4$Sb$_{12}$ however has a comparably low thermal conductivity exhibiting no visible secondary phases in the PXRD data. It appears to be that already at a lower indium filling fraction a low thermal conductivity is attained, even without exhibiting precipitates of secondary material. The lowest doped sample clearly shows an onset of bipolar thermodiffusion already at $500\,\mathrm{K}$. This furthermore suggests that the In$_{0.05}$Co$_4$Sb$_{12}$ possesses a relatively low doping concentration and can be regarded as an intrinsic semiconductor, which is revealed by the low effective charge carrier density n_H in comparison to all other indium filled skutterudites.

In addition it is of interest, which of the scattering mechanisms in this inter-

mediate temperature range is prevailing for the indium filled skutterudites. For this reason the lattice thermal conductivity was calculated after the Debye model and consequently adjusted to the corresponding κ_l data of the specimens. For the calculation of κ_l the Debye approximation (see section 1.4) was applied.

The values from Debye temperature ($\Theta = 287\,\text{K}$) and sound velocity ($v = 2700\,\text{m s}^{-1}$), as well as the starting parameters for A, B and C were taken from literature[10] [105, 145]. For indium a resonant frequency is not known and as a result a typical value in the THz region for ω_0 was taken. Furthermore due to the observations in the SEM and the synthesis method the grain size was assumed to be relatively high.[11] These values however were not changed, thus in case the behavior of the indium atom is not comparable with other typical filler elements, the ω_0 value may be regarded as a systematical error within this approximation.

The data from temperature dependent Seebeck coefficient measurements of the In:CoSb$_3$ samples show mainly two different characteristics. (I) For low filling fraction of indium the sample exhibits a behavior of a more intrinsic semiconductor, reflected in the high absolute Seebeck coefficient and the starting decrease at about $500\,\text{K}$. First can be explained by the low effective charge carrier density, which directly contributes to a high Seebeck coefficient S. This trend can be best described by the Mott-relation ("metallic formula for S") [146–148]:

$$S = \frac{\pi^2 k_B^2 T}{3e} \left. \frac{d(\ln \sigma(E))}{dE} \right|_{E=E_F} \tag{4.1}$$

and

$$\sigma = \int_{-\infty}^{+\infty} dE \left(-\frac{\partial N}{\partial E} \right) \cdot \sigma(E) \quad , \tag{4.2}$$

where $\sigma(E)$ is the electrical conductivity determined as a function of the Fermi energy E_F, k_B is the Boltzmann constant, e is the electronic charge and T the absolute temperature. As can be seen in the eq.(4.1) and eq.(4.2) maximum S can be achieved when a large asymmetry in the density of states N within a small energy range (typically few $k_B T$) above and below the Fermi

---

[10]A is in the range of $10^{-41}\,\text{s}^3$, B in the range of $10^{18}\,\text{s K}^{-1}$ and C in the range of $10^{-33}\,\text{s}^{-3}$.

[11]ω_0 was set to $10 \times 10^{13}\,\text{Hz}$ and L was set to $30\,\mu\text{m}$ (L did not significantly contribute to the calculated lattice thermal conductivity value).
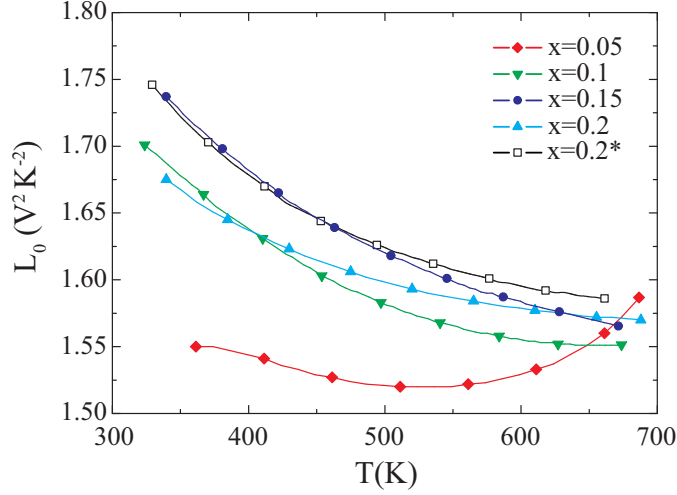
Figure 4.14: *Calculated temperature dependent Lorenz number L_0 (see sec.1.4) of the $In_xCo_4Sb_{12}$ specimens, with different concentrations of the filler element indium ($x = 0.05, 0.1, 0.15, 0, 2$ and 0.2^*). The $x = 0.2^*$ sample indicates a $In_{0.2}Co_4Sb_{12}$ specimen, which was prepared with a changed synthesis parameter (quenched after the annealing period) [133].*

level persists. High asymmetry is achieved for a low charge carrier density at the Fermi level, or a strongly non-parabolic band.

The decrease of the Seebeck coefficient for the $In_{0.05}Co_4Sb_{12}$ skutterudite material at higher temperatures are caused by the thermally excited intrinsic charge carriers, which then increase the effective charge carrier density leading to a decline of the absolute Seebeck coefficient. This effect is common for pure or low doped semiconductors, because the excited charge carriers are typically unimportant for highly doped semiconductors.

(II) The other, higher filled In:CoSb₃ specimens have a substantial different trend in the Seebeck coefficient data. All samples show a considerable lower absolute Seebeck coefficient in comparison to the low indium filled material. The increase of the charge carriers is due to the amount of indium in the skutterudite material and has a detrimental effect on the Seebeck coefficient. Furthermore no intrinsic excitation is visible and the absolute Seebeck coefficient increases almost linearly with temperature for all higher indium filled samples (i.e. $x =0.01$, 0.15 and 0.2).
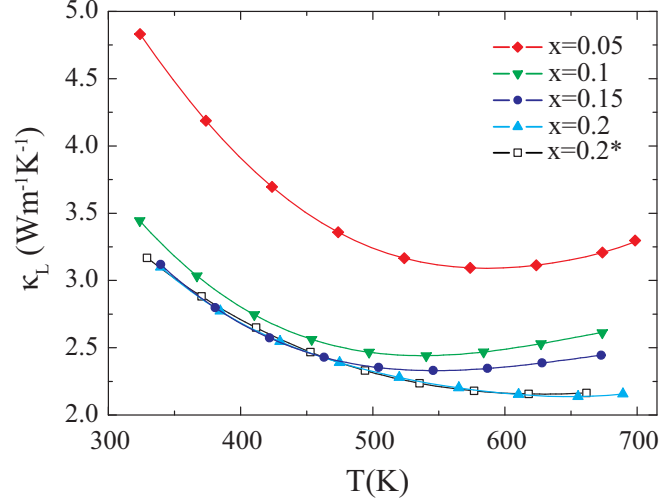
Figure 4.15: *Calculated lattice thermal conductivity κ_l as a function of temperature (see sec.1.4) of the $In_xCo_4Sb_{12}$ specimens, with different concentrations of the filler element indium ($x = 0.05, 0.1, 0.15, 0.2$ and 0.2^*). The $x = 0.2^*$ sample indicates a $In_{0.2}Co_4Sb_{12}$ specimen, which was prepared with a changed synthesis parameter (quenched after the annealing period) [133].*

The electrical conductivity of the samples supports the fact that the low indium filled sample exhibits an intrinsic semiconductor behavior and the other skutterudite specimens show, due to higher filling fractions of indium, a degenerate semiconductor behavior, i.e. these perform rather like metals. Latter can be seen in the vastly enhance electrical conductivity, which is considerably higher than in the case for the $In_{0.05}Co_4Sb_{12}$ sample. Notable is that highest electrical conductivity is achieved for the $In_{0.15}Co_4Sb_{12}$ specimen and not for the sample with highest indium content ($x = 0.2$). This can be contributed to the impurity phases, which do not possess high electrical conductivities (e.g. $CoSb_2$) and moreover enhance the scattering of charge carriers at the phase boundaries and hence lowers the charge carrier mobility. Hall measurements at room temperature were carried out to obtain the effective mobility of the charge carriers μ_H and the effective charge carrier density n_H. The effective charge carrier densities of the $In:CoSb_3$ specimens are in the range of $10^{19}\,cm^{-3}$, which is typical for highly doped thermoelectric materi-
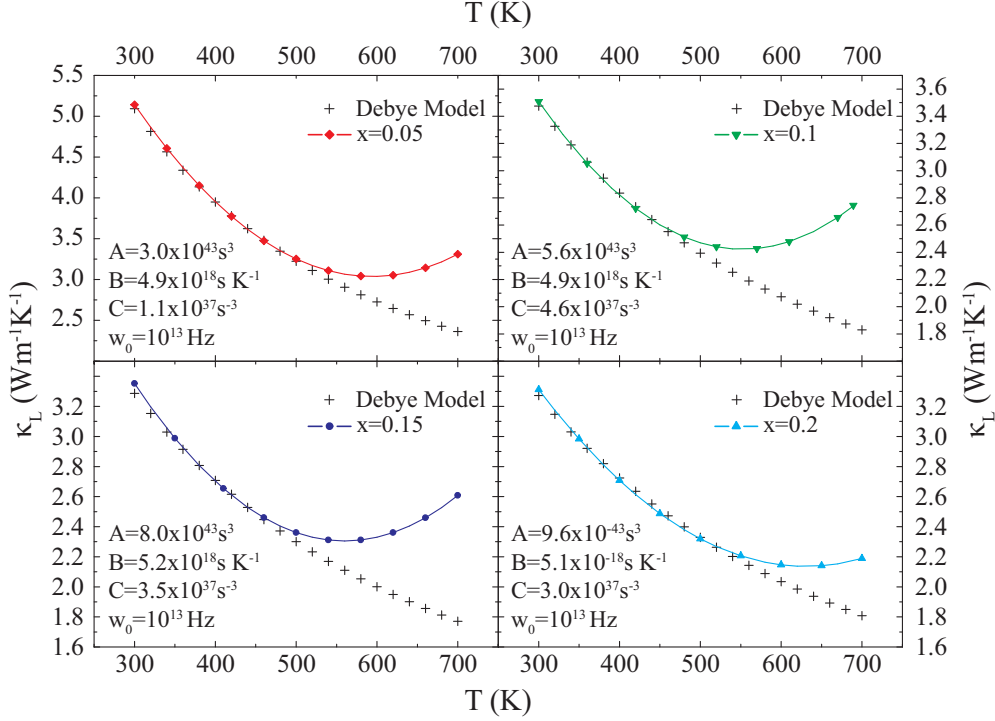
Figure 4.16: *Calculated lattice thermal conductivity according to the Debye model (see sec.1.4 and the lattice thermal conductivity from fig.4.15 of the In$_x$Co$_4$Sb$_{12}$ specimens, with different concentrations of the filler element indium ($x = 0.05, 0.1, 0.15$ and 0.2)). The calculated values (plus symbols) from the Debye model are shown as a function of temperature. The parameter values of A,B,C and ω_0 for the calculation are denoted in the particular diagram. The parameter L was set to $30\,\mu m$, however did not significantly contribute to the calculated κ_l value.*

als and is increasing with ascending filling fraction of indium. The measured carrier concentration together with the indium filling fraction provide information about the degree of ionization of the filling atom. The effective charge carrier density ascends with the addition of indium, though not linear, which means that the level of ionization changes with the addition of indium or that only a fractional part of the starting composition occupies the void lattice site in the skutterudite crystal. This non-linearity may denote a (I) change of the starting composition within the synthesis/annealing process,

(II) formation of secondary phases or (III) a decline of the effective charge contribution to the skutterudite material [143]. Point (III) is in other words a steady decrease of the ionization level of the indium atoms, which cannot be discussed in detail, because the minority charge carrier density for the low filled skutterudite samples is not known and may be of high importance in this context. Nevertheless is should be mentioned that the compensation of additional valence electrons in the skutterudite phase (which are provided by the filler element) can lead to a strong change in the electronic structure within the crystal structure [149]. In that case it can be assumed that the electronic compensation of these additional charge carriers can only take place to a certain extent and hence could lead to decrease of the effective oxidation state of the indium ion at higher filling fractions near the solubility limit.

The trend of the effective charge carrier mobility supplements the behavior of $n(x)$ as a function of the indium fraction x, which decreases with the addition of indium. This can be explained by an enhanced scattering of the electrons by the filler elements, which act as ionized impurities. For high filling fraction (e.g. $In_{0.2}Co_4Sb_{12}$) scattering at boundaries can set in, which causes another reduction of the electron mobility. It is reported that the effective mass can be dependent on the effective charge carrier density itself [143]. This may also contribute to the vast reduction of the charge carrier mobility of the indium filled skutterudite material.

A Pisarenko plot (a $S - n$ diagram) can provide this information about the effective mass m^* of a material system.[12] To obtain the effective mass a single parabolic band approximation was applied, which is valid to a certain extent for skutterudites [150, 151]. In further scientific papers it was shown that with ascending effective charge carrier density of the skutterudite compounds a higher effective mass can be obtained [143] and references therein. For this reason the approximation by a single parabolic band is only valid to some extent.[13]

---

[12]The effective mass m^* is here defined as 'carrier effective mass', which is identical with the 'density of states effective mass' in the isotropic case for a parabolic electronic band structure where only acoustic phonon scattering is considered.

[13]A more detailed consideration of the electronic band structure of the skutterudite material will surely improve the accuracy of the lattice thermal conductivity calculation.
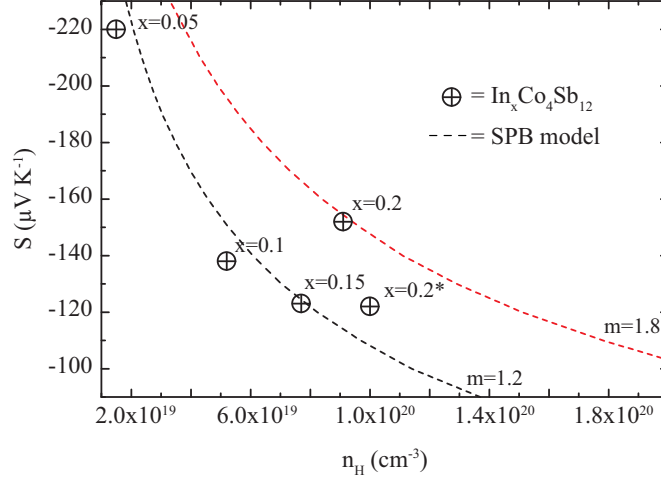
Figure 4.17: *Calculated Seebeck coefficient S according to a single parabolic band model (see sec.1.4) as a function of the charge carrier density n_H and a constant mass of the charge carrier m. The particular data points within the diagram are the effective charge carrier densities n_H from Hall measurements at room temperature vs. the correspondent Seebeck coefficient of the material (derived from the local Seebeck coefficient data). The specimens are indium filled skutterudites with different concentrations of the filler element indium (exact starting compositions are denoted in the diagram).*

Secondary Phases in In:CoSb₃ Skutterudites: Secondary phases in the form of small precipitates/nanocomposites can under certain circumstances enhance the thermoelectric properties of a material (e.g. [23, 55]). In a report about melt-spun indium and cerium added CoSb₃ material it is assumed that nanosized precipitates of InSb can suppress the thermal conductivity, without deteriorating much the electrical conductivity of the bulk material [118]. On the other side, many impurity phases seem to be not suitable as these are bad electrical conductors, have low Seebeck coefficients or possess a completely different crystal structure[14]. Furthermore secondary phases can induce circular currents due to a different Seebeck coefficient in comparison to the matrix material, which as a result can reduce the thermo-

---

[14]Latter can lead to a degradation of the mechanical properties due to weak chemical/physical bonding between the matrix and the precipitates.
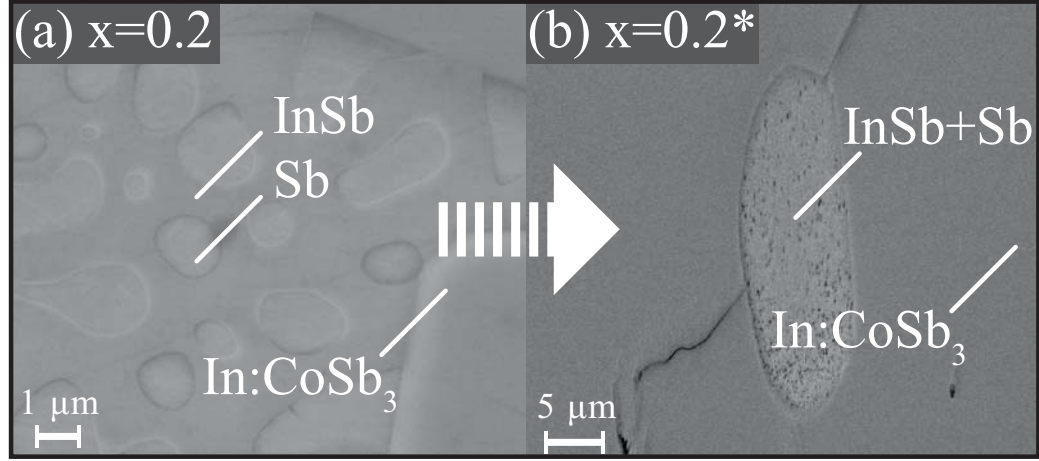
Figure 4.18: *SEM images of two skutterudite specimens with an identical composition showing secondary phases (InSb, Sb) at the grain boundaries. The $In_{0.2}Co_4Sb_{12}$ specimens differ in its annealing process parameters. The specimen which is shown left was synthesized as described in (see sec.4.2.1) and the right image shows a specimen, which was additionally quenched after the annealing period [133].*

electric efficiency of the bulk material drastically. The InSb phase however possesses a high Seebeck coefficient and can exhibit a relatively good electrical conductivity (e.g. see [152–154]).

In this work mostly no secondary phases were observed in the $In:CoSb_3$ skutterudite material by SEM and PXRD. Only for the skutterudite material with highest indium content ($x = 0.2$) impurity phases were detectable. Due to the long annealing duration and the steady cooling step the precipitates exhibit large grain sizes up to several hundreds of micrometer. Furthermore they feature a substructure, where EDX analysis suggests that it consists of spherical Sb isles surrounded by an InSb phase.

This structure of the secondary phases can be massively influenced by the cooling step in the annealing period, which is in detail discussed in [133]. Within this work the $In_{0.2}Co_4Sb_{12}$ material was additionally quenched in the end of the annealing period. The result showed a totally different structure of these secondary phases, without changing the matrix microstructure at all. The precipitates formed an elliptical shape and possess a diffuse intermixture of elementary Sb and InSb, which was revealed by EDX measurements.

It is notable that In together with Sb forms only one binary intermetallic phase, which is the compound InSb. This intermetallic phase has a melting temperature of $798\,\mathrm{K}$ and is liquid during the applied annealing temperature of $1073\,\mathrm{K}$.

The thermoelectric properties of this material show that the quenched sample ($\mathrm{In_{0.2}Co_4Sb_{12}^{qu}}$) has an enhanced thermoelectric figure of merit up to 15%, which is mainly based on the vast improvement of the electrical conductivity of the material (around 30%) and a concomitant reduction of the lattice thermal conductivity (around 8%).[15] The decrease of the lattice thermal conductivity may be contributed to the different substructure of the secondary phases. However due to the higher electrical conductivity and the decrease of the Seebeck coefficient of around 8% in comparison to the slow cooled sample, it can be speculated whether the quenched sample has a higher incorporated fraction of In in the skutterudite matrix and therefore cause (I) a lower Seebeck coefficient value, (II) lower lattice thermal conductivity and (III) higher electrical conductivity. Hall measurements of the quenched sample reveal that the effective charge carrier density is around 12% higher than the original sample ($n=1.03 \times 10^{20}\,\mathrm{cm^{-3}}$).

This fact suggests that more indium was dissolved in the skutterudite matrix and hence increased the effective charge carrier density (and the thermoelectric properties in general), based on a small modification of the synthesis route. The main improvement of the electrical conductivity is however caused by a dramatic change of the effective mobility of the charge carriers (around 20%) in the quenched specimen. Consequently the scattering of electrons was significantly decreased. Another notable observation in these two skutterudite specimens was that considerable amounts of Sb appeared in form of InSb and elementary Sb. Due to stoichiometric reasons[16] it is suggested that Sb is displaced from its lattice site in the skutterudite crystal or is thermodynamically favored to exist as secondary phases in the skutterudite material. Elementary Co was never found in the PXRD or SEM evaluation.

Indium as a filler element: It is of recent interest, why indium is vastly enhancing the thermoelectric properties of the skutterudite material [64, 118].

---

[15]The superscript "qu" in the chemical formula denotes the modified synthesis route to make a better distinction of the "original" sample with the identical composition.

[16]i.e. no excess addition of Sb in the synthesis procedure of the $\mathrm{In_{0.2}Co_4Sb_{12}}$ material
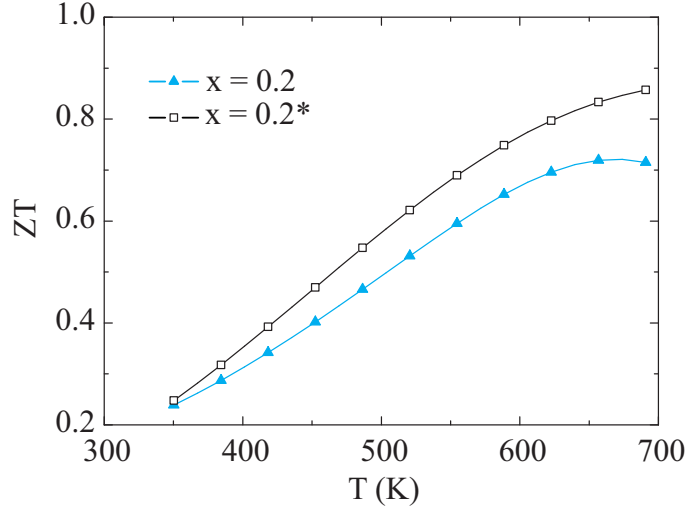
Figure 4.19: *Figure of merit as a function of temperature of two skutterudite specimens with an identical composition. The* $In_{0.2}Co_4Sb_{12}$ *specimens differ in its annealing process parameters. The specimen which is denoted as "x = 0.2" was synthesized as described in (see sec.4.2.1) and the other specimen, denoted as "x = 0.2*", was additionally quenched after the annealing period [133].*

The first intuitive suggestion was that it may occupy the $2a$ Wyckoff position and acts like any other filler element like several lanthanides [117]. This is quite reasonable, because the effect of indium is quite alike to that of a typical filler element, i.e. dramatic reduction of the thermal resistivity, increase of the electrical conductivity and only a small deterioration of the Seebeck coefficient. All these properties are already achieved with a small fraction of indium (max. $1.36\,at\%$), which is equivalent to many other filler elements with a rather low oxidation state ($< 3^+$). However there seem to be only a small number of elements with low electronegativity which can be contributed to that kind of bonding between the Sb atoms (which surround the void lattice site and form the cage) and the filler element. For this reason an empirical rule was reported, under which it is suggested that the electronegativity of the filler element subtracted with the electronegativity of antimony should not be as low as 0.80 [64], otherwise the element will not properly

bond and therefore does not occupy the void lattice site permanently. It was furthermore stated that thallium, which is chemically related to indium, indeed does not obey this rule of thumb, however it is still doubted whether indium can enter the void or not [64, 118].

Several investigations were made to gain more knowledge about the localization of indium in the skutterudite bulk material. (I) SEM together with EDX analysis of the skutterudite as-cast material suggest that the indium concentration within the skutterudite material is about $1\,at\%$ and ranges therefore in the right order of magnitude. However it has to be considered that the EDX detector has an error of measurement, which is equal or greater than the measured concentration of indium. Additionally in the EDX analysis the line intensities of Sb and In overlap and cause for this reason a superposition of both. These obstacles do not occur for the analysis by TEM/EDX. In this case sample preparation by simply grinding the material or by a focused ion beam allows to investigate only on the skutterudite matrix at higher energies. Latter is necessary to obtain the Kα indium signal, which is well separated from any other intensity lines. The diagram 4.6 shows that an indium signal is observable and therefore clearly reveals the appearance of indium in the skutterudite phase. Even for low indium concentrations, such like the $In_{0.05}Co_4Sb_{12}$ material a distinct signal can be observed [133].

(II) A chemical perspective on this issue may suggest that indium can occupy all three lattice positions within the skutterudite structure, namely the $2a$ filler position, the lattice site of Sb ($24g$ Wyckoff position) and the lattice site of Co ($8c$ Wyckoff position) in the skutterudite crystal.

In perovskites, which have a crystal structure comparable to the skutterudites, the most important factor in substitution reaction is the effective ionic size of the host and substituent ions and the closer the sizes the greater is the likelihood of successful substitution. For so-called $A_2BB'O_6$ perovskites the B cation can be a rare earth or indium[17] (see e.g. [156, 157]). Consequently the indium can substitute a (small) rare earth ion at an electronpositive lattice site. This scenario may be transferred to the skutterudite crystal structure, where the $2a$ position is mainly accessible by rare earth elements.

Despite the case indium would occupy the position of Sb then a significant decrease of the lattice parameter would be expected since the ion radii of antimony and indium are very different (Sb^{-1}, In^{+1}, In^{+3}). The oxidation state of In^{+1} is found in indium containing chalcogenides and would form

---

[17]from [155]

an electron deficient skutterudite compound and possibly cause a descending lattice parameter of the skutterudite crystal structure. An oxidation state of In^{+3} would worsen the charge imbalance and further decrease the lattice parameter due to its small ionic radius.[18] The lattice parameter of the examined skutterudite material however shows an increase of the lattice parameter with increasing filling fraction of indium. For highest filling fraction in this series ($x = 0.2$) a saturation of the lattice expansion is visible (see fig.4.1). This finding gives rise to the assumption that indium may not occupy the Sb lattice site, or only to a minor extent.

Whether indium does occupy the 24g Wyckoff position at all may be answered in a more empirical way. In the SEM/EDX and PXRD analysis especially fractions of elementary antimony and InSb can be observed for indium filled skutterudite material near the reported fraction limit. Based on the fact that stoichiometric portions of the elementary constituents were used to synthesize the skutterudite material, it is a consequence that every Sb atom, which is forming secondary phases or is abundant as pure element, is missing in the skutterudite material. Thus it is possible that indium displaces the Sb atoms in the crystal structure, when the skutterudite compound is near the reported filling fraction. A formation of secondary phases with antimony would be a consequence out of the substitution by indium.

The Co site in the skutterudite crystal structure is an electron positive lattice site and therefore can be in principle occupied by a cation, such as the In^{+1} or In^{+3} ion. Latter would substitute the cobalt isoelectronically. The effective ionic radius of Co^{+3} in a six-fold coordination (low spin) is reported to be $r_{Co^{3+}} = 0.685\,\text{Å}$ [144] and is therefore around 35% smaller than the In^{+3} ion. This fact naturally decreases the likeliness of a successful substitution. Furthermore no elementary Co was found in PXRD or SEM/EDX evaluation since stoichiometric portions of the elements was used for the synthesis. Another fact is the doping effect of In in the skutterudite material - which means that an oxidation state of In^{3+} can be almost excluded. However from a chemical point of view a substitution of the cobalt ion by indium with an oxidation state of 1+ seems to be improbable but not impossible.

(III) The thermoelectric properties reveal that indium suppresses the lattice thermal conductivity, increases the electrical conductivity and exhibit a neg-

---

[18]For In^{+3} an ion radius of $r_{In^{+3}} = 1.06\,\text{Å}$ is reported [144]. There are only few reports about the ionic radius of Sb^{-1} (e.g. [158] reporting $r_{Sb^{-1}} = 2.95\,\text{Å}$). For this reason the atomic radius of Sb can be a more helpful reference point: $r_{Sb} = 1.45\,\text{Å}$

ative Seebeck coefficient. Reports on Sn filled skutterudite compounds show that in the case of filling ($2a$) and doping ($24g$) the material can either possess a n-type or a p-type behavior, which is reflected by a negative and a positive Seebeck coefficient, which were measured in different studies [159] and references therein. Due to the negative Seebeck coefficient of all In:CoSb₃ samples in this work a substitution of Sb by In can be excluded as main mechanism in the skutterudite crystal structure. The occupation of the $2a$ void position is clearly favorable since it would cause a negative Seebeck coefficient and an increased electrical conductivity due to an electron charge transfer to the skutterudite matrix. Furthermore the reduction of the thermal conductivity is more pronounced for indium filled skutterudites than for doped CoSb₃ material and it can be doubted that a substitution by indium would cause such a high depression of the κ_l[19]. In addition a substitution of Co would be most probably not cause a dramatic change of the thermal conductivity, since the Sb atoms are mainly responsible for the thermal transport within the skutterudite material [65, p.167].

Structural investigations by neutron powder diffraction were carried out to identify the "rattling" mode of indium filled skutterudites. This is made possible by determination of the thermal parameter of indium as a function of the temperature. Filled skutterudites show mostly a significant increase of the thermal parameter, which is due to the activation of the rattling mode at higher temperatures [65].

We carried out studies on single indium filled skutterudites and double cerium and indium filled skutterudites to determine whether this high thermal parameter at the Wyckoff $2a$ position is visible in indium single and double filled skutterudites (for double filled skutterudite see sec.4.3.2). Neutron powder diffraction was preferred over x-ray diffraction because it has by far a better contrast[20], which is based on the fact that Sb and In possess very close scattering lengths for x-rays.

The results from Rietveld refinement show that for the low and high indium filled sample an occupation of the $2a$ lattice site is verifiable. The particular occupancy is in both cases lower than the starting composition, which leads

---

[19]In the samples InSb as precipitates were absent, or in case of the high indium filled skutterudites big grains of InSb occurred (several $100\,\mu m$).

[20]i.e. the differences of the bound coherent neutron scattering length in the particular elements - especially In ($4.065\,fm$), Sb ($5.57\,fm$), Co ($2.49\,fm$) and Ce ($4.84\,fm$). The data is extracted from the internal table of the FULLPROF program, which is identical with the data from the National Institute of Standards and Technology [160].

to the assumption that indium was lost during the synthesis or annealing period. The lattice parameter is also a further indication for the occupancy of the void lattice site and it is increasing with ascending portion of indium.[21] This observation is in agreement with the results from the PXRD evaluation. The maximum lattice parameter for indium filled skutterudites is $9.0568\,\text{Å}$ and is therefore significantly higher than the lattice parameter found in our specimens [117]. When the data in [117] is compared to the results from the neutron powder diffraction measurements a composition of around $In_{0.15}Co_4Sb_{12}$ can be assumed. However it should be noted that the preparation method for these indium filled skutterudite is different and may have an influence on the lattice parameter of the skutterudite material.[22] The lattice parameter as a function of temperature furthermore exhibits a low increase in the range of approx. $\approx 12\,\text{K}$ to $50\,\text{K}$ and becomes steeper for higher temperatures ($\approx 50\,\text{K}$ to $300\,\text{K}$). This behavior is comparable to many other filled skutterudites within this temperature range of $10\,\text{K}$ to $300\,\text{K}$ [161].

The thermal parameter of Sb and Co as a function of temperature are both increasing with ascending temperature. In the case of Sb the values of both specimens are almost identical, the thermal parameter of Co is by trend slightly higher, however within the accuracy of measurement. In the work of Iversen et al. [162] the room temperature values for both thermal parameter are in the same range and is closest to the value of $La_{0.1}Co_4Sb_{12}$ having an U_{iso} value of $U_{iso}(Co) = 0.0039\,\text{Å}^2$ and $U_{iso}(Sb) = 0.0055\,\text{Å}^2$, respectively. The values of $In_{0.2}Co_4Sb_{12}$ in this work are $U_{iso}(Co) = 0.0040\,\text{Å}^2$ and $U_{iso}(Sb) = 0.0056\,\text{Å}^2$.

The thermal parameter of indium at the $2a$ position is very different for both specimens, which is caused by the absolute fraction of indium in the skutterudite phase. In the low indium filled sample a thermal parameter could not be refined (i.e. $U_{iso}(In) = 0\,\text{Å}^2$) even though the material possesses an excellent crystallinity. The refined occupancy and expansion of the lattice parameter of this sample are however too low to determine the thermal parameter of the indium atom. For this reason it can be almost compared to an unfilled skutterudite material and thus demonstrates that for almost pure $CoSb_3$ material no ADP at the $2a$ position can be determined.

This is different for the high indium filled sample, where a steep increase

---

[21]This is based on the fact, that in case of substitution ($8c$, $24g$) a decrease of the lattice parameter is expected.

[22]Further quantitative measurements have to be carried out to clarify the exact chemical composition of the examined specimens.

in the thermal parameter is visible. This denotes a weak bonding of the indium atom at the lattice site and/or a great disorder of the filler elements within the skutterudite phase. In comparison to other filled skutterudites the atomic displacement parameter is best compared with the $Sm_{0.1}Co_4Sb_{12}$ and therefore possess a relatively low ADP. The reported value from He et al. [117] is significantly higher than the evaluated value in this work. In many filled skutterudites the ADP does significantly change with the filling fraction of the impurity atom (see therefore the before mentioned work from Iverson et al. [162]), however Sales et al. suggested that Tl, which is chemically related to In, can change its ADP with respect to the filling fraction within the skutterudite structure [138]. In this work however it is reported that the ADP is increasing with increasing filling fraction - the concentrations of Tl are (much) larger than the examined indium specimens in this work. Nevertheless it is of high interest, why these ADPs of He et al. and the evaluated ADPs are very different (more than doubled).[23]

The occupancy parameter of the $2a$ lattice site of the low indium filled sample and moreover the strong increase of the ADP as a function of temperature in the high indium filled sample strongly indicates that the indium atom is a *regular* filler element in the skutterudite material, such as many species.

4.3   Ce,In:CoSb$_3$ and Gd,In:CoSb$_3$ Skutterudites

Skutterudites offer a vast structural flexibility and can incorporate several different impurity atoms in the void lattice site of the skutterudite crystal structure [62]. For an enhancement of the thermoelectric properties (i.e. $\kappa(T)$, $\sigma(T)$, $S(T)$) in the intermediate temperature range (i.e. 300 K to 700 K) the substitution of the void with - at least - two elements, especially from the lanthanides series, have shown great improvements in the thermal resistivity and electrical conductivity leading to a reasonable increase of ZT. The combinatorial possibilities of double filled skutterudites are of course extensive and for this reason a selection of two distinct lanthanides was made: (I) cerium and (II) gadolinium.

---

[23]He et al. [117]: $In_{0.2}Co_4Sb_{12}$:U_{iso}(In)= 0.036 Å^2; In this work: $In_{0.2}Co_4Sb_{12}$:U_{iso}(In)= 0.015 Å^2 - here the starting compositions are stated, which may be different to the actual chemical composition of the specimens.

(I) Already single cerium filled skutterudites have shown good figure of merit (around $ZT = 0.7$ at $700\,\mathrm{K}$) in past investigations [65, 163]. Cerium exhibits a valence state of 3^+ and therefore donates a significant amount of charge carriers to the skutterudite structure. The electronic configuration of Ce comprises two $4f$ and two $6s$ valence electrons, in which the $5p$ and the $5s$ electrons in most cases act as good shielding of the $4f$ electrons [164]. For this reason a Ce^{3+} oxidation state provides one $4f$ electron together with two electrons of the $6s$ shell. Cerium was one of the first filling elements in the skutterudite structure leading to a high ZT in the intermediate temperature range and possesses a filling fraction limit of 10% in the $CoSb_3$ material (i.e. $Ce_{0.1}Co_4Sb_{12}$) [71].

(II) Gadolinium filled skutterudites are fabricated by a high-pressure synthesis in the case of RuP_3 [85] and by a conventional melting/annealing process in the case of $Co_xFe_{x-1}Sb_3$ and $IrSb_3$ [165, 166]. Gd filled $CoSb_3$ is doubted to exist due to the low ion radii of Gd^{3+} and therefore no filling fraction is known for Gd in $CoSb_3$ [167]. However charge compensation can enable the skutterudite structure to incorporate the Gd ion into the void lattice site, because it presumably lowers the formation enthalpy of the Gd filled skutterudites [165, 167]. Expansion of the lattice parameter may on the other side cause an increase of the void volume and consequently deteriorate the bonding between the Gd ion and the Sb atoms and destabilize the Gd filled skutterudite phase. For the gadolinium and indium filled $CoSb_3$ material it is of interest, how secondary phases may influence the thermoelectric properties and whether the electronic and structural impact by indium may change the capacity to incorporate the Gd ion or not.

The investigation of Gd,In:$CoSb_3$ and Ce,In:$CoSb_3$ material will focus on the thermoelectric properties, structural changes in relation to the filling fraction and the secondary phases, which are possibly formed at low filling fractions.

4.3.1   Experimental Details

Polycrystalline samples of $Ce_xIn_xCo_4Sb_{12}$ and $Gd_xIn_xCo_4Sb_{12}$ (both with $x = 0.05, 0.1, 0.15$ and 0.2) samples were synthesized by induction melting followed by thermal annealing - comparable to the synthesis route of the In:$CoSb_3$ material (see sec.4.2.1). Stoichiometric quantities of indium, cobalt, antimony and the particular rare earth (gadolinium, cerium), were melted for $1.5\,\mathrm{h}$ at $1423\,\mathrm{K}$ in an evacuated silica tube, which was subsequently quenched to avoid peritectic decomposition. In order to obtain a homogenized as-cast

material, the silica tube was additionally rocked and manually tilted during the induction melting process.

In the case of the $Ce_{0.1}In_{0.1}Co_4Sb_{12}$ sample the starting ingredients were elementary Sb, In and a Ce-Co alloy. Latter was a precursor material, which was prepared by stoichiometric amounts of cerium and cobalt. The material was alloyed by an arc melter in inert atmosphere. The Ce-Co alloy was then put together with stoichiometric amounts of antimony and indium. The subsequent steps are identical to that of the other Ln,In:CoSb₃ specimens.

The purity of all used elements was at least 99.99% or higher. Annealing was carried out in a programmable furnace at 973 K for 168 h with a heating rate of $2\,\mathrm{K\,min^{-1}}$ from room temperature to 973 K. Sample preparation, short-term compaction and (temperature dependent) measurements were carried out similarly to the In:CoSb₃ material (see therefore sec.4.2.1).

4.3.2   Results

This section comprises the results from phase and structural analysis of the as-cast material (Ln,In:CoSb₃ with Ln=Ce,Gd) and in the following the Seebeck coefficient, electrical and thermal conductivity data as a function of temperature. Hall measurements and neutron powder diffraction data of the skutterudite material are presented in the end of this section.

The powder X-ray diffraction patterns of the Ce,In:CoSb₃ (see fig.4.20) and Gd,In:CoSb₃ as-cast material (see fig.4.22) show in most cases a highly crystalline skutterudite phase after the induction melting and the annealing process - except for the $Ce_{0.1}In_{0.1}Co_4Sb_{12}$ specimen, where the main phases are elementary Sb and CoSb₂ and only a minor fraction of the skutterudite phase can be detected.[24]

 For lowest addition of cerium and indium ($x = 0.05$) the skutterudite material exhibits no visible secondary phases in the PXRD pattern. This does not apply for higher Ce and In filled samples and as a consequence minor fractions of different phases are observable: InSb, CeSb₂ and Sb. The CeSb₂ unit cell is orthorhombic and belongs to the space group No. 64 (Cmce). It has two unique positions for Sb and Ce. The lattice parameter are after Wang et al. [168] $a = 6.295\,\text{Å}$, $b = 6.124\,\text{Å}$ and $c = 18.21\,\text{Å}$. For details of

---

[24]The $Ce_{0.1}In_{0.1}Co_4Sb_{12}$ material was synthesized by using a Ce,Co alloy and is therefore different from the synthesis route of the other Ce,In:CoSb₃ samples; see details in the experimental section sec.4.3.1.
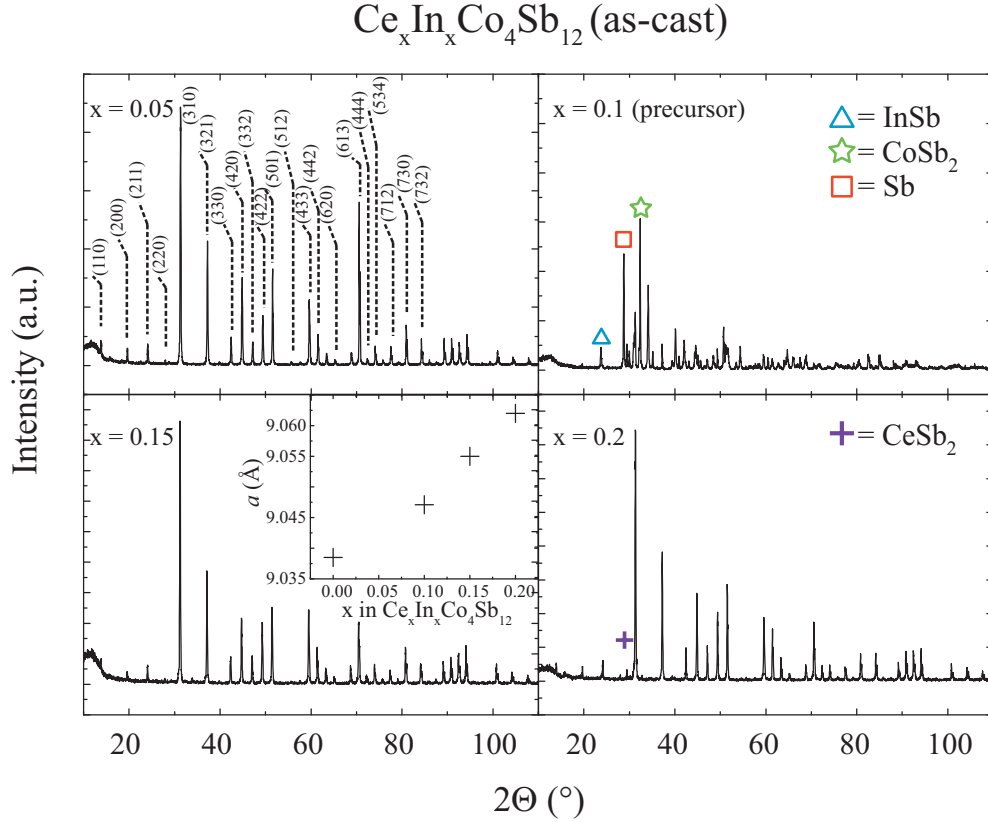
Figure 4.20: *Powder X-ray diffraction patterns of* $Ce_xIn_xCo_4Sb_{12}$ *as-cast material with* $x = 0.05, 0.1, 0.15$ *and* 0.2*, prepared by induction melting at* $1423\,K$ *for* $1.5\,h$ *and subsequent annealing at* $973\,K$ *for* $168\,h$*. In the diffractogram of the powder material with* $x = 0.05$ *the lattice planes of the skutterudite phase are indicated and the inset diagram depicts the corresponding lattice parameter a. In other diffractograms secondary material is indicated by symbols.*

the structural properties of the other impurity phases it is referred to section 4.2.2. The fraction of the secondary phases is only in the region of 1% and several intensities lines (e.g. from $CeSb_2$) do not follow the regular intensity distribution in the PXRD pattern - an indication of a preferred orientation (of growth), or a texture within the powder sample.

As already mentioned, the $Ce_{0.1}In_{0.1}Co_4Sb_{12}$ specimen does not exhibit a skutterudite structure after the preparation step. The material in this stage

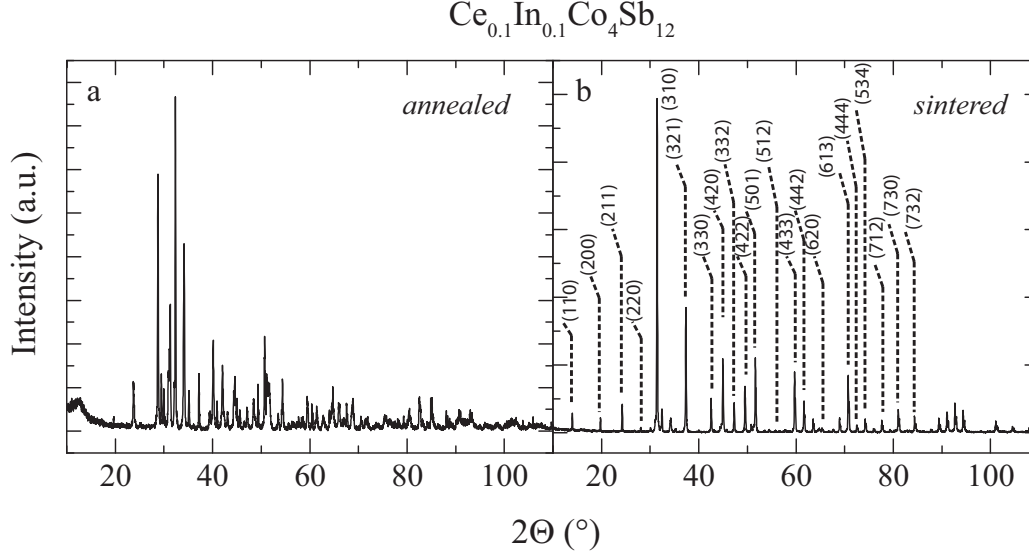$$Ce_{0.1}In_{0.1}Co_4Sb_{12}$$

Figure 4.21: *Powder X-ray diffraction patterns of the $Ce_{0.1}In_{0.1}Co_4Sb_{12}$ material. Left diffractogram (a) shows the annealed powder material and the right diffractogram (b) the powder material of the short-term sintered specimen. The lines in (b) indicate the lattice planes of the skutterudite phase (hkl). For details on the preparation see sec.4.3.1.*

is composed of elementary Sb and the thermodynamically stable intermetallic phase $CoSb_2$. This was changed by short-term compaction of the material. During the short sintering process the skutterudite structure crystallized and is according to the PXRD pattern the predominant phase after the compaction step (see fig.4.21). The determined lattice parameter of the formed skutterudite phase at room temperature is $a = 9.047$ Å.

All gadolinium and indium filled skutterudite specimens show small fractions of secondary phases in the PXRD patterns. The main difference in comparison to Ce,In:CoSb₃ is clearly that $GdSb/GdSb_2$ attribute to the diffraction pattern instead of $CeSb_2$ (partly additional intensity lines from the LaB_6 standard are observable). GdSb has a face-centered cubic crystal cell geometry (Fm3m, No.225, JCPDS No. 15-0832) with a typical lattice parameter of $a = 6.217$ Å. $GdSb_2$ is comparable to $CeSb_2$ and crystallize in the orthorhombic $SmSb_2$ crystal structure with a lattice parameter of $a = 6.157$ Å,

$b = 5.986\,\text{Å}$ and $c = 17.83\,\text{Å}$ [169]. According to the diffraction pattern, GdSb is the predominant phase compared to $GdSb_2$, which may exist only to a low extent in the matrix. The fraction of all secondary phases is low and presumably not significantly higher than 1-2%. However, a quantitative evaluation of the secondary phases in the PXRD pattern may be troublesome due to the low and partly broad intensities together with a possible texturing of the particular phases.

The different concentrations of the filler elements cause changes in the lattice parameter for both series, the $Ce,In{:}CoSb_3$ (sample with $x = 0.1$ was excluded) and the $Gd,InCoSb_3$ samples (see fig.4.20 and fig.4.22). With ascending fractions of Ce and In the lattice parameter increases almost linearly from $a = 9.046\,\text{Å}$ for the $Ce_{0.05}In_{0.05}Co_4Sb_{12}$ specimen up to a value of $a = 9.062\,\text{Å}$ for the $Ce_{0.2}In_{0.2}Co_4Sb_{12}$ specimen. The $Gd,In{:}CoSb_3$ specimens show a nonlinear increase of the lattice parameter and the magnitude of a is as a function of the filler fraction not as high as for the $Ce,In{:}CoSb_3$ samples. Furthermore it is notable that the specimen with lowest Gd and In content does not possess the lowest lattice parameter. However a steady increase of the lattice parameter is observed for higher filling fractions of Gd and In. Investigation with SEM show large grains of the skutterudite phase ($> 100\,\mu\text{m}$) in most of the $Ln,In{:}CoSb_3$ specimens. The as-cast material appears to be dense with a low number of pores in the material. These irregularities increase with ascending concentration of the filler elements and thus more craters, groves and secondary material are visible.

The $Ce,In{:}CoSb_3$ specimen with lowest filling ($x = 0.05$) does not show any visible precipitates in the material. The EDX analysis of the main phase validates the skutterudite phase in terms of the relation of quantity of antimony and cobalt: The measured values are around $23\,\text{at}\%$ for Co, $76\,\text{at}\%$ for Sb and the filler elements have a proportion of less than $1\,\text{at}\%$. It should be noted that the values for the filling elements remain relatively constant, however range within the accuracy of measurement. Highest filling fraction of Ce and In ($x = 0.2$) in this series show a considerable amount of secondary phases. Predominantly InSb, $CeSb_2$ and Sb are found and partly a Sb phase is observed near an InSb phase and vice versa. The grain size of $CeSb_2$ is larger in comparison to the InSb material, however both are in the μm scale. The material with lowest filling of Gd and In ($x = 0.05$) shows already precipitates of $GdSb_2/GdSb$ and Sb in the SEM. These phases cannot be clearly distinguished, because the EDX analysis shows an overbalance of Sb and a phase separation is not clearly visible. The $Gd_{0.1}In_{0.1}Co_4Sb_{12}$ specimen pos-
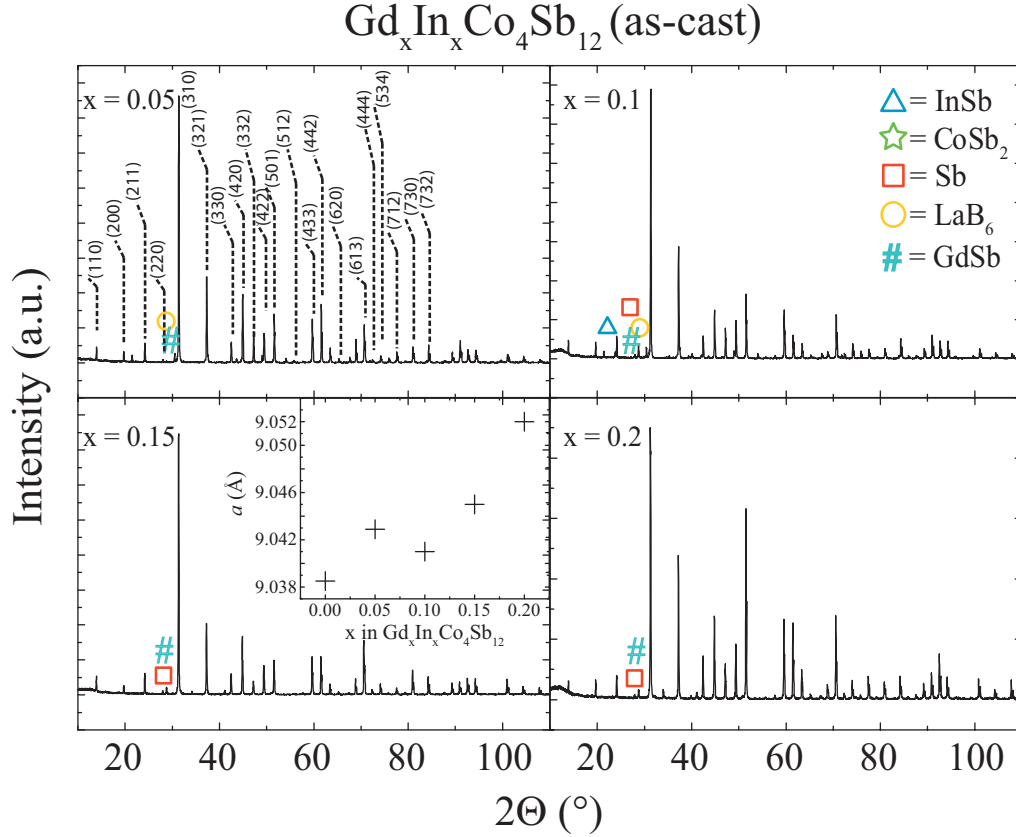
Figure 4.22: *Powder X-ray diffraction patterns of* $Gd_xIn_xCo_4Sb_{12}$ *as-cast material with* $x = 0.05, 0.1, 0.15$ *and* 0.2, *prepared by induction melting at* $1423\,K$ *for* $1.5\,h$ *and subsequent annealing at* $973\,K$ *for* $168\,h$. *In the diffractogram of the powder material with* $x = 0.05$ *the lattice planes of the skutterudite phase are indicated and the inset diagram depicts the corresponding lattice parameter a. In other diffractograms secondary material is indicated by symbols.*

sesses larger fractions of secondary material in comparison to the lower filled sample with additionally detectable amounts of InSb. The shape of the GdSb or GdSb₂ phase is often times rod-shaped. The Sb phase can be elliptical ($x = 0.05$) or for the $Gd_{0.1}In_{0.1}Co_4Sb_{12}$ specimen with a higher concentration of Gd and In the precipitates exhibit sharp edges and is located at the grain boundaries of the skutterudite matrix. The specimens with even higher filling
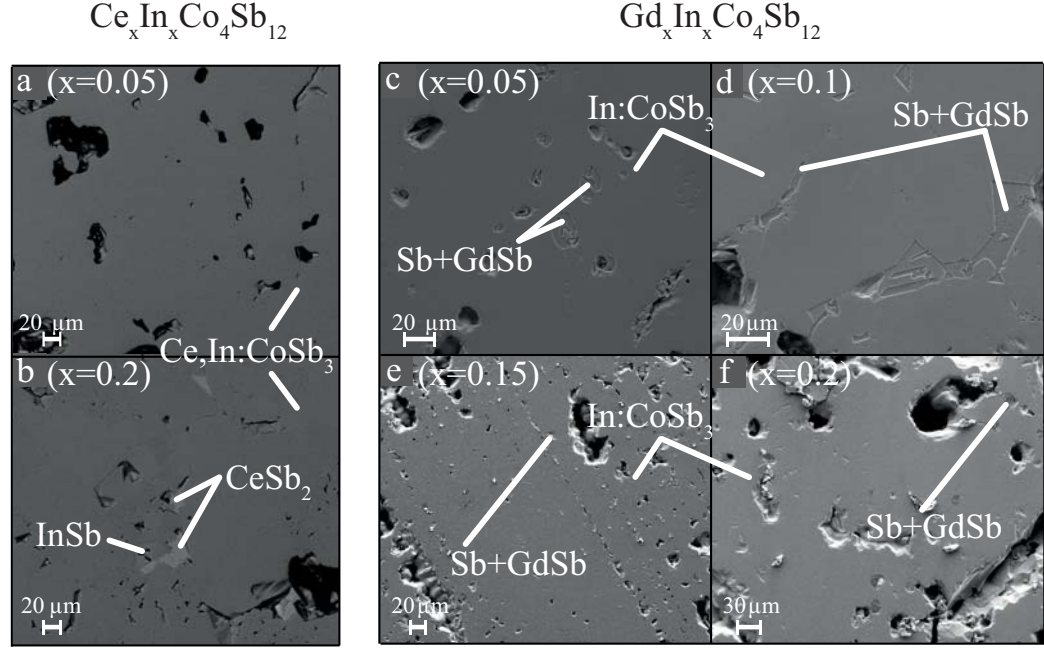
$$Ce_xIn_xCo_4Sb_{12}$$ $$\qquad\qquad Gd_xIn_xCo_4Sb_{12}$$

Figure 4.23: *left: SEM images of as-cast* $Ce_xIn_xCo_4Sb_{12}$ *with* $x = 0.05$ *(a) and* 0.2 *(b) showing Sb, InSb and* $CeSb_2$ *precipitates of surrounding cobalt-antimony based skutterudite domains, when indicated. The* $Ce_xIn_xCo_4Sb_{12}$*; right: SEM images of as-cast* $Gd_xIn_xCo_4Sb_{12}$ *with* $x = 0.05$ *(c),* $x = 0.1$ *(d),* $x = 0.15$ *(e) and* 0.2 *(f) showing Sb, GdSb precipitates of surrounding cobalt-antimony based skutterudite domains. EDX analysis showed fractions of In in the* $CoSb_3$ *material.*

fractions ($x = 0.15$ and 0.2) contain similar secondary phases. However for these samples the microstructure is considerably changed and a high number of irregularities within the matrix occur.

Figure 4.24 shows the macroscopic spatial distribution of the Seebeck coefficient $S(x,y)$ along the sample ingots with $x = 0.05, 0.1, 0.15$ and 0.2 of cerium and indium. A typical area of $7\,\mathrm{mm}$ in length and $1\,\mathrm{mm}$ in width was scanned on a cross-section of the ingot samples. Almost all samples show n-type behavior at room temperature and exhibit a narrow distribution of

S values, which can be seen in the histogram of the PSM-data.[25] Latter indicates that the double filled skutterudites (with lanthanides and indium) exhibit almost homogeneously distributed S values across the particular ingots. The Seebeck coefficients of the Ce,In:CoSb$_3$ as-cast material, which are obtained by a Gaussian fit of the $S(x,y)$ histogram, are $-158\,\mu\text{V}\,\text{K}^{-1}$ ($x = 0.05$), $-0.3\,\mu\text{V}\,\text{K}^{-1}/14\,\mu\text{V}\,\text{K}^{-1}$ ($x = 0.1$), $-113\,\mu\text{V}\,\text{K}^{-1}$ ($x = 0.15$) and $-101\,\mu\text{V}\,\text{K}^{-1}$ ($x = 0.2$), respectively.

For the Gd,In:CoSb$_3$ sample series the absolute Seebeck coefficients are by trend lower (see fig.4.25): $-197\,\mu\text{V}\,\text{K}^{-1}$ for $x = 0.05$, $-170\,\mu\text{V}\,\text{K}^{-1}$ for $x = 0.1$, $-140\,\mu\text{V}\,\text{K}^{-1}$ for $x = 0.15$ and $-138\,\mu\text{V}\,\text{K}^{-1}$ for $x = 0.2$.

Figure 4.26 shows the temperature dependent Seebeck coefficient data from around $300\,\text{K}$ to $700\,\text{K}$ for short-term sintered Ln,In:CoSb$_3$ skutterudite material, which had at least a relative theoretical density of 98%. All samples exhibit n-type behavior, which corresponds to the results from the local Seebeck measurement $S(x,y)$ of the as-cast material.

For the Ce,In:CoSb$_3$ compacted specimens the magnitude of the Seebeck coefficient increases almost linearly with temperature. The Ce,In:CoSb$_3$ samples show that with increasing filling fraction a clear reduction of the absolute value of the Seebeck coefficient occurs, beginning - e.g. at $500\,\text{K}$ - from $-236\,\mu\text{V}\,\text{K}^{-1}$ for $x = 0.05$, $-221\,\mu\text{V}\,\text{K}^{-1}$ for $x = 0.1$, $-151\,\mu\text{V}\,\text{K}^{-1}$ for $x = 0.15$ to $-128\,\mu\text{V}\,\text{K}^{-1}$ for $x = 0.2$. Furthermore figure 4.26 contains the local Seebeck coefficient measurement mean value of the *short-term sintered* samples.[26] The $S(x,y)$ analysis of the samples comprised about 200 measurement points with a relatively high interspace on the surface of the short-term compacted sample and a Gaussian fit was used to determine the room temperature Seebeck coefficient value.

It should be noted that the Ce$_{0.1}$In$_{0.1}$Co$_4$Sb$_{12}$ specimen exhibits a considerably different behavior. As already mentioned the corresponding powder X-ray diffractogram of the as-cast material does not possess the skutterudite phase as the main phase. This is changed after short-term compaction of the material (see fig.4.21), which is also reflected in the markedly different Seebeck coefficients of the as-cast material and the short-term specimen ($-0.3\,\mu\text{V}\,\text{K}^{-1}/14\,\mu\text{V}\,\text{K}^{-1}$ vs. -169$\,\mu\text{V}\,\text{K}^{-1}$).

For the Gd,In:CoSb$_3$ specimens similarities to the Ce,In:CoSb$_3$ and In:CoSb$_3$

---

[25]The Ce$_{0.1}$In$_{0.1}$Co$_4$Sb$_{12}$ material was synthesized by using a Ce,Co alloy (see sec.4.3.1).
[26]For the single indium filled skutterudite samples only as-cast material was measured by the local Seebeck coefficient instrument.
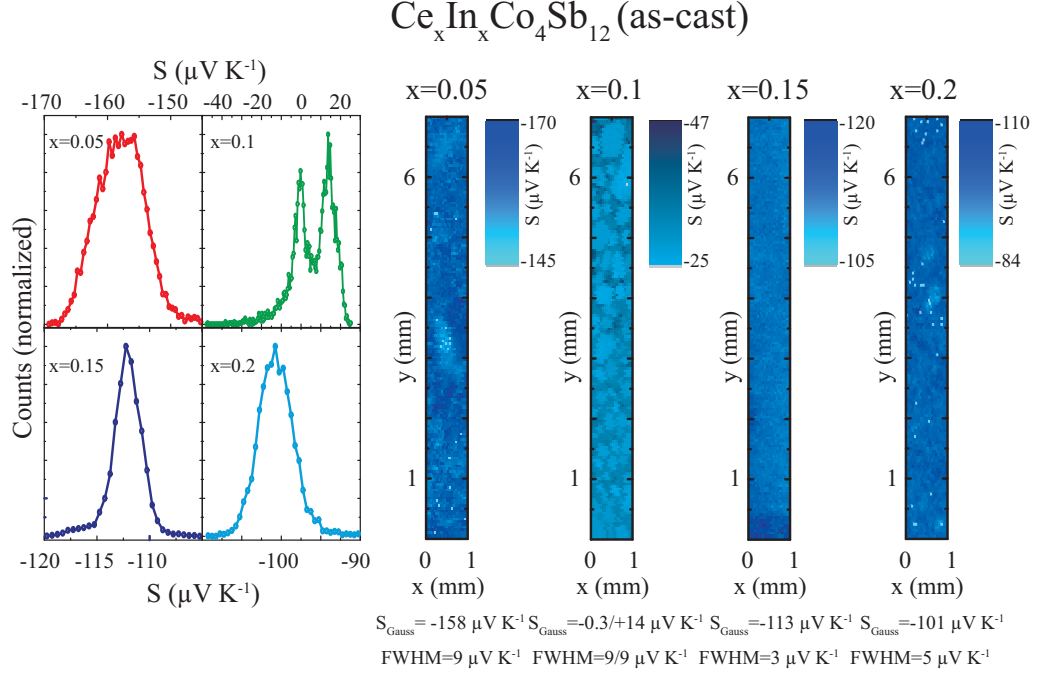
Figure 4.24: *S(x, y) data (cross-sectional area) taken from annealed $Ce_xIn_xCo_4Sb_{12}$ material (x = 0.05, 0.1, 0.15 and 0.2) showing the spatial distribution of the Seebeck coefficient S(x, y) (right) and the corresponding histograms (left). The full width half maximum (FWHM) values are denoted below as well as the maximum S values, which were obtained by a Gaussian fit of the histogram data points.*

samples are identifiable: In addition to the n-type behavior, a decrease of the Seebeck coefficient with increasing filling fraction of gadolinium and indium can be observed - except for the $Gd_{0.1}In_{0.1}Co_4Sb_{12}$ sample. The absolute Seebeck coefficient values at e.g. $500\,K$ are $-208\,\mu V\,K^{-1}$ for $x = 0.05$, $-223\,\mu V\,K^{-1}$ for $x = 0.1$, $-194\,\mu V\,K^{-1}$ for $x = 0.15$ and $-180\,\mu V\,K^{-1}$ for $x = 0.2$. This implies in relation to the $Ce,In:CoSb_3$ specimens that filling with gadolinium and indium has less impact on the magnitude of the Seebeck coefficient than the cerium and indium filled compacted skutterudite samples. Furthermore the temperature characteristic of the $Gd,In:CoSb_3$ Seebeck coefficient values does not change its linear behavior, which is found for almost all compacted $Gd,In:CoSb_3$ specimens - again, except for the $Gd_{0.1}In_{0.1}Co_4Sb_{12}$ sample, which possesses an inflection point at around $600\,K$.
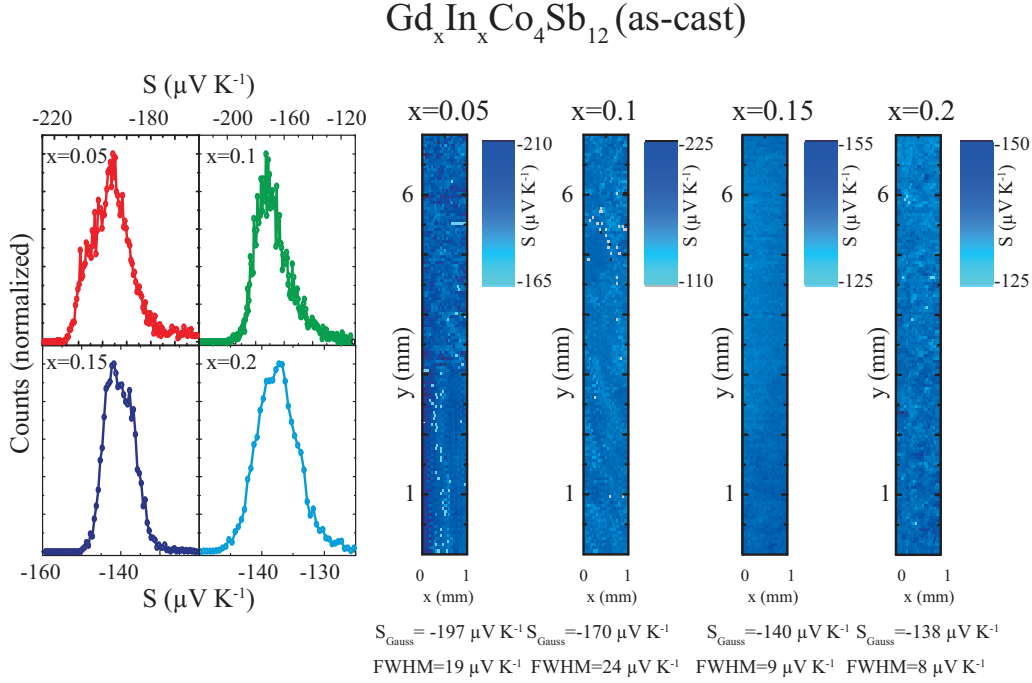
Figure 4.25:   *S(x, y) data (cross-sectional area) taken from annealed* $Gd_x In_x Co_4 Sb_{12}$ *material (x = 0.05, 0.1, 0.15 and 0.2) showing the spatial distribution of the Seebeck coefficient S(x, y) (right) and the corresponding histograms (left). The full width half maximum (FWHM) values are denoted below as well as the maximum S values, which were obtained by a Gaussian fit of the histogram data points.*

 Figure 4.27 shows the temperature dependence of the electrical conductivity σ of Ce,In:CoSb₃ and Gd,In:CoSb₃ short-term sintered specimens. It can be observed that the electrical conductivity is generally increasing with the amount of filler elements (i.e. Ce/In, Gd/In) in the skutterudite material and is highest for the samples with $x = 0.2$.

The Ce,In:CoSb₃ specimens show a monotonic decline of the electrical conductivity as a function of the temperature. The absolute σ values are - by far - the highest among all measured samples in this thesis and reach almost $2000\,\mathrm{S\,cm^{-1}}$ at room temperature for $x = 0.2$.

The Gd,In:CoSb₃ compacted samples have a much lower electrical conductivity (in parts less than half), when the data is compared to the Ce,In:CoSb₃ compacted samples, and show almost the same slope among each other.
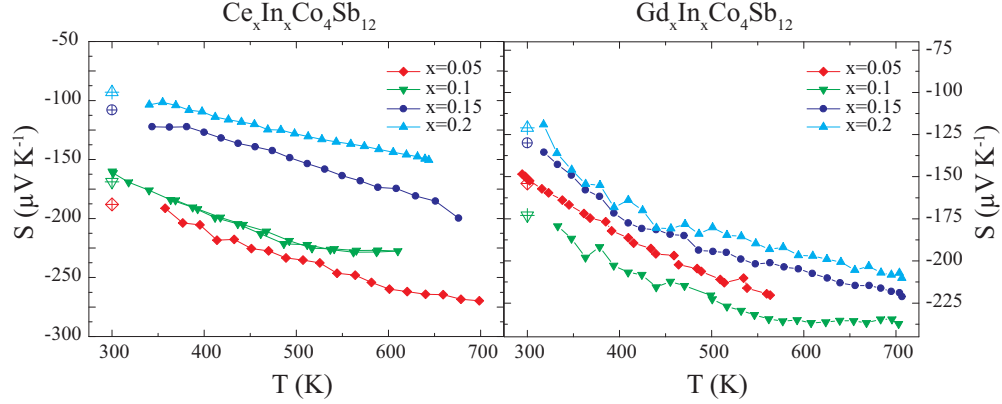
Figure 4.26: *The Seebeck coefficient S as a function of temperature of*
$Ce_xIn_xCo_4Sb_{12}$ *and* $Gd_xIn_xCo_4Sb_{12}$ *short-term compacted material (x =*
0.05, 0.1, 0.15 and 0.2) from 300 *to* 700 K. *The room temperature values*
are taken from the $S(x, y)$ *data of the short-term sintered specimens. The*
$Ce_{0.1}In_{0.1}Co_4Sb_{12}$ *and the* $Gd_{0.05}In_{0.05}Co_4Sb_{12}$ *specimens were measured by*
the differential Seebeck voltages method (see sec.3.2.2).

When the results from the electrical conductivity measurements are com-
pared to the Seebeck coefficient measurements, the effect of gadolinium and
indium filled skutterudites is again considerably weaker than with cerium
and indium double filled skutterudite material.
  Figure 4.28 shows the thermal conductivity data of the double filled skut-
terudite material. The results validate that the addition of cerium and in-
dium to the cobalt-antimony based skutterudites drastically reduces the ther-
mal conductivity. The values range between $3\,\mathrm{W\,m^{-1}\,K^{-1}}$ and $4\,\mathrm{W\,m^{-1}\,K^{-1}}$
for all Ce,In:CoSb$_3$ specimens and descend with ascending temperature. How-
ever the samples vary little within the given temperature of 300 K to 700 K.
This applies especially for the higher doped samples which have a $\Delta\kappa$ of about
$0.5\,\mathrm{W\,m^{-1}\,K^{-1}}$ in this temperature range. Almost all Ce:In:CoSb$_3$ samples
show a flattening of the thermal conductivity starting at around 550 K. It
is notable that the sample with lowest filling fraction of cerium and indium
($x = 0.05$) has partly lower thermal conductivity values than compacted spec-
imens, with a higher filling fraction. In other words the $Ce_{0.05}In_{0.05}Co_4Sb_{12}$
sample possesses a steeper slope in the $\kappa-T$ diagram than higher filled skut-
terudite specimens.

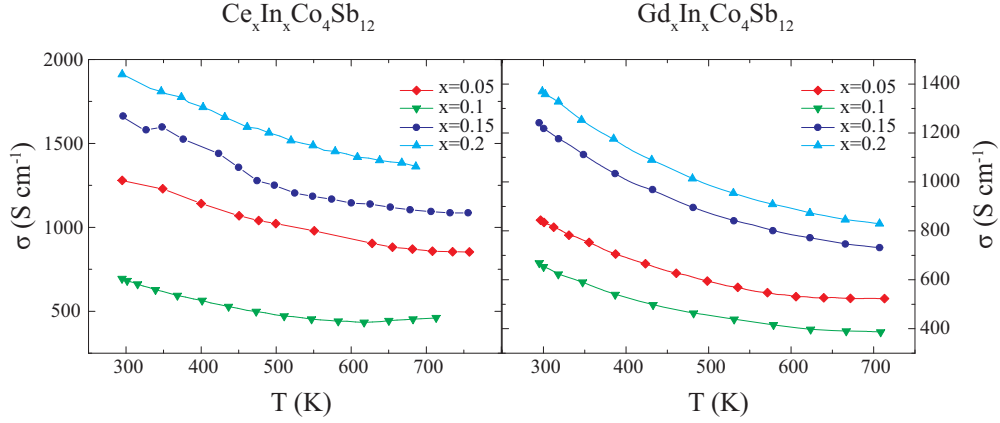Figure 4.27: *Temperature dependent electrical conductivity σ of short-term sintered $\mathrm{Ce}_x\mathrm{In}_x\mathrm{Co}_4\mathrm{Sb}_{12}$ and $\mathrm{Gd}_x\mathrm{In}_x\mathrm{Co}_4\mathrm{Sb}_{12}$ skutterudite specimens with $x = 0.05, 0.1, 0.15$ and 0.2*

The $\mathrm{Ce}_{0.1}\mathrm{In}_{0.1}\mathrm{Co}_4\mathrm{Sb}_{12}$ specimen exhibits the lowest thermal resistivity and electrical conductivity in the Ce,In:CoSb₃ sample series, which clearly corresponds to the high absolute Seebeck coefficient data - together with the PXRD pattern, which proved significant amounts of the secondary material. The results of the thermal conductivity data of the Gd,In:CoSb₃ compacted material are considerably different. The thermal conductivity values as a function of temperature start at slightly higher values (around $4.5\,\mathrm{W\,m^{-1}\,K^{-1}}$) for the low filled sample ($x = 0.05$) and reaches values below $3\,\mathrm{W\,m^{-1}\,K^{-1}}$ for higher filled samples, such as $\mathrm{Gd}_{0.15}\mathrm{In}_{0.15}\mathrm{Co}_4\mathrm{Sb}_{12}$ and $\mathrm{Gd}_{0.2}\mathrm{In}_{0.2}\mathrm{Co}_4\mathrm{Sb}_{12}$. The Gd,In:CoSb₃ specimens show a decrease of the thermal conductivity as a function of temperature until the inflection point at around $575\,\mathrm{K}$. From there on the values strongly ascend. This strong effect is not observed for most Ce,In:CoSb₃ samples, but for single filled In:CoSb₃ compacted material, especially the specimen with $x = 0.05$.

Hall measurements of the compacted samples were carried out at $300\,\mathrm{K}$ and are denoted in table 4.3. The table 4.3 shows the effective charge carrier density n_H, the Hall mobility μ_H and the corresponding electrical conductivity σ at room temperature. The data validates that with ascending concentration of Ce and In in the skutterudite material the effective charge carrier density increases beginning from $n = 9.2 \times 10^{19}\,\mathrm{cm^{-1}}$ for $x = 0.05$ up to a value of
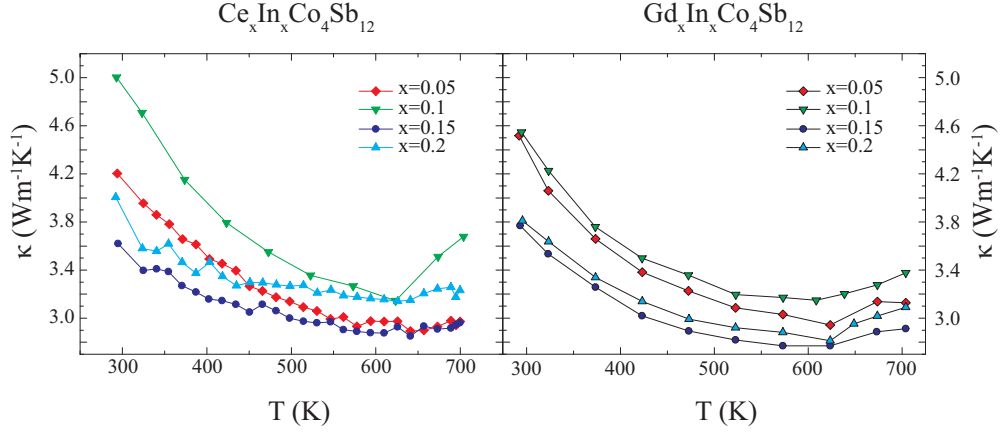
Figure 4.28: *Temperature dependent thermal conductivity κ of short-term sintered $\mathrm{Ce}_x\mathrm{In}_x\mathrm{Co}_4\mathrm{Sb}_{12}$ and $\mathrm{Gd}_x\mathrm{In}_x\mathrm{Co}_4\mathrm{Sb}_{12}$ skutterudite specimens with $x = 0.05, 0.1, 0.15$ and 0.2*

$n = 8.7 \times 10^{20}\,\mathrm{cm}^{-1}$ with $x = 0.2$. The Hall mobility μ_{H} of the Ce,In:CoSb$_3$ samples is inversely proportional and is therefore highest for a cerium and indium fraction with $x = 0.05$ ($\mu_{\mathrm{H}} = 76\,\mathrm{cm}^2\,\mathrm{V}^{-1}\,\mathrm{s}^{-1}$) and lowest for $x = 0.2$ with a Hall mobility of $\mu_{\mathrm{H}} = 20\,\mathrm{cm}^2\,\mathrm{V}^{-1}\,\mathrm{s}^{-1}$.

The Hall measurement results of Gd,In:CoSb$_3$ specimens are comparable to those values of the Ce,In:CoSb$_3$ specimens. Here the effective charge carrier density increases on average with ascending filling fraction, but to a smaller extent than in the case of the Ce,In:CoSb$_3$ samples. Furthermore the Hall mobility values follow the trend and are inversely proportional to the filling degree with Gd and In. The exception is the $\mathrm{Gd}_{0.1}\mathrm{In}_{0.1}\mathrm{Co}_4\mathrm{Sb}_{12}$ sample, which shows a considerable lower effective charge carrier density as well as a lower electrical conductivity, when it is compared to the lower filled sample with $x = 0.05$. As a result of the effective charge carrier density and the lower electrical conductivity the Hall mobility of the $\mathrm{Gd}_{0.1}\mathrm{In}_{0.1}\mathrm{Co}_4\mathrm{Sb}_{12}$ sample possesses the highest Hall mobility among all other Gd,In:CoSb$_3$ specimens. In figure 4.29 the temperature dependence of the dimensionless figure of merit ZT of the compacted Ce,In:CoSb$_3$ and Gd,In:CoSb$_3$ specimens is shown. The ZT values were calculated from fitted values of the temperature dependent Seebeck coefficient together with the electrical and thermal conductivity data. All specimens show a gradual increase of ZT as a function

	$n_{\mathrm{H}}(10^{19}\,\mathrm{cm}^{-3})$	$\mu_{\mathrm{H}}(\mathrm{cm}^2\,\mathrm{V}^{-1}\,\mathrm{s}^{-1})$	$\sigma(\,\mathrm{S}\,\mathrm{cm}^{-1})$
$\mathrm{Ce}_x\mathrm{In}_x\mathrm{Co}_4\mathrm{Sb}_{12}$			
$x = 0.05$	9.2	76	1118
$x = 0.1$	9.5	55	832
$x = 0.15$	60	22	2129
$x = 0.2$	87	20	2768
$\mathrm{Gd}_x\mathrm{In}_x\mathrm{Co}_4\mathrm{Sb}_{12}$			
$x = 0.05$	11	56	961
$x = 0.1$	4.8	101	771
$x = 0.15$	15	58	1428
$x = 0.2$	22	49	1699

Table 4.3: *Results from Hall and electrical conductivity measurements of the compacted* $\mathrm{Ln}_x\mathrm{In}_x\mathrm{Co}_4\mathrm{Sb}_{12}$ *(Ln=Ce,Gd) material with* $x = 0.05, 0.1, 0.15$ *and* 0.2 *at* $300\,\mathrm{K}$ *showing the effective charge carrier density* n_{H}, *the Hall mobility* μ_{H} *and the electrical conductivity* σ, *respectively.*

of temperature starting from around $300\,\mathrm{K}$ to $700\,\mathrm{K}$.

According to the diagram the Ce,In:CoSb₃ sample with lowest filling fraction $(x = 0.05)$ possesses the highest ZT with a $ZT_{\mathrm{max}} = 1.1$ at $700\,\mathrm{K}$ among all other skutterudite specimens. The Ce,In:CoSb₃ specimens with higher filling fractions have due to a significantly lower absolute S value a vastly reduced ZT. It is noteworthy that the sample with highest filling fraction $(x = 0.2)$ has one of the lowest figure of merit ZT within the Ce,In:CoSb₃ sample series, which is opposed to most of the reported results on In:CoSb₃, where with higher filling fractions by trend an increase of the ZT is observable [117, 118]. The Gd,In:CoSb₃ samples show in comparison to the Ce,In:CoSb₃ compacted samples a lower electrical conductivity, absolute Seebeck coefficient and thermal resistivity and thus a lower ZT as a function either of the filling fraction or temperature. Highest ZT in the Gd,In:CoSb₃ series is obtained for $\mathrm{Gd}_{0.15}\mathrm{In}_{0.15}\mathrm{Co}_4\mathrm{Sb}_{12}$ having a $ZT_{\mathrm{max}} = 0.83$ at $700\,\mathrm{K}$. The compacted sample with $x = 0.2$ however show almost the same ZT over a wide temperature range versus the $x = 0.15$ compacted material, which is based on the higher electrical conductivity of the $\mathrm{Gd}_{0.2}\mathrm{In}_{0.2}\mathrm{Co}_4\mathrm{Sb}_{12}$ sample and can subsequently compensate the lower Seebeck coefficient. Low filling fractions of gadolinium and indium filled skutterudites lead to a low figure of merit.
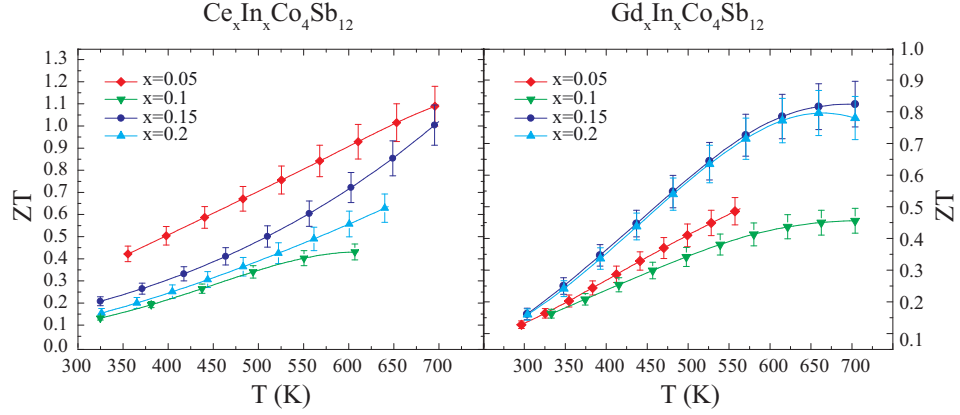
Figure 4.29: *Temperature dependence of the dimensionless figure of merit ZT for short-term sintered* $Ce_xIn_xCo_4Sb_{12}$ *and* $Gd_xIn_xCo_4Sb_{12}$ *material with* $x = 0.05, 0.1, 0.15$ *and* 0.2. *The error is considered to be around* 8% *and is based on a calculation of errors of the particular measuring instruments:* $\Delta S = 2\,\mu V\,K^{-1}$, $\Delta\sigma = 2\,S\,cm^{-1}$, $\Delta T = 0.2\,K$, $\Delta\kappa = 0.2\,W\,m^{-1}\,K^{-1}$.

Neutron powder diffraction measurements of the Ce,In:CoSb$_3$ Skutterudite material

The neutron powder diffraction data of $Ce_{0.05}In_{0.1}Co_4Sb_{12}$ was recorded together with the single indium filled samples presented in the section 4.2.2 at four different temperatures (12 K, 50 K, 150 K and 300 K). The pattern of the powder diffraction measurement can be seen in figure 4.30, figure 4.31 and the Rietveld refinement results are shown in table 4.4 and furthermore in figure 4.32. The data is presented together with the single indium filled samples to facilitate the distinctions between single In filled skutterudite specimens and the double filled skutterudite sample.

The lattice parameter of the $Ce_{0.05}In_{0.1}Co_4Sb_{12}$ specimen increases from about 9.0298 Å at 12 K to 9.0463 Å at room temperature. It increases with almost the same slope as both single indium filled specimens. The absolute value ranges between the $In_{0.05}Co_4Sb_{12}$ and $In_{0.2}Co_4Sb_{12}$ samples and approaches the high indium filled specimen.

The thermal parameters of Co and Sb are by trend higher than those of the

	$Ce_{0.05}In_{0.1}Co_4Sb_{12}$
R_P (%)	2.75
R_{WP} (%)	2.53
R_{exp} (%)	1.29
χ^2	3.83
a (Å)	9.046 26(2)
U_{iso}(In/Ce) (Å^2)	0.003(2)
U_{iso}(Co) (Å^2)	0.0042(1)
U_{iso}(Sb) (Å^2)	0.005 95(6)
y(Sb)	0.335 07(5)
z(Sb)	0.157 91(5)
Occ.(In) (%)	6.8
Occ.(Ce) (%)	3.0
$\alpha_{150K-300K}$ ($10^{-6}\,K^{-1}$)	8.3

Table 4.4: *Results from the Rietveld refinement of the time-of-flight neutron powder diffraction measurements of the $Ce_{0.05}In_{0.1}Co_4Sb_{12}$ specimen at room temperature - the R-factors are taken from the measurement at the lowest temperature. The occupancy of Co, Sb and In was refined equal to the data set in table 4.2. The occupancy of Ce was individually refined - the evaluation of the U_{iso} value at the 2a Wyckoff position represents a superposition of Ce and In. $\alpha_{150K-300K}$ is the linear thermal expansion evaluated from the lattice parameter at 150 K and 300 K, respectively, after [141]. The uncertainty is denoted as follows: e.g. 0.335 07(5) = 0.33507 ± 0.00005.*

single indium filled samples and moreover when it is compared to the data from Mi et al. [162] the thermal parameters are more alike to the values of the cerium single filled material. The thermal parameter of the 2a position (assumably Ce and In) however is much different to the data from Mi et al. and shows a low number of around U_{iso}(In/Ce)=(0.003 Å^2). The thermoelectric properties of these specimens, which originate from the same as-cast materials as the samples for the neutron powder diffraction data, are of special interest, because the revised effect on the structural properties of the skutterudite material will have a macroscopic impact on the transport properties. In figure 4.33 the temperature dependent Seebeck coefficient, the
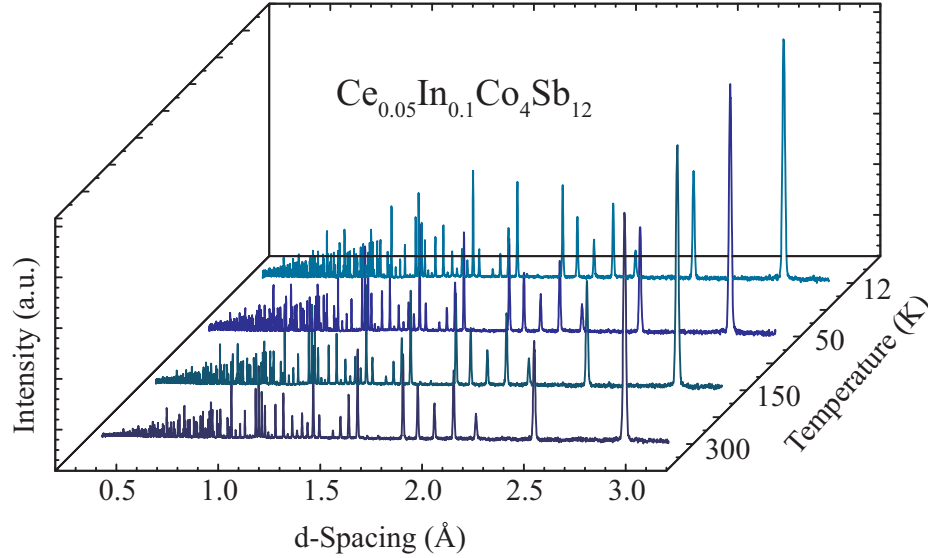
Figure 4.30:   *The time-of-flight neutron powder diffraction data of the* $Ce_{0.05}In_{0.1}Co_4Sb_{12}$ *specimen. The diagram shows the intensity in arbitrary units as a function of d-spacing in [Å] and different temperatures* 12 K, 50 K, 150 K *and* 300 K.

electrical/(lattice) thermal conductivity and the figure of merit are displayed. The Seebeck coefficient data of all three samples exhibits n-type behavior and is consequently alike to the previous single and double filled skutterudites. Highest absolute Seebeck coefficient is approached by the lowest single filled skutterudite specimen ($In_{0.05}Co_4Sb_{12}$) and exhibits a maximum S at around 550 K and descends again for higher temperatures. The other two samples show lower absolute Seebeck coefficients, which increase almost linearly with ascending temperature and start to flatten at 600 K and 650 K, respectively. The $Ce_{0.05}In_{0.1}Co_4Sb_{12}$ specimen shows among all other three specimens the lowest absolute S value.

The electrical conductivity data as a function of temperature shows results, which are comparable to the Seebeck coefficient data. The electrical conductivity of all three specimens decrease within the temperature range of 300 K to 700 K. The double filled skutterudite sample possesses the highest and the $In_{0.05}Co_4Sb_{12}$ specimen the lowest electrical conductivity. Latter features a flattening in the electrical conductivity data at around 600 K, which supports
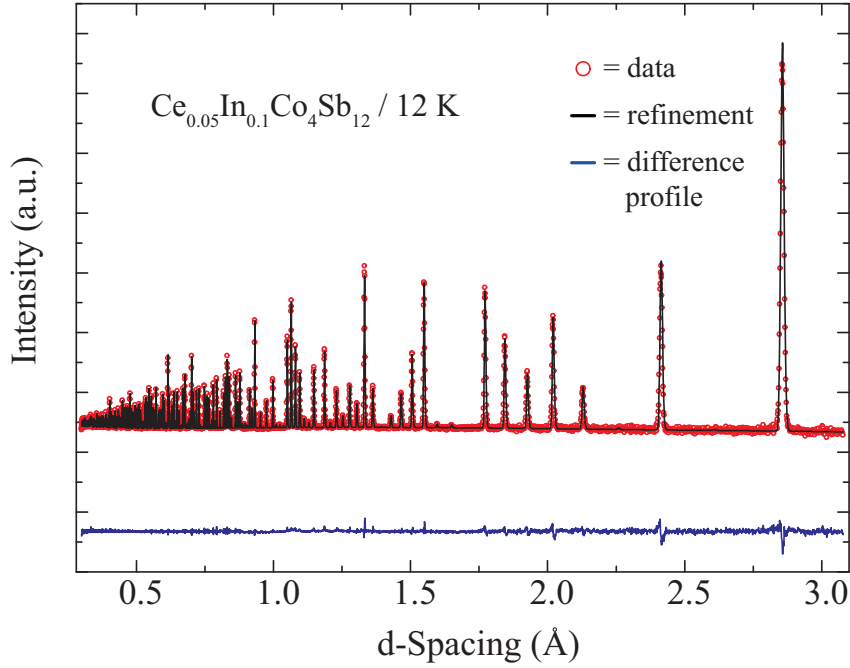
Figure 4.31: *Data and Rietveld refinement of the time-of-flight neutron powder diffraction data of* $Ce_{0.05}In_{0.1}Co_4Sb_{12}$ *specimen at* $12\,K$. *The difference profile is shown below the data points (blue solid line).*

the visible effect in the Seebeck coefficient data.

The thermal conductivity values of the three specimens lie between 3 and $5.5\,\mathrm{W\,m^{-1}\,K^{-1}}$ in the given temperature range. The low indium filled sample $(In_{0.05}Co_4Sb_{12})$ shows a steep fall of the thermal conductivity up to $550\,\mathrm{K}$ and increases again for higher temperatures. The double cerium and indium filled specimen $(Ce_{0.05}In_{0.1}Co_4Sb_{12})$ starts already at a lower thermal conductivity value, when it is compared to the $In_{0.05}Co_4Sb_{12}$ sample. The slope of the double filled skutterudite material however is not as high as the low indium filled sample and flattens furthermore at a temperature of $525\,\mathrm{K}$. The skutterudite sample with highest indium content possesses the lowest thermal conductivity in this series. The slope of the thermal conductivity data is more comparable to the low indium filled specimen and exhibits a minima
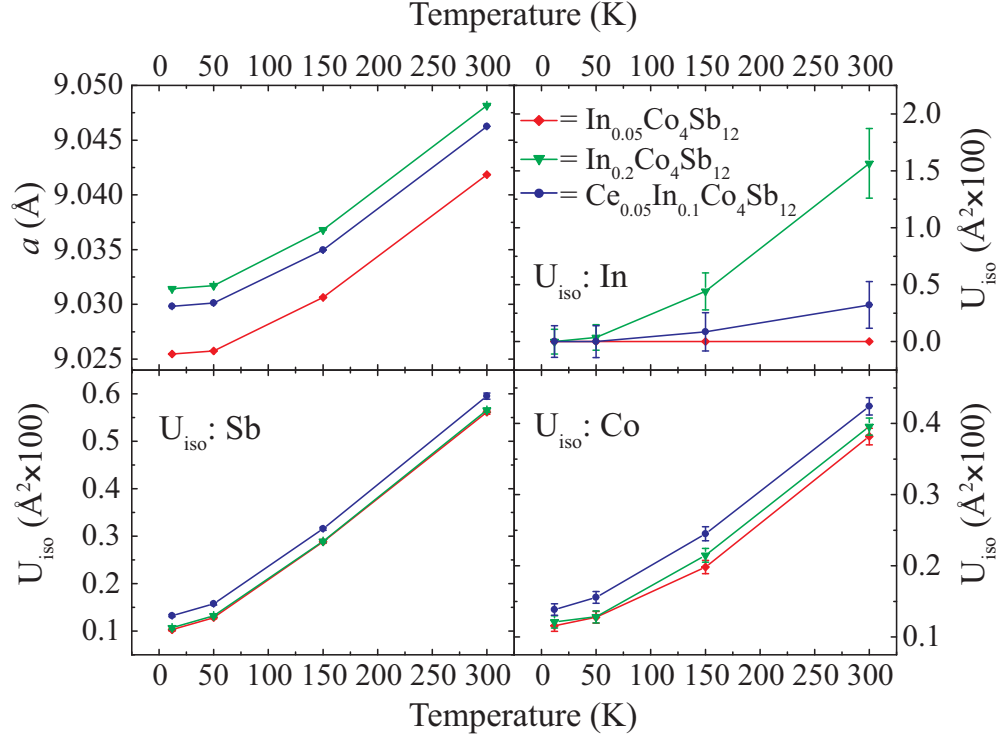
Figure 4.32: *Results from the Rietveld refinement of the temperature dependent time-of-flight neutron powder diffraction measurement of double cerium and indium filled skutterudites (*In$_{0.05}$Co$_4$Sb$_{12}$*, *In$_{0.2}$Co$_4$Sb$_{12}$ *and* Ce$_{0.05}$In$_{0.1}$Co$_4$Sb$_{12}$*). Top left diagram shows the temperature dependent lattice parameter* a*. Top right, bottom left and bottom right diagrams display the atomic displacement parameter* U$_{iso}$ *of the particular elements as a function of temperature.*

at 600 K and a small increase of the thermal conductivity is visible for higher temperatures.

The calculated lattice thermal conductivity for the low filled sample is almost unchanged with respect to the thermal conductivity. This is contributed to the high absolute Seebeck coefficient and the low electrical conductivity of the sample. The other two specimens show considerable changes between the lattice thermal conductivity κ_l and the overall thermal conductivity κ. Due to the high electrical conductivity of the Ce$_{0.05}$In$_{0.1}$Co$_4$Sb$_{12}$ specimen the

lattice thermal conductivity is almost identical to the high indium filled sample. In the sum the figure of merit ZT is highest for the double cerium and indium filled skutterudite sample ($Ce_{0.05}In_{0.1}Co_4Sb_{12}$) approaching a value of $ZT_{\max} = 0.9$ at 700 K. However the high indium filled specimen possesses an equally high figure of merit up to around 575 K and is then saturating at higher temperatures.

4.3.3   Discussion

The thermoelectric properties of both double filled skutterudites (i.e. Ce/In and Gd/In) show notable high figure of merits in a temperature range from 300 K to 700 K. The Gd,In:CoSb$_3$ samples exhibit thermoelectric properties related to that of single filled In:CoSb$_3$ material and possess at high filling fractions of gadolinium and indium a figure of merit close to $ZT = 0.83$ at 700 K. On the other hand the cerium and indium doubled filled samples show a vast improvement in comparison to pure CoSb$_3$ material and even single filled In:CoSb$_3$ specimens in terms of the thermoelectric properties. It is noteworthy that the sample with lowest filling of cerium and indium already exceeds a figure of merit of one starting from about 640 K.

The Synthesis   of double filled skutterudite material is almost identical to the process of single indium filled skutterudites (see sec.4.2.1). However there are (vast) differences, which occur at the particular steps of the synthesis. First, the synthesis process is carried out solely under inert atmosphere, because both rare earth elements (Gd, Ce) easily oxidize in air. Additionally powders from rare earths can be pyrophoric and as a consequence were not used in this synthesis approach.[27] After sealing the silica tube the constituents were melted in an induction furnace. In this silica tube an exothermal reaction takes place during the inductive melt process, which is most probably a reaction of antimony and the particular rare-earth. Experiments with an arc melter were carried out for the $Ce_{0.1}In_{0.1}Co_4Sb_{12}$ material to produce a precursor out of cerium and cobalt. The advantage of this process is that the strong exothermal reaction can be displaced within a more controlled surrounding, i.e. in a water cooled copper cup under inert atmosphere. On

---

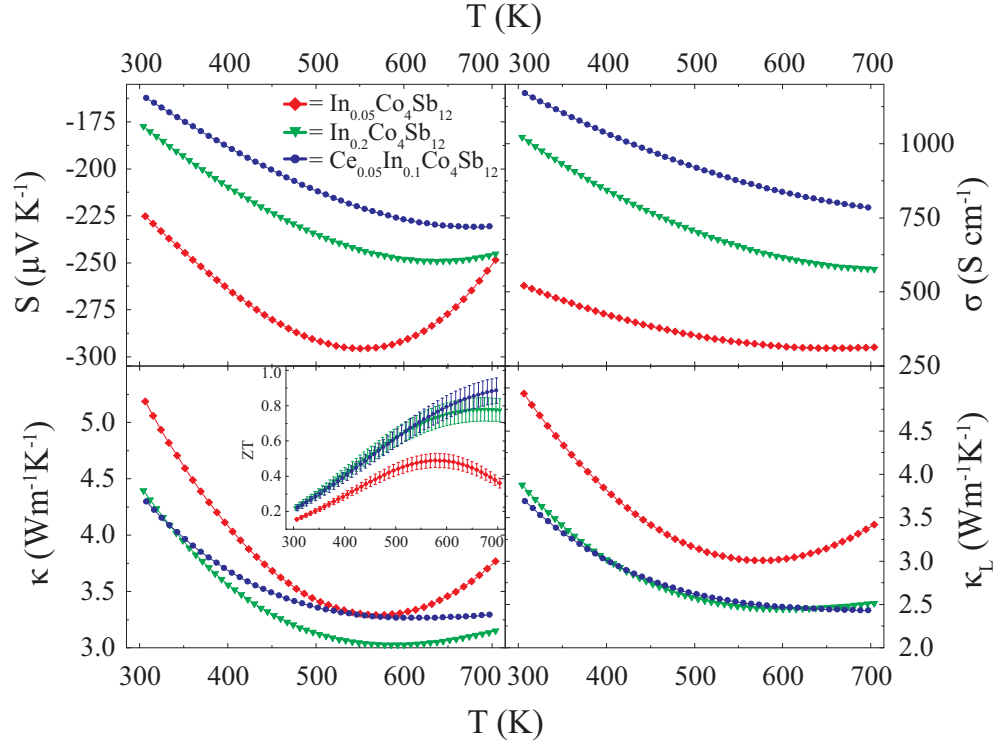[27]Preliminary experiments with cerium powder failed due to severe oxidation problems.

Figure 4.33: *Temperature dependent thermoelectric properties of short-term sintered* $In_{0.05}Co_4Sb_{12}$, $In_{0.2}Co_4Sb_{12}$ *and* $Ce_{0.05}In_{0.1}Co_4Sb_{12}$ *specimens. The samples origin from the same as-cast materials as the samples used for the neutron powder diffraction measurements. The diagrams show the Seebeck coefficient S (top left), the electrical conductivity* σ *(top right), thermal conductivity* κ *(bottom left) and the calculated lattice thermal conductivity* κ_l *(bottom right) as a function of temperature in the range of* 300 K *to* 700 K. *In the inset of the thermal conductivity diagram the figure of merit of all three specimens is displayed as a function of temperature. All three specimens were measured by the differential Seebeck voltages method (see sec.3.2.2).*

the other side, the PXRD pattern of the annealed $Ce_{0.1}In_{0.1}Co_4Sb_{12}$ powder material shows that Sb and $CoSb_2$ are the predominant phases and the skutterudite phase was almost not formed. This was changed by short-term sintering of the powder. After the compaction the skutterudite phase was formed, however considerable amounts of secondary material remains in the

material (see fig.4.21). This behavior may be attributed also to the high annealing temperature, which can have a negative effect on the crystallization process of the material. Since elementary Sb is assumed to be liquid in the annealing period the filled skutterudite phase may not have the chance to crystallize. Experiments have shown that a reduction of the annealing temperature to $973\,\mathrm{K}$ enables a formation of the skutterudite phase during the annealing process. This reveals very clearly that the constraints for the formation of filled skutterudites are stronger than for unfilled skutterudites, at least for the selected annealing temperature.

Another observation is that the melt of Ln,In:CoSb₃ material exhibits a completely different viscosity, which can be best compared to highly alloyed steels. This is considerably different to single indium filled skutterudite material, which possesses a significantly lower viscosity than the Ln,In:CoSb₃ material in the liquid state.

Measurements of the local Seebeck coefficient can detect differences in the effective doping level on the surface of the as-cast material and for this reason can be possibly used as a measure of the local distribution of the filler elements. This means that a local Seebeck coefficient measurement and the corresponding histogram can predict, whether the filler elements are finely distributed to a large extent in the synthesized material, or not. Latter is determined by the change of the Seebeck coefficient as a function of the filler fraction, which is validated in the results of the different Seebeck coefficients of the specimens (e.g. see fig.4.9). The analysis of the local Seebeck coefficient data of Ln,In:CoSb₃ material suggests that most probably due to the higher viscosity in comparison to In:CoSb₃ material a homogenization is more difficult to obtain. Many attempts were necessary to obtain a skutterudite material, with homogeneously distributed S values and thus with an uniform filling/doping of the whole skutterudite material.

Structural and Thermoelectric Properties: The used filler elements have a considerable impact on the structure of the skutterudite crystal, which are different for Ce,In:CoSb₃ and Gd,In:CoSb₃ specimens, respectively. The lattice parameter of the Ce,In:CoSb₃ specimens starts already at a higher value and increases more rapidly in comparison to the single In:CoSb₃ samples. The lattice parameter of the low filled Ce,In:CoSb₃ specimen ($x = 0.05$) is $a = 9.046\,\text{Å}$ and increases up to a value of $a = 9.062\,\text{Å}$ for the material with

highest filling fraction ($Ce_{0.2}In_{0.2}Co_4Sb_{12}$). This finding suggests that cerium is to a large extent incorporated in the skutterudite crystal and consequently exhibits a lattice parameter expansion, which is alike to that reported in literature for single filled cerium skutterudites [62, 65].[28] For the single filled Ce:CoSb$_3$ material a maximum lattice parameter of 9.046 Å is reported [151], which is significantly lower than the maximum value, which was obtained in these Ce,In:CoSb$_3$ samples. Hence it can be assumed that a reasonable part of the lattice parameter expansion is most likely attributed to the presence of cerium *and* indium in the skutterudite crystal structure.

For the Gd,In:CoSb$_3$ material the change of the CoSb$_3$ crystal structure is not as high as with the Ce,In:CoSb$_3$ specimens. The lattice parameter starts with $a = 9.041$ Å for $Gd_{0.1}In_{0.1}Co_4Sb_{12}$ and ends with a maximum lattice parameter of $a = 9.052$ Å for the composition $Gd_{0.2}In_{0.2}Co_4Sb_{12}$. It is of interest that the lowest filled sample exhibits a higher lattice parameter than the next higher filled $Gd_{0.1}In_{0.1}Co_4Sb_{12}$ specimen. This is a strong indication that the starting composition was changed in such a way that the effective doping and filling of the skutterudite material is higher for the $Gd_{0.05}In_{0.05}Co_4Sb_{12}$ sample than the $Gd_{0.1}In_{0.1}Co_4Sb_{12}$ specimen. This is supported by the fact that the temperature dependent electrical conductivity follows this trend under which the lowest filled Gd,In:CoSb$_3$ sample has a higher σ than the $Gd_{0.1}In_{0.1}Co_4Sb_{12}$ specimen - and therefore suggest a higher effective doping/filling. Carried out Hall measurements reveal this fact and show a considerable lower effective charge carrier density for the Gd,In:CoSb$_3$ sample with $x = 0.1$. Accordingly the determination of the exact composition of these two compounds would be desirable.[29]

For the highest filling level with gadolinium and indium a lattice parameter is observed, which corresponds to the reported maximum lattice parameter of single indium filled CoSb$_3$ skutterudites ($a = 9.0563$ Å from [117]). This means that indium is either fully incorporated in the skutterudite structure, or gadolinium may be additionally substituting/entering sites within the skutterudite structure - or both.

Gadolinium possesses seven $4f$, two $6s$ and one further $5d$ valence electron having a typical oxidation state of 3^+ or less often 2^+, which makes it in principle suitable for an electropositive lattice site in the skutterudite structure,

---

[28]These studies report mostly on skutterudite material, which contains an additional amount of iron. Fe itself has an influence on the lattice parameter and thus these two effects cannot be clearly separated.

[29]e.g. by an inductively induced plasma mass spectrometer measurement (ICP-MS)

such like the Wyckoff position $8c$ or less likely the $2a$ position. The gadolinium ion possess an ionic radius, which is smaller than that of cerium[30], and for this reason it is doubted, whether gadolinium can occupy the filler position permanently due to a weak bonding to the Sb-framework. However when certain conditions are fulfilled the Gd ion can occupy the interstitial void [165].[31]

In this work it can be almost excluded that Gd does *predominantly* fill the $2a$ void in the skutterudite structure, due to the results from the Rietveld refinement and the determined lattice parameter.[32] In this case a higher lattice parameter would be expected. A lattice site substitution of Gd in the skutterudite crystal is also unlikely. This would probably lead to a significant change in the electrical conductivity, or in the case of isoelectronic substitution, a (dramatic) decrease in the lattice parameter.[33] The increased thermal resistivity and the evidence of secondary phases in the material indicate that Gd will first and foremost form impurity phases (GdSb/GdSb$_2$).

SEM and PXRD analyses reveal that almost all Ln,In:CoSb$_3$ (Ln=Gd,Ce) as-cast materials show mainly the skutterudite phase with a high grade of crystallinity. Secondary phases are not observable for the Ce$_{0.05}$In$_{0.05}$Co$_4$Sb$_{12}$ specimen. For higher filling fractions traces of impurity phases (e.g. CeSb$_2$/CoSb$_2$ for Ce$_{0.15}$In$_{0.15}$Co$_4$Sb$_{12}$) can be observed in the PXRD patterns. However only for highest filling fraction with $x = 0.2$ a relatively intense signal is visible for CeSb$_2$[34] and InSb. This indicates that for higher filling fractions with cerium and indium the solubility limit in the skutterudite crystal is reached/exceeded and the actual filling fraction of Ce and In is most probably less than the starting nominal composition. Nevertheless the lattice parameter still ascends with increasing addition of Ce an In. Thus the formation of secondary material and the incorporation of filler elements in the skutterudite crystal can be regarded as competing processes. This again can be attributed to the synthesis procedure and especially the annealing step,

---

[30]Gd^{3+} radius in eight-fold coordination $r_{Gd} = 1.19\,\text{Å}$, Ce^{3+} in eight-fold coordination $r_{Ce} = 1.28\,\text{Å}$ [144]

[31]It is reported that the provided charge carriers from the Gd ion has to be compensated by e.g. Co substitution with Fe.

[32]A statement, whether Gd enters to a (very) small extent the lattice void site of CoSb$_3$, cannot be made.

[33]The reported ionic radius of Co^{+3} in six-fold coordination and low-spin configuration is $r_{Co} = 0.685\,\text{Å}$.

[34]Reflections and lattice parameters are taken from Wang [168].

where the crystallization of the skutterudite material takes place.

The thermoelectric properties of double filled skutterudites show high ZT values in the investigated intermediate temperature range, especially Ce,In:CoSb$_3$ material exhibits a ZT, which is significantly above 1 at higher temperatures. The figure of merit ZT as a function of temperature decrease with increasing filling fraction of Ce and In. In many investigations, high(er) filling levels contribute to an improved figure of merit of the skutterudite material, especially due to the high Seebeck coefficient values. For this reason the distinctions of ZT vs. filling fraction x between this work and other studies may be contributed to the different synthesis procedures, which are in other studies far away from steady state conditions (e.g. melt-spinning with subsequent short-term annealing). In this investigation a more steady state synthesis was approached, comprising induction melting with a subsequent long annealing step at high temperature and a steady cooling down period. In the case of gadolinium and indium filled CoSb$_3$ material, the samples possess values of ZT not significantly higher than for single filled In:CoSb$_3$ material. For instance the maximum ZT for the lowest double filled Gd,In:CoSb$_3$ and single filled In:CoSb$_3$ specimen ($x = 0.05$) does not differ in magnitude, but shifts from $550\,\mathrm{K}$ to a temperature value of around $600\,\mathrm{K}$.

The lattice thermal conductivity values for the double filled Ln,In:CoSb$_3$ specimens was derived by applying the Wiedemann-Franz law (see sec.1.4). The diagrams are shown in figure 4.34.

 The values of the lattice thermal conductivity in figure 4.34 are for skutterudite samples with small Ce and In filling fractions slightly lower in comparison to the single filled In:CoSb$_3$ specimens and therefore validates the effectiveness of double filled skutterudites. The vastly enhanced electrical conductivity of Ce,In:CoSb$_3$ specimens, contributes however to an increased total thermal conductivity. Specimens with high fractions of cerium and indium show even lower lattice thermal conductivity values up to a minimum lattice thermal conductivity of $\kappa_{\mathrm{l_{min}}} = 1.66\,\mathrm{W\,m^{-1}\,K^{-1}}$ at $640\,\mathrm{K}$ for the Ce$_{0.2}$In$_{0.2}$Co$_4$Sb$_{12}$ sample. Main reason of the high lattice thermal resistivity is the increasing filling fraction of Ce an In in the skutterudite structure, which is revealed by the ascending lattice parameter, and presumably to a lesser degree by the occurrence of secondary material. Latter is of interest in the case of the Ce$_{0.2}$In$_{0.2}$Co$_4$Sb$_{12}$ specimen, where a significant amount[35] of finely distributed impurity phases was found. It should be noted that at

---

[35]The total volume fraction of secondary phases is in the region of 1% to 2%
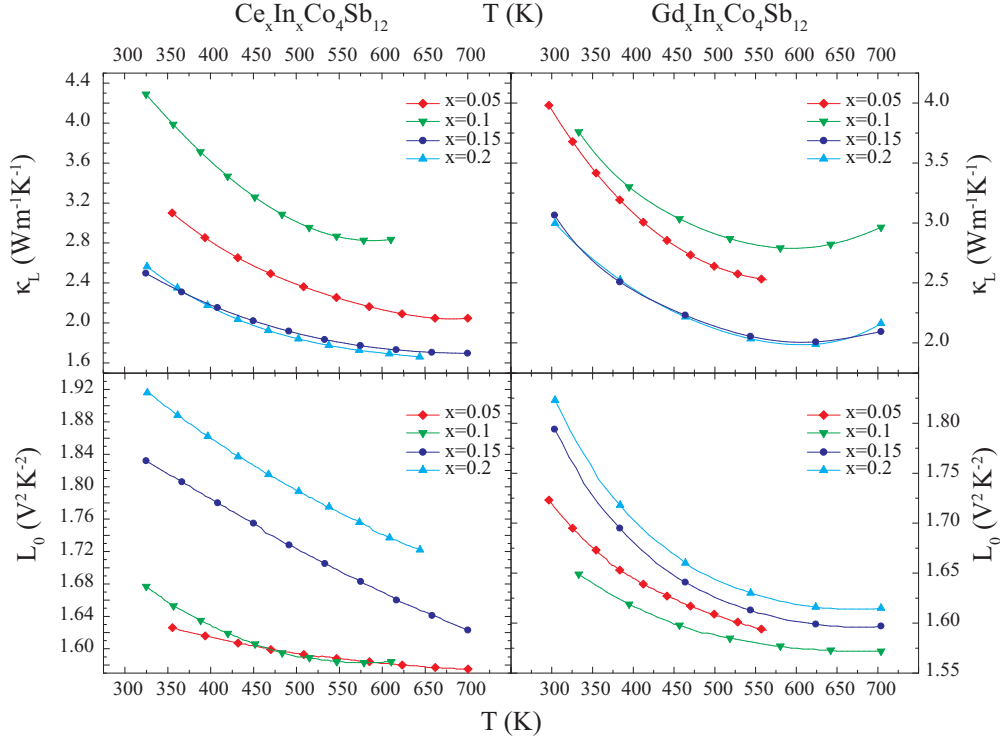
Figure 4.34: *Calculated lattice thermal conductivity κ_l and the Lorenz number L_0 of Ce,In:CoSb₃ and Gd,In:CoSb₃ specimens with the composition $x = 0.05, 0.1, 0.15$ and 0.2 as a function of temperature. The left diagrams represents the data from the Ce,In:CoSb₃ specimens and the right diagrams the data from the Gd,In:CoSb₃ specimens, respectively.*

this level of filling, the fraction limit in the skutterudite material may be already exceeded, because the individual filling fraction limits typically do not increase with double filling of the skutterudite material.[36] (see work of Xi et al. [103])

This leads to the assumption that the observation of finely distributed secondary phases in high filled Ce,In:CoSb₃ specimens does not detrimentally affect the electrical conductivity of the skutterudite material. For higher

---

[36]Filling fraction limit of Ce in CoSb₃ is reported to be 10%, of In it is reported to be 22%. However, as mentioned in the previous paragraph the formation of secondary phases does not necessarily start with reaching the filling fraction limit.

amounts of secondary phases this might be different: The $Ce_{0.1}In_{0.1}Co_4Sb_{12}$ sample shows a $CoSb_2$ phase with a volume fraction of around 10% and a charge carrier density, which is comparable to the $Ce_{0.05}In_{0.05}Co_4Sb_{12}$ specimen.[37] The comparison of the Hall mobilities μ_H shows that the specimen with $x = 0.1$ has a considerably reduced Hall mobility and thus shows a lower electrical conductivity. As expected the secondary phases have a negative influence on the skutterudite material, when its volume fraction is reasonably high. For (much) lower amounts the precipitates do not significantly lower the electrical conductivity, but enhance the thermal resistivity in form of the increased grain boundary density.

The $Gd,In:CoSb_3$ specimens show a somewhat different trend of the lattice thermal conductivity in comparison to the $Ce,In:CoSb_3$ samples. In figure 4.35 the κ_l data of the $Gd,In:CoSb_3$ samples is presented together with the single filled indium skutterudite specimens. It is clearly observable that the lattice thermal conductivity of the single filled indium skutterudite material is by trend higher than the $Gd,In:CoSb_3$ specimens.[38] Furthermore the lowest lattice thermal conductivities in this series are obtained for the $Gd_{0.2}In_{0.2}Co_4Sb_{12}$ and $Gd_{0.15}In_{0.15}Co_4Sb_{12}$, which exhibit almost the same value and an identical temperature dependence. This leads to the assumption that the occurrence of the secondary phases increases significantly the lattice thermal resistivity and the effect is in addition saturated at the filling fraction of $x = 0.15$ with gadolinium and indium. This is supported by the fact that these two compositions ($x = 0.15$ and 0.2) have furthermore the identical temperature dependence of the figure of merit ZT: The increased electrical conductivity of the highest gadolinium and indium filled skutterudite specimen with $x = 0.2$ is compensated by a minor decrease of the absolute Seebeck coefficient and leads to an almost identical figure of merit for the specimen with the lower filling fraction of $x = 0.15$. Moreover it is noteworthy that indeed the specimen with highest Gd and In filling fraction ($x = 0.2$) exhibits a higher lattice parameter than the lower filled sample with $x = 0.15$, but both possess an identical lattice thermal conduc-

---

[37]The determination of the volume fraction of $CoSb_2$ was obtained by the analysis of the PXRD pattern of the ground short-term sintered specimen.

[38]The specimen with starting composition of $Gd_{0.15}In_{0.15}Co_4Sb_{12}$ has shown a significantly lower lattice parameter, electrical conductivity and absolute Seebeck coefficient in comparison to the $Gd_{0.05}In_{0.05}Co_4Sb_{12}$ specimen. Thus it was concluded that the starting composition was changed to some extent and is therefore not shown in fig.4.35.
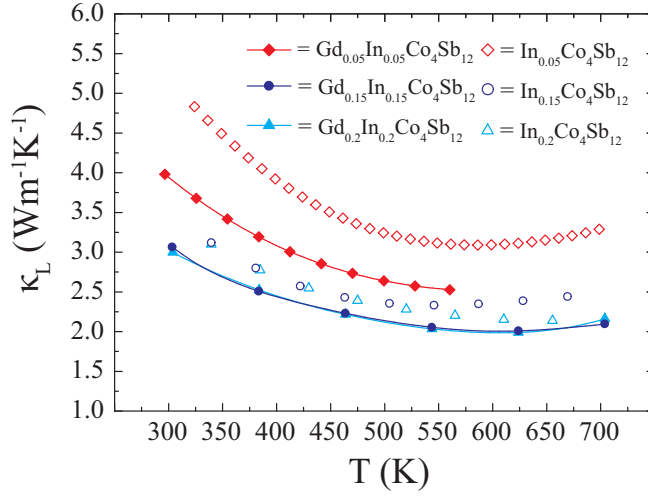
Figure 4.35: *Calculated lattice thermal conductivity κ_1 of Gd,In:CoSb₃ and In:CoSb₃ specimens with the composition $x = 0.05, 0.15$ and 0.2 as a function of temperature. The empty symbols represent the data of the In:CoSb₃ specimens and the filled symbols with lines represent the data of the Gd,In:CoSb₃ specimens.*

tivity.[39] For this reason the question arises, why an apparently higher filling level of the skutterudite material does not exhibit a lower lattice thermal conductivity? It can therefore be speculated that a higher lattice parameter of the skutterudite phase (presumable high occupancy of $2a$ lattice sites) not necessarily cause a higher thermal resistivity - or simply, the calculation of the lattice thermal conductivity suffers a systematic error, due to the non-parabolic property of the band structure.

The Pisarenko plot (a $S - n$ diagram) shows the Seebeck coefficient as a function of the effective charge carrier density at room temperature (see fig.4.36). The colored curves are calculations, where a single parabolic band model is assumed with different constant effective masses and a scattering exponent r of -1, which denotes an acoustic phonon scattering as the dominant

---

[39]The lattice thermal conductivity is calculated after the Single Parabolic Band Model and represents an assumption and is valid only for a certain extent for skutterudite materials.

phonon scattering process (see sec.1.4). For the Ce,In:CoSb$_3$ specimens it is easily observable that a considerable higher effective charge carrier density is obtained in comparison to the single indium filled skutterudites. This behavior is found for several other (rare earth) filled skutterudite materials and consequently is revealed for the Ce,In:CoSb$_3$ system. For the Gd,In:CoSb$_3$ material system this effect is indeed less pronounced, however it can be observed that an increase of the effective mass from about $m^* = 1.8$ to $m^* = 2.5$ takes place with increase of the effective charge carrier density n_{H}.

From these findings it can be concluded that the Seebeck coefficient of the Ln,In:CoSb$_3$ material system is strongly dependent on the effective charge carrier density of the material. This behavior does not apply for the single filled In:CoSb$_3$ system, where the effective mass changes only to a minor extent and as a consequence has a considerably lower Seebeck coefficient with values of the identical effective charge carrier density in comparison to the Ln,In:CoSb$_3$ specimens. The optimum of the charge carrier density with regard to a high figure of merit ZT locates most probably in the range of $1 \times 10^{20}\,\mathrm{cm}^{-3}$. For higher charge carrier densities the ZT does not overcome a value of 1.

Secondary Phases in Ln,In:CoSb$_3$ Skutterudites (Ln=Ce,Gd):   Besides the secondary phases, which were observed in the double filled Ce,In:CoSb$_3$ and Gd,In:CoSb$_3$ as-cast material, a further study on Ce,In:CoSb$_3$ material was carried out, similarly to the work in [133] and in section 4.2.3. In this study the focus issue was the impurity material of Ce and In filled skutterudite and whether these impurities can be affected by changing one parameter in the synthesis route to a certain extent. Latter was realized by an additional quenching of the skutterudite material directly after the annealing period of 168 h (see [170]).

The temperature dependent thermoelectric properties, i.e. the electrical and thermal conductivity, and the calculated lattice thermal conductivity, of different concentrations with Ce and In ($x = 0.05, 0.1, 0.15$ and 0.2) are shown in figure 4.37. The room temperature Seebeck coefficient values of these specimens with modified annealing parameters were obtained by the local Seebeck measurement instrument and are presented in the $S - n$ diagram in figure 4.36.

The results from the Pisarenko diagram support the assumption that the modified synthesis procedure does not vastly affect the behavior of the See-
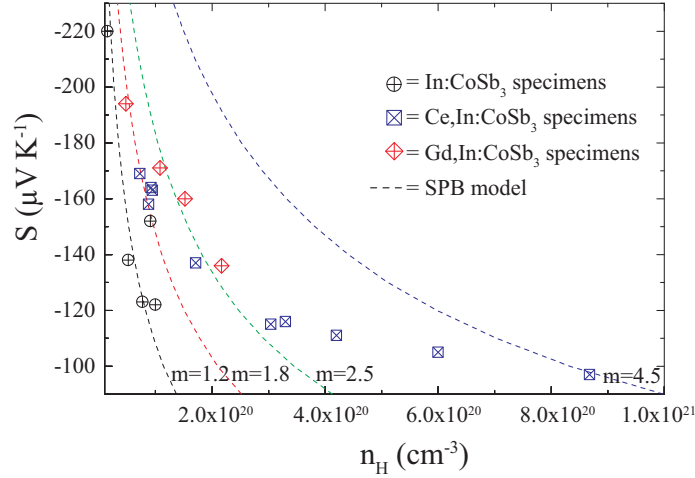
Figure 4.36: *Calculated Seebeck coefficient S according to a single parabolic band model (see sec.1.4) as a function of the charge carrier density nboltz and a constant mass of the charge carrier m. The particular data points within the diagram are the effective charge carrier densities n_H from Hall measurements at room temperature vs. the correspondent Seebeck coefficient of the short-term sintered specimens (derived from the local Seebeck coefficient data). The specimens are In, Ce/In and Gd/In filled skutterudites with different concentrations of the filler elements.*

beck coefficient as a function of the effective charge carrier density. For this reason it can be concluded that the Seebeck coefficient in the Ce,In:CoSb₃ material system is mostly affected by the effective charge carrier density. The impact of the microstructure of the specimens on the Seebeck coefficient is in contrast presumably insignificant.

More dramatic differences are observable with the electrical and thermal conductivity of the modified Ce,In:CoSb₃ material. The electrical conductivity data of the quenched Ce,InCoSb₃ specimens is lower and to some extent the (lattice) thermal conductivity considerably higher than the conventional Ce,In:CoSb₃ material and as a consequence exhibit by trend a lower figure of merit. This can be to some extent explained by the microstructure of the material. In [170] we observed that the low filled $Ce_{0.05}In_{0.05}Co_4Sb_{12}^{qu}$ specimen shows decomposition effects of the material from the skutterudite phase
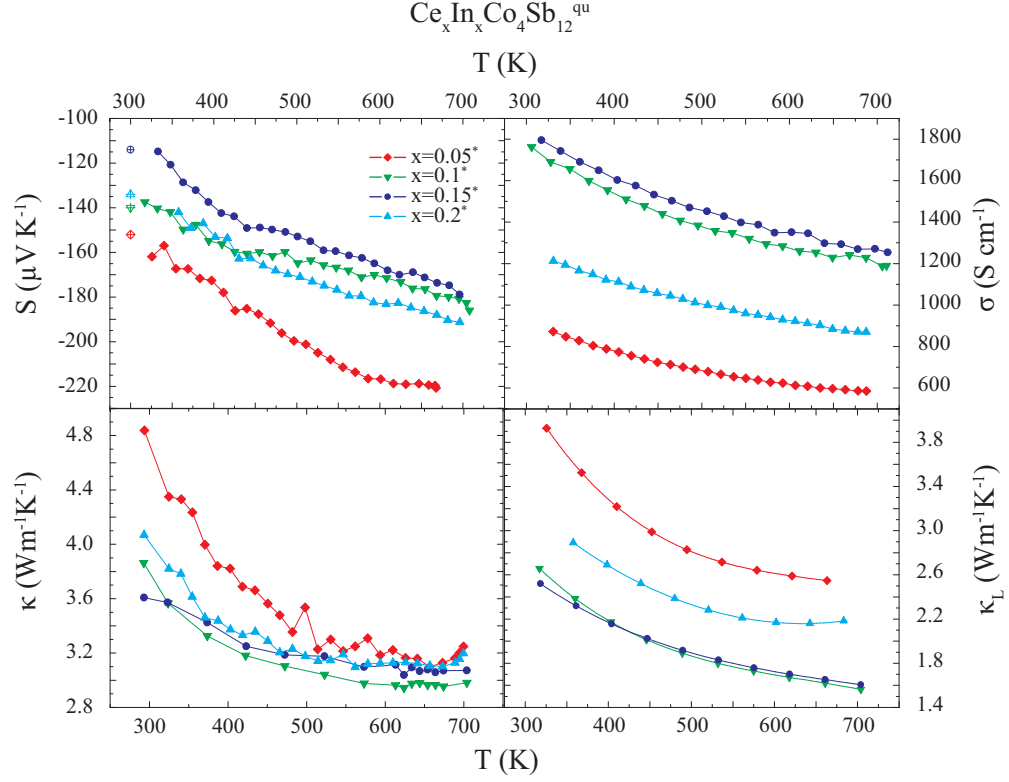
Figure 4.37: *Temperature dependent thermoelectric properties of short-term sintered* $\mathrm{Ce}_x\mathrm{In}_x\mathrm{Co}_4\mathrm{Sb}_{12}^{\mathrm{qu}}$ *skutterudite specimens with* $x = 0.05, 0.1, 0.15$ *and* 0.2*. The diagrams show the Seebeck coefficient S (top left), the electrical conductivity* σ *(top right), thermal conductivity* κ *(bottom left) and the calculated lattice thermal conductivity* κ_l *(bottom right) as a function of temperature in the range of* $350\,\mathrm{K}$ *to* $700\,\mathrm{K}$*. All presented specimens experienced a different annealing procedure in comparison to the* $\mathrm{Ce}_x\mathrm{In}_x\mathrm{Co}_4\mathrm{Sb}_{12}$*. For details it is referred to the section 4.3.3. For a better distinction the Ce,In:CoSb$_3$ specimens with the modified synthesis parameter are denoted with a "qu" as superscript and the different concentrations are denoted with an additional star symbol. The* $\mathrm{Ce}_{0.1}\mathrm{In}_{0.1}\mathrm{Co}_4\mathrm{Sb}_{12}^{\mathrm{qu}}$ *specimen was measured by the differential Seebeck voltages method (see sec.3.2.2).*

into elementary Sb and InSb. This causes a vast phase inhomogeneity in the material, which was observed in the electron microscopy analysis and in the local Seebeck coefficient measurement. Latter revises a macroscopic transformation of the specimen, by reason that the scanned area of the as-cast material was about $7\,\text{mm}^2$ large.

This decomposition effect is until now, not fully understood. From the work in [133] we know that the binary phase diagrams (e.g. In-Sb) have to be considered and that the formation of secondary material is vastly dependent on the thermodynamical processes of the filler element(s) with the main constituents (especially Sb). It is obvious that the formation of InSb is a main driving force in the (Ln),In:CoSb₃ system, however the question why the skutterudite material can be quite sensitive to the annealing temperature is not yet answered. Here a systematically investigation on possible ternary phases and deviations from the Co-Sb phase diagram would be of high benefit.

For higher Ce and In filled samples the condition can be more complex. We observed for the $\text{Ce}_{0.2}\text{In}_{0.2}\text{Co}_4\text{Sb}_{12}^{\text{qu}}$ specimen a reduced electrical conductivity with a concomitant higher lattice thermal conductivity in comparison to the conventional specimen with the identical starting composition of $x = 0.2$ the lattice thermal conductivity was calculated by a constant Lorenz number and is therefore significantly different to the calculated lattice thermal conductivity in this work.[40] However this does not occur for lower In and Ce filled specimens with $x = 0.1$ and 0.15. Clarification brings the measurement of the effective charge carrier density. The results from the Hall measurement reveal that the quenched samples (denoted as "qu") have by trend a lower charge carrier density, but a higher effective charge carrier mobility. Here the secondary material plays a crucial role, because it impacts the effective mobility by frequency, distribution and its size. With regard to an optimized thermoelectric material, this study showed that lower filling fractions of Ce and In with no visible precipitates is most ideal. Nanosized InSb precipitates, were never observed with TEM and SEM in this work (see therefore [118]). Compositions with $x = 0.1$ and 0.15 are also effective in terms of high ZT and are actually improved little by the additional quenching step. These compositions may be good candidates for a more rapid synthesis procedure (e.g. spin melting), due to a formation of precipitates, which are assumably

---

[40]In [170] For details on the more accurate determination of the Lorenz number it is referred to sec.1.4.

small and may not deteriorate the effective charge carrier mobility and on the other side give access to higher charge carrier densities/effective masses, which in the end can result to a vastly enhanced ZT.

Thermal Parameter and Thermoelectric Properties of the Skutterudite Specimens: The thermoelectric properties of the short-term sintered $In_{0.05}Co_4Sb_{12}$, $In_{0.2}Co_4Sb_{12}$ and $Ce_{0.05}In_{0.1}Co_4Sb_{12}$ specimens were determined in the temperature range of $300\,K$ to $700\,K$. These compacted samples originate from the same as-cast materials, which was used for the neutron powder diffraction measurement. The results do not considerably deviate from other samples with the same starting composition within this work, i.e. the $In_{0.05}Co_4Sb_{12}$ and $In_{0.2}Co_4Sb_{12}$ specimens. The low filled indium sample exhibits a behavior of a more intrinsic semiconductor, with evidence of bipolar thermodiffusion in the thermal conductivity data starting from around $575\,K$. The high indium filled specimen is more comparable to a metal and shows high electrical conductivity together with a monotonically increasing absolute Seebeck coefficient as a function of temperature. The thermal conductivity of the high indium filled sample is significantly reduced by contrast with the low indium filled specimen. The double cerium and indium filled sample however possesses an unique starting composition in this work.[41] The thermoelectric properties of the double skutterudite material shows in comparison to the $In_{0.2}Co_4Sb_{12}$ sample a higher electrical conductivity (at $500\,K$ about 30% higher), lower absolute Seebeck coefficient (at $500\,K$ around 9% lower) and an almost similar lattice thermal conductivity. The double filled skutterudite specimen yields a figure of merit of 0.9 at $700\,K$ and has therefore the highest ZT in this series.

The refined thermal parameters indicate detectable differences among the examined neutron powder diffraction samples. The $Ce_{0.05}In_{0.1}Co_4Sb_{12}$ specimen has by trend a higher U_{iso} for Co and Sb than the single indium filled samples (which are almost identical for both values). This is most probably attributed the filler element cerium, which obviously has a measurable effect on the two main constituents of the skutterudite material [162]. The main

---

[41]The composition was chosen in consideration of the individual filling fraction limits of cerium and indium, which were divided by two - to avoid the occurrence of secondary phases as much as possible and achieve a high filling fraction of both elements at the same time

focus however lies in the $2a$ Wyckoff position, which has in the case of the $Ce_{0.05}In_{0.1}Co_4Sb_{12}$ sample a traceable thermal parameter with a relatively high measuring error. However within the accuracy of measurement a value of around $U_{iso}(In/Ce)= 0.003\,\text{Å}^2$ was determined from the Rietveld refinement. Thus it can be concluded that the atomic displacement parameter is considerably reduced from single filled cerium (see [162]) or indium (see sec.4.2.2) skutterudite material to double cerium and indium filled skutterudite specimens. Another possible explanation is the variation of the atomic displacement parameter as a function of the filler occupancy, which is in the case of the double filled skutterudite specimen 6.8% for In and 3.0% for Ce, respectively (refined values) - and therefore considerably lower than the reported filling fraction of cerium in $CoSb_3$ (4.9% [162]) and the indium fraction in the $In_{0.2}Co_4Sb_{12}$ sample (13%, see sec.4.2.2).

Moreover it can be concluded from the high lattice parameter, the thermal parameters and the thermoelectric properties (especially the low lattice thermal conductivity) that cerium and indium most probably occupy the vacant lattice site of the skutterudite crystal.

Chapter 5

Summary

The thesis investigated on the thermoelectric and structural properties of $CoSb_3$ skutterudite material. The material was modified by several elements such as indium, cerium and gadolinium, which have a significant impact on the crystal structure and moreover on the thermoelectric properties. The $CoSb_3$ skutterudite material was synthesized by induction melting and subsequent long-term annealing mostly from elementary constituents. Series of indium filled (In:$CoSb_3$), cerium and indium (Ce,In:$CoSb_3$) and gadolinium and indium (Gd,In:$CoSb_3$) specimens with different concentrations of the filler elements (In, Ce, Gd) were prepared for structural investigations and (high temperature) thermoelectric characterization.

The as-cast material, i.e. the skutterudite material directly after the annealing process, was examined by X-ray and neutron powder diffraction. Also measurements of the local Seebeck coefficient and electron microscopy analysis on a cut-out of the as-cast material were carried out.

The thermoelectric properties of the short-term sintered samples of the skutterudite material were determined within the temperature range of around $300\,\mathrm{K}$ to $700\,\mathrm{K}$. The temperature dependent measurements encompassed the Seebeck coefficient, electrical and thermal conductivity. Hall measurements were carried out at room temperature to identify the effective charge carrier density and the effective charge carrier mobility.

The thermoelectric properties of the single indium filled skutterudite specimens showed that the figure of merit ZT strongly increases between the filling fraction of indium between $x = 0.05$ and $x = 0.1$, when x denotes the fraction of the indium content ($In_x Co_4 Sb_{12}$). The $In_{0.05} Co_4 Sb_{12}$ specimen possesses a behavior of an intrinsic semiconductor, i.e. the trend of the

Seebeck coefficient has an inflection point at around $550\,\mathrm{K}$ and the thermal conductivity exhibits a significant bipolar thermodiffusion around the same temperature range. The single indium filled skutterudite samples with higher indium concentration exhibit a more metallic behavior (monotonic decrease of σ and κ as a function of temperature, with a concomitant increase of the absolute Seebeck coefficient S).

Furthermore the synthesis parameters have a significant influence on the thermoelectric properties of the indium filled skutterudite material and can enhance the figure of merit, especially for high filling fractions with indium, which was revealed in the case of two different $In_{0.2}Co_4Sb_{12}$ specimens. The modified synthesis parameter (quenching after the annealing period) showed that the effective charge carrier is increased and the size and shape of the precipitates are considerably changed.

The thermoelectric properties can also be enhanced by addition of two elements to the $CoSb_3$ skutterudite material. Gadolinium and indium filled skutterudite specimens ($Gd_xIn_{0.05}Co_4Sb_{12}$) showed a considerable amount of secondary material already for low filling fractions. The occurrence of these precipitates can significantly enhance the lattice thermal resistivity, however the mobility of the charge carriers can be affected - with a final outcome of a ZT, which is almost similar to single indium filled skutterudite specimens. The thermoelectric properties of the short-term sintered $Ce,In:CoSb_3$ specimens show the highest figure of merit values among all samples investigated in this thesis. However the figure of merit ZT as a function of the concentration of the filler elements is different to the single filled $In:CoSb_3$ specimens. Here the lowest filled sample ($Ce_{0.05}In_{0.05}Co_4Sb_{12}$), exhibiting no visible precipitates, possesses a vastly enhanced ZT significantly above 1 at around $700\,\mathrm{K}$. Specimens with higher filling fractions of cerium and indium still have high ZT values just below 1. This different behavior can be most probably explained by the increase of the effective charge carrier mass as a function of the effective charge carrier density, which was revealed by Hall measurements. In other words the skutterudite material with high charge carrier densities deviate significantly from a single parabolic band model and the material can possess higher Seebeck coefficients with a concomitant high effective charge carrier density. The high effective mass adds to a high Seebeck coefficient together with an increased electrical conductivity and thus leads to an improved ZT. The microstructure of double filled skutterudites can be complex, due to the multiplicity of possible secondary phases. In the case of $Gd,In:CoSb_3$ or high filled $Ce,In:CoS_3$ skutterudite material, $LnSb_2$

(Ln=Gd, Ce) phases, elementary antimony and InSb are the most occurring precipitates. The size and shape are mostly in the range of several $100\,\mu m$, which can be attributed to the induction melting and long-term annealing (slow heating and cooling rate). When the annealing parameters are changed equally to the experiment with the single indium filled specimen, the shape and size of InSb and Sb can be considerably changed. However the $LnSb_2$ intermetallic phases remain unchanged, due to its high melting temperatures. The thermoelectric properties and particular the figure of merit of these double filled skutterudite specimens do not benefit from the additional treatment and rather tend to show decomposition effects.

The structural investigations with high resolution neutron powder diffraction reveal that for single indium filled skutterudite material the $2a$ Wyckoff position is occupied. Furthermore the temperature dependent measurement of the $In_{0.2}Co_4Sb_{12}$ specimen exhibits a strong increase of the thermal parameter of indium, which represents a significant atomic displacement and is typical for the filler element in cage compounds.

The examined double cerium and indium filled skutterudite specimen with the starting composition $Ce_{0.05}In_{0.1}Co_4Sb_{12}$ also shows an occupation of the void lattice site ($2a$ Wyckoff) by cerium *and* indium. The thermal parameter of the $2a$ position increases equally as a function of temperature, however the absolute value is considerably decreased. The thermoelectric properties of these examined specimens coincide with previous results and the double filled $Ce,In:CoSb_3$ specimen also shows a potential figure of merit of 0.9 at $700\,K$.

The indium single filled skutterudite show promising thermoelectric properties within the temperature range between $300\,K$ and $700\,K$. Indium acts as regular filler element and the secondary phases can contribute to an enhanced figure of merit ZT, when the synthesis and annealing parameters are optimized. Double filling of the skutterudite material further enhance the lattice thermal resistivity with a concomitant high Seebeck coefficient and electrical conductivity, especially for cerium and indium.

Bibliography

[1] T.J. Seebeck. Ueber die magnetische Polarisation der Metalle und Erze durch Temperatur-Differenz. *Annalen der Physik*, 82(2):133–160, 1826.

[2] J.C.A. Peltier. Nouvelles experiences sur la caloriecete des courans electriques. *Annales de Chimie et de Physique*, LVI:371–387, 1834.

[3] W. Thomson. On a mechanical theory of thermoelectric currents. *Proceedings of the Royal Society of Edinburgh*, III:91–98, 1851.

[4] W. Thomson. Account of researches in thermo-electricity. *Proc. R. Soc. Lond.*, 7:49–58, 1854.

[5] E.H. Hall. On a new action of the magnet on electrical currents. *American Journal of Mathematics*, 2:287–292, 1879.

[6] M. Telkes. The efficiency of thermoelectric generators I. *Journal of Applied Physics*, 18(12):1116–1127, 1947.

[7] A.F. Ioffe. Energeticheskie osnovy termoelektricheskikh bataryei iz poluprovodnikov. USSR Academy of Sciences, 1950.

[8] A.F. Ioffe. *Semiconductor thermoelements, and Thermoelectric cooling.* Infosearch, ltd., 1957.

[9] H.J. Goldsmid. *Applications of Thermoelectricity.* Butler & Tanner Ltd., 1960.

[10] D. Jänsch. *Thermoelektrik: Eine Chance für die Automobilindustrie.* Reihe Technik. Expert-Verlag GmbH, 2008.

[11] T. Kajikawa. Status and future prospects on the development of thermoelectric power generation systems utilizing combustion heat from municipal solid waste. In *Proceedings ICT 1997 - XVI International Conference on Thermoelectrics*, pages 28 –36, 1997.

[12] G.J. Snyder, J.R. Lim, C.K. Huang, and J.P. Fleurial. Thermoelectric microdevice fabricated by a MEMS-like electrochemical process. *Nature Materials*, 2(8):528–531, August 2003.

[13] D.M. Rowe. *CRC Handbook of Thermoelectrics*. CRC Press, 1995.

[14] C. LaBounty, A. Shakouri, P. Abraham, and J.E. Bowers. Monolithic integration of thin-film coolers with optoelectronic devices. *Optical Engineering*, 39(11):2847–2852, 2000.

[15] T.M. Tritt. *Thermoelectric materials 2000: The next generation materials for small-scale refrigeration and power generation applications.* Materials Research Society symposia proceedings. Materials Research Society, 2001.

[16] S.B. Riffat and X. Ma. Thermoelectrics: A review of present and potential applications. *Applied Thermal Engineering*, 23(8):913–935, 2003.

[17] Lord Rayleigh. On the thermodynamic efficiency of the thermopile. *Philosophical Magazine Series 5*, 20:361–363, 1885.

[18] E. Altenkirch. Ueber den Nutzeffekt der Thermosaeule. *Physikalische Zeitschrift*, 10:560–568, 1909.

[19] E. Altenkirch. Elektrothermische Kaelteerzeugung und reversible elektrische Heizung. *Physikalische Zeitschrift*, 12:920–924, 1911.

[20] L. Boltzmann. Weitere Studien ueber das Waermegleichgewicht unter Gasmolekuelen. *Sitzungsberichte der Mathematisch Naturwissenschaftlichen Classe der Kaiserlichen Akademie der Wissenschaften*, 66, 2. Abtheilung(Bd. 63):275–370, 1872.

[21] L. Onsager. Reciprocal relations in irreversible processes. I. *Phys. Rev.*, 37:405–426, 1931.

[22] J.M. Ziman. *Electrons and Phonons. The Theory of Transport Phenomena in Solids.* Oxford University Press, London, 1960.

[23] G.S. Nolas, J. Sharp, and H.J. Goldsmid. *Thermoelectrics: Basic principles and new materials developments.* Springer series in materials science. Springer, 2001.

[24] V.I. Fistul. *Heavily doped semiconductors (Translated from Russian by Albin Tybulewicz).* Monographs in semiconductor physics. Plenum Press, 1969.

[25] A. May. *High-temperature transport in lanthanum telluride and other modern thermoelectric materials.* PhD thesis, California Institute of Technology, 2010.

[26] E. Mueller. *Bandstruktur und Ladungstraegerstreuung in p-leitenden $(Bi_{1-x}Sb_x)_2 Te_3$-Mischkristallen: Modellierung der thermoelektrischen Eigenschaften im Temperaturbereich* $100-300$ K, volume 19. Duesseldorf. VDI-Verl., 1998.

[27] H. Froehlich and C. Kittel. Remark on the paper by Prof. G. Busch. *Physica*, 20(7-12):1086, 1954.

[28] T.M. Tritt. *Thermal conductivity: theory, properties, and applications.* Physics of solids and liquids. Kluwer Academic/Plenum Publishers, 2004.

[29] P. Debye. Zur Theorie der spezifischen Waerme. *Annalen der Physik (Leipzig)*, 39 (4):789–839, 1912.

[30] N.W. Ashcroft and N.D. Mermin. *Solid state physics.* Science: Physics. Saunders College, 1976.

[31] H. Bross. Der Einfluss von Fehlstellen auf die Gitterwaermeleitfaehigkeit bei tiefen Temperaturen. *physica status solidi (b)*, 2(5):481–516, 1962.

[32] A. Matthiessen and C. Vogt. On the influence of temperature on the electric conducting-power of alloys. *Philosophical Transactions of the Royal Society of London*, 154:167–200, 1864.

[33] K. Lichtenecker. Der elektrische Leitungswiderstand kuenstlicher und natuerlicher Aggregate. *Physikalische Zeitschrift*, 25:225–233, 1924.

[34] G. D. Mahan. Figure of merit for thermoelectrics. *Journal of Applied Physics*, 65(4):1578–1583, 1989.

[35] G. A. Slack. *Solid State Physics*, volume 34. Academic, New York, 1979.

[36] H. Kim, M. Kaviany, J.C. Thomas, A. Van der Ven, C. Uher, and B. Huang. Structural order-disorder transitions and phonon conductivity of partially filled skutterudites. *Phys. Rev. Lett.*, 105(26):265901, 2010.

[37] H.J. Goldsmid. *Electronic refrigeration*. Pion, 1986.

[38] Y. Pei, X. Shi, A. LaLonde, H. Wang, L. Chen, and G.J. Snyder. Convergence of electronic bands for high performance bulk thermoelectrics. *Nature*, 473(7345):66–69, May 2011.

[39] M. M. Koza, M. R. Johnson, R. Viennois, H. Mutka, L. Girard, and D. Ravot. Breakdown of phonon glass paradigm in La- and Ce-filled Fe_4Sb_{12} skutterudites. *Nature Materials*, 7(10):805–810, October 2008.

[40] L.D. Hicks and M.S. Dresselhaus. Thermoelectric figure of merit of a one-dimensional conductor. *Phys. Rev. B*, 47:16631–16634, June 1993.

[41] A. Khitun, K.L. Wang, and G. Chen. Thermoelectric figure of merit enhancement in a quantum dot superlattice. *Nanotechnology*, 11(4):327, 2000.

[42] T. C. Harman, P. J. Taylor, M. P. Walsh, and B. E. LaForge. Quantum dot superlattice thermoelectric materials and devices. *Science*, 297(5590):2229–2232, 2002.

[43] R. Venkatasubramanian, E. Siivola, T. Colpitts, and B. O'Quinn. Thin-film thermoelectric devices with high room-temperature figures of merit. *Nature*, 413:597–602, 2001.

[44] X. Fan, G. Zeng, E. Croke, C. LaBounty, C.C. Ahn, D. Vashaee, A. Shakouri, and J.E. Bowers. High cooling power density SiGe/Si micro-coolers. *Electronics Letters*, 37(2):126–127, 2001.

[45] D. Vashaee and A. Shakouri. Thermionic power generation at high temperatures using SiGe/Si superlattices. *Journal of Applied Physics*, 101(5):053719, 2007.

[46] X. Fan, G. Zeng, C. LaBounty, J.E. Bowers, E. Croke, C.C. Ahn, S. Huxtable, A. Majumdar, and A. Shakouri. SiGeC/Si superlattice microcoolers. *Applied Physics Letters*, 78(11):1580–1582, 2001.

[47] W.S. Capinski and H.J. Maris. Thermal conductivity of GaAs/AlAs superlattices. *Physica B: Condensed Matter*, 219-220(0):699 – 701, 1996.

[48] T. Koga, X. Sun, S.B. Cronin, and M.S. Dresselhaus. Carrier pocket engineering to design superior thermoelectric materials using GaAs/AlAs superlattices. *Applied Physics Letters*, 73(20):2950–2952, 1998.

[49] J. M. Zide, D. O. Klenov, S. Stemmer, A. C. Gossard, G. Zeng, J. E. Bowers, D. Vashaee, and A. Shakouri. Thermoelectric power factor in semiconductors with buried epitaxial semimetallic nanoparticles. *Applied Physics Letters*, 87(11):112102, 2005.

[50] A. I. Boukai, Y. Bunimovich, J. Tahir-Kheli, J. Yu, W. A. Goddard III, and J. R. Heath. Silicon nanowires as efficient thermoelectric materials. *Nature*, 451:168–171, 2008.

[51] A. I. Hochbaum, R. Chen, R. D. Delgado, W. Liang, E. C. Garnett, M. Najarian, A. Majumdar, and P. Yang. Enhanced thermoelectric performance of rough silicon nanowires. *Nature*, 451(7175):163–167, January 2008.

[52] L.D. Chen, T. Kawahara, X.F. Tang, T. Goto, T. Hirai, J.S. Dyck, W. Chen, and C. Uher. Anomalous barium filling fraction and n-type thermoelectric performance of $Ba_yCo_4Sb_{12}$. *Journal of Applied Physics*, 90(4):1864–1868, 2001.

[53] P.F.P. Poudeu, J. D'Angelo, H. Kong, A. Downey, J.L. Short, R. Pcionek, T.P. Hogan, C. Uher, and M.G. Kanatzidis. Nanostructures versus solid solutions: Low lattice thermal conductivity and enhanced thermoelectric figure of merit in $Pb_{9.6}Sb_{0.2}Te_{10-x}Se_x$ bulk materials. *Journal of the American Chemical Society*, 128(44):14347–14355, 2006.

[54] C.J. Vineis, A. Shakouri, A. Majumdar, and M. G. Kanatzidis. Nanostructured thermoelectrics: Big efficiency gains from small features. *Advanced Materials*, 22(36):3970–3980, 2010.

[55] Y. Lan, A.J. Minnich, G. Chen, and Z. Ren. Enhancement of thermoelectric figure-of-merit by a bulk nanostructuring approach. *Advanced Functional Materials*, 20(3):357–376, 2010.

[56] J. Sootsman, D. Chung, and M. Kanatzidis. New and old concepts in thermoelectric materials. *Angewandte Chemie International Edition*, 48(46):8616–8639, 2009.

[57] A.J. Minnich, M.S. Dresselhaus, Z.F. Ren, and G. Chen. Bulk nanostructured thermoelectric materials: current research and future prospects. *Energy Environ. Sci.*, 2:466–479, 2009.

[58] M. Zebarjadi, K. Esfarjani, M. S. Dresselhaus, Z. F. Ren, and G. Chen. Perspectives on thermoelectrics: From fundamentals to device applications. *Energy Environ. Sci.*, 5:5147–5162, 2012.

[59] K.F. Boebert. *Ueber das Modumer Blaufarbenwerk in Norwegen.* Archiv fuer Mineralogie, Geognosie, Bergbau und Huettenkunde. G. Reimer, Berlin, 1847.

[60] A. Breithaupt. Ueber eine neue Kies-Spezies von Skutterud. *Annalen der Physik und Chemie*, 9:115–116, 1827.

[61] I. Oftedal. Die Kristallstruktur von Skutterudit und Speiskobalt-Chloanthit. *Z. Kristallogr.*, A66:517–546, 1928.

[62] D.M. Rowe. *Thermoelectrics Handbook: Macro to Nano.* CRC/Taylor & Francis, 2006.

[63] W. Jeitschko and D. Braun. $LaFe_4P_{12}$ with filled $CoAs_3$-type structure and isotypic lanthanoid-transition metal polyphosphides. *Acta Crystallographica Section B*, 33(11):3401–3406, 1977.

[64] X. Shi, W. Zhang, L. D. Chen, and J. Yang. Filling fraction limit for intrinsic voids in crystals: Doping in skutterudites. *Phys. Rev. Lett.*, 95(18):185503, 2005.

[65] T.M. Tritt. *Recent trends in thermoelectric materials research I*, volume 69 of *Semiconductors and semimetals*. Academic Press, 2001.

[66] K. Momma and F. Izumi. VESTA3 for three-dimensional visualization of crystal, volumetric and morphology data. *Journal of Applied Crystallography*, 44(6):1272–1276, 2011.

[67] G.J. Snyder. California University of Technology. pers. comm.

[68] G. Rose. *Das Kristallo-Chemische Mineralsystem*. Engelmann, Wilhelm, 1852.

[69] L.D. Dudkin and N.K. Abrikosov. A physicochemical investigation of cobalt antimonide. *Zhurnal Neorganicheskoi Khimii*, I, (9):2096–2105, 1956.

[70] D.T. Morelli and G.P. Meisner. Low temperature properties of the filled skutterudite $CeFe_4Sb_{12}$. *Journal of Applied Physics*, 77(8):3777–3781, 1995.

[71] B. C. Sales, D. Mandrus, and R. K. Williams. Filled Skutterudite Antimonides: A New Class of Thermoelectric Materials. *Science*, 272(5266):1325–1328, 1996.

[72] V. Keppens, D. Mandrus, B. C. Sales, B. C. Chakoumakos, P. Dai, R. Coldea, M. B. Maple, D. A. Gajewski, E. J. Freeman, and S. Bennington. Localized vibrational modes in metallic solids. *Nature*, 395(6705):876–878, October 1998.

[73] H. Kitagawa, M. Hasaka, T. Morimura, H. Nakashima, and S. Kondo. Skutterudite structure and thermoelectric property in $Ce_fFe_{8-x}Co_xSb_{24}$ (f =0-2, x=0-8). *Materials Research Bulletin*, 35(2):185 – 192, 2000.

[74] A. Grytsiv, P. Rogl, S. Berger, C. Paul, E. Bauer, C. Godart, B. Ni, M.M. Abd-Elmeguid, A. Saccone, R. Ferro, and D. Kaczorowski. Structure and physical properties of the thermoelectric skutterudites $Eu_yFe_{4-x}Co_xSb_{12}$. *Phys. Rev. B*, 66(9):094411, 2002.

[75] Q.M. Lu, J.X. Zhang, X. Zhang, Y.Q. Liu, D.M. Liu, and M.L. Zhou. Effects of double filling of la and ce on thermoelectric properties of

$Ce_mLa_nFe_{1.0}Co_{3.0}Sb_{12}$ compounds by spark plasma sintering. *Journal of Applied Physics*, 98(10):106107, 2005.

[76] D. Berardan, E. Alleno, C. Godart, M. Puyet, B. Lenoir, R. Lackner, E. Bauer, L. Girard, and D. Ravot. Improved thermoelectric properties in double-filled $Ce_{y/2}Yb_{y/2}Fe_{4-x}(Co/Ni)_xSb_{12}$ skutterudites. *Journal of Applied Physics*, 98(3):033710, 2005.

[77] W. Schnelle, A. Leithe-Jasper, H. Rosner, R. Cardoso-Gil, R. Gumeniuk, D. Trots, J. A. Mydosh, and Yu. Grin. Magnetic, thermal, and electronic properties of iron-antimony filled skutterudites MFe_4Sb_{12} (M=Na,K,Ca,Sr,Ba,La,Yb). *Phys. Rev. B*, 77(9):094421, 2008.

[78] G.J. Snyder and E.S. Toberer. Complex thermoelectric materials. *Nature Materials*, 7(2):105–114, February 2008.

[79] R.P. Hermann, R. Jin, W. Schweika, F. Grandjean, D. Mandrus, B.C. Sales, and G.J. Long. Einstein oscillators in thallium filled antimony skutterudites. *Phys. Rev. Lett.*, 90(13):135505, 2003.

[80] J. Yang, W. Zhang, S.Q. Bai, Z. Mei, and L.D. Chen. Dual-frequency resonant phonon scattering in $Ba_xR_yCo_4Sb_{12}$ (R = La, Ce, and Sr). *Applied Physics Letters*, 90(19):192111, 2007.

[81] X. Shi, J. Salvador, J. Yang, and H. Wang. Thermoelectric properties of n-type multiple-filled skutterudites. *Journal of Electronic Materials*, 38(7):930–933, July 2009.

[82] S.Q. Bai, X. Shi, and L.D. Chen. Lattice thermal transport in $Ba_xRE_yCo_4Sb_{12}$ (RE = Ce, Yb, and Eu) double-filled skutterudites. *Applied Physics Letters*, 96(20):202102, 2010.

[83] T. Caillat, A. Borshchevsky, and J.-P. Fleurial. Novel transition metal compounds with promising thermoelectric properties. In *International Thermoelectric Society, XIIth International Conf. on Thermoelectrics Yokohama, Japan*, 1993.

[84] H. Fukuoka and S. Yamanaka. High-pressure synthesis, structure, and electrical property of iodine-filled skutterudite $I_{0.9}Rh_4Sb_{12}$: First anion-filled skutterudite. *Chemistry of Materials*, 22(1):47–51, 2010.

[85] C. Sekine, H. Saito, T. Uchiumi, A. Sakai, and I. Shirotani. Micro-probed raman scattering study of ternary ruthenium phosphides with filled skutterudite-type structure. *Solid State Communications*, 106(7):441 – 445, 1998.

[86] D.J. Singh and I.I. Mazin. Calculated thermoelectric properties of La-filled skutterudites. *Phys. Rev. B*, 56(4):1650–1653, 1997.

[87] B. C. Sales, D. Mandrus, B. C. Chakoumakos, V. Keppens, and J. R. Thompson. Filled skutterudite antimonides: Electron crystals and phonon glasses. *Phys. Rev. B*, 56(23):15081–15089, 1997.

[88] J. L. Feldman, D. J. Singh, I. I. Mazin, D. Mandrus, and B. C. Sales. Lattice dynamics and reduced thermal conductivity of filled skutterudites. *Phys. Rev. B*, 61(14):9209–9212, 2000.

[89] R.P. Hermann, F. Grandjean, and G.J. Long. Einstein oscillators that impede thermal transport. *American Journal of Physics*, 73(2):110–118, 2005.

[90] G.P. Meisner, D.T. Morelli, S. Hu, J. Yang, and C. Uher. Structure and lattice thermal conductivity of fractionally filled skutterudites: Solid solutions of fully filled and unfilled end members. *Phys. Rev. Lett.*, 80(16):3551–3554, 1998.

[91] G.S. Nolas, D.T. Morelli, and T.M. Tritt. Skutterudites: A phonon-glass-electron crystal approach to advanced thermoelectric energy conversion applications. *Annual Review of Materials Science*, 29:89–116, 1999.

[92] J. Callaway. Model for lattice thermal conductivity at low temperatures. *Phys. Rev.*, 113:1046–1051, 1959.

[93] B. Abeles. Lattice thermal conductivity of disordered semiconductor alloys at high temperatures. *Phys. Rev.*, 131:1906–1911, 1963.

[94] M. Noh, J. Thiel, and D.C. Johnson. Synthesis of crystalline super-lattices by controlled crystallization of modulated reactants. *Science*, 270(5239):1181–1184, 1995.

[95] M.D. Hornbostel, E.J. Hyer, J. Thiel, and D.C. Johnson. Rational synthesis of metastable skutterudite compounds using multilayer precursors. *Journal of the American Chemical Society*, 119(11):2665–2668, 1997.

[96] A. Moechel, I. Sergueev, N. Nguyen, G.J. Long, F. Grandjean, D.C. Johnson, and R.P. Hermann. Lattice dynamics in the $FeSb_3$ skutterudite. *Phys. Rev. B*, 84:064302, 2011.

[97] G. Rogl, A. Grytsiv, E. Bauer, P. Rogl, and M. Zehetbauer. Thermoelectric properties of novel skutterudites with didymium: $DD_y(Fe_{1-x}Co_x)_4Sb_{12}$ and $DD_y(Fe_{1-x}Ni_x)_4Sb_{12}$. *Intermetallics*, 18(1):57 – 64, 2010.

[98] M.S. Toprak, C. Stiewe, D. Platzek, S. Williams, L. Bertini, E. Mueller, C. Gatti, Y. Zhang, M. Rowe, and M. Muhammed. The impact of nanostructuring on the thermal conductivity of thermoelectric $CoSb_3$. *Advanced Functional Materials*, 14(12):1189–1196, 2004.

[99] J.L. Mi, X.B. Zhao, T.J. Zhu, and J.P. Tu. Thermoelectric properties of n-type $CoSb_3$ nanocomposite prepared by in-situ solvothermal synthesis and hot pressing. *Journal of Inorganic Materials*, 23 (4):715–718, 2008.

[100] W.Y. Zhao, C.L. Dong, P. Wei, W. Guan, L.S. Liu, P.C. Zhai, X.F. Tang, and Q.J. Zhang. Synthesis and high temperature transport properties of barium and indium double-filled skutterudites $Ba_xIn_yCo_4Sb_{12-z}$. *Journal of Applied Physics*, 102(11):113708, 2007.

[101] G. Rogl, A. Grytsiv, P. Rogl, E. Bauer, M.B. Kerber, M. Zehetbauer, and S. Puchegger. Multifilled nanocrystalline p-type didymium - skutterudites with $zt > 1.2$. *Intermetallics*, 18(12):2435 – 2444, 2010.

[102] R. Liu, J. Yang, X. Chen, X. Shi, L. Chen, and C. Uher. p-type skutterudites $R_xM_yFe_3CoSb_{12}$ (R, M = Ba, Ce, Nd, and Yb): Effectiveness of double-filling for the lattice thermal conductivity reduction. *Intermetallics*, 19(11):1747 – 1751, 2011.

[103] L. Xi, J. Yang, W. Zhang, L. Chen, and J. Yang. Anomalous dual-element filling in partially filled skutterudites. *Journal of the American Chemical Society*, 131(15):5560–5563, April 2009.

[104] L. Xi, J. Yang, C. Lu, Z. Mei, W. Zhang, and L. Chen. Systematic study of the multiple-element filling in caged skutterudite $CoSb_3$. *Chemistry of Materials*, 22(7):2384–2394, April 2010.

[105] G.S. Nolas, G. Fowler, and J. Yang. Assessing the role of filler atoms on the thermal conductivity of filled skutterudites. *Journal of Applied Physics*, 100(4):043705, 2006.

[106] F.A. Garcia, D.J. Garcia, M.A. Avila, J.M. Vargas, P.G. Pagliuso, C. Rettori, M.C.G. Passeggi, S.B. Oseroff, P. Schlottmann, B. Alascio, and Z. Fisk. Coexisting on-center and off-center Yb^{+3} sites in $Ce_{1-x}Yb_xFe_4P_{12}$ skutterudites. *Phys. Rev. B*, 80(5):052401, 2009.

[107] K. Matsuhira, C. Sekine, M. Wakeshima, Y. Hinatsu, T. Namiki, K. Takeda, I. Shirotani, H. Sugawara, D. Kikuchi, and H. Sato. Systematic study of lattice specific heat of filled skutterudites. *Journal of the Physical Society of Japan*, 78(12):124601, 2009.

[108] J.R. Salvador, J. Yang, X. Shi, H. Wang, A.A. Wereszczak, H. Kong, and C. Uher. Transport and mechanical properties of Yb-filled skutterudites. *Philosophical Magazine*, 89(19):1517–1534, 2009.

[109] L. Zhang, G. Rogl, A. Grytsiv, S. Puchegger, J. Koppensteiner, F. Spieckermann, H. Kabelka, M. Reinecker, P. Rogl, W. Schranz, M. Zehetbauer, and M.A. Carpenter. Mechanical properties of filled antimonide skutterudites. *Materials Science and Engineering: B*, 170(1-3):26 – 31, 2010.

[110] H.H. Saber, M.S. El-Genk, and T. Caillat. Tests results of skutterudite based thermoelectric unicouples. *Energy Conversion and Management*, 48(2):555 – 567, 2007.

[111] R. Hara, S. Inoue, H.T. Kaibe, and S. Sano. Aging effects of large-size n-type $CoSb_3$ prepared by spark plasma sintering. *Journal of Alloys and Compounds*, 349(1-2):297 – 301, 2003.

[112] X. Tang, W. Xie, H. Li, W. Zhao, Q. Zhang, and M. Niino. Preparation and thermoelectric transport properties of high-performance p-type Bi_2Te_3 with layered nanostructure. *Applied Physics Letters*, 90(1):012102, 2007.

[113] H. Li, X. Tang, X. Su, and Q. Zhang. Preparation and thermoelectric properties of high-performance Sb additional $Yb_{0.2}Co_4Sb_{12+y}$ bulk materials with nanostructure. *Applied Physics Letters*, 92(20):202114, 2008.

[114] H. Li, X. Tang, and Q. Zhang. Microstructure and thermoelectric properties of Yb-filled skutterudites prepared by rapid solidification. *Journal of Electronic Materials*, 2009.

[115] Q.S. Guo, H. Li, X.L. Su, and X.F. Tang. Microstructure and themoelectric properties of p-type filled skutterudite $Ce_{0.3}Fe_{1.5}Co_{2.5}Sb_{12}$ prepared by melt-spinning method. *Acta Physica Sinica*, 59 (9):6666–6672, 2010.

[116] K. Biswas, S. Muir, and M.A. Subramanian. Rapid microwave synthesis of indium filled skutterudites: An energy efficient route to high performance thermoelectric materials. *Materials Research Bulletin*, 46(11):2288–2290, 2011.

[117] T. He, J. Chen, H.D. Rosenfeld, and M.A. Subramanian. Thermoelectric properties of indium-filled skutterudites. *Chemistry of Materials*, 18(3):759–762, 2006.

[118] H. Li, X. Tang, Q. Zhang, and C. Uher. High performance $In_xCe_yCo_4Sb_{12}$ thermoelectric materials with in situ forming nanostructured InSb phase. *Applied Physics Letters*, 94(10):102114, 2009.

[119] J.K. Lee, S.M. Choi, W.S. Seo, Y.S. Lim, H.L. Lee, and I.H. Kim. Thermoelectric properties of spark plasma sintered $In_xYb_yLa_{0.3-x-y}Co_4Sb_{12}$ skutterudite system. *Renewable Energy*, 42(0):36–40, 2012.

[120] L. Deng, X.P. Jia, T.C. Su, S.Z. Zheng, X. Guo, K. Jie, and H.A. Ma. Effects of double filling of Pb and Ba on thermoelectric properties of $Pb_xBa_yCo_4Sb_{11.5}Te_{0.5}$ compounds by HPHT. *Solid State Communications*, 151(20):1483 – 1485, 2011.

[121] K. Biswas, M.S. Good, K.C. Roberts, M.A. Subramanian, and T.H. Hendricks. Thermoelectric and structural properties of high-performance In-based skutterudites for high-temperature energy recovery. *Journal of Materials Research*, 26:1827–1835, 2011.

[122] H. Okamoto. Co-Sb (cobalt-antimony). *Journal of Phase Equilibria*, 12:244–245, 1991.

[123] D. Platzek, A. Zuber, C. Stiewe, G. Baehr, P. Reinshaus, and E. Mueller. An automated microprobe for temperature dependent spatial scanning of the seebeck coefficient. *Proceedings of the 22nd International Conference on Thermoelectrics, LaGrande-Motte, France, Aug 17-21 IEEE: New York, 2004*, pages 528–532, 2003.

[124] S. Zastrow. Aufbau einer Hochtemperatur-Hall-Seebeck-Sigma-Messanlage zur Charakterisierung der elektronischen Transporteigenschaften von Thermoelektrischen Material auf Basis von Indiumgefuellten Kobalt-Antimon-Skutteruditen. Master's thesis, German Aerospace Center (DLR), 2010.

[125] W.A. Wakeham and M.J. Assael. *The Measurement, Instrumentation, and Sensors Handbook*. The electrical engineering handbook series. CRC Press, 1999.

[126] W.J. Parker, R.J. Jenkins, C.P. Butler, and G.L. Abbott. Flash method of determining thermal diffusivity, heat capacity, and thermal conductivity. *Journal of Applied Physics*, 32(9):1679–1684, 1961.

[127] C. Stiewe. *Nanostrukturierte $CoSb_3$-Skutterudite*. PhD thesis, Justus-Liebig-Universitaet Giessen, 2009.

[128] V.K. Pecharsky and P.Y. Zavalij. *Fundamentals of Powder Diffraction and Structural Characterization of Materials*. Springer, 2009.

[129] http://www.ornl.gov.

[130] D.B. Williams and C.B. Carter. *Transmission electron microscopy: Diffraction*. Transmission Electron Microscopy: A Textbook for Materials Science. Plenum Press, 1996.

[131] L. Reimer. *Scanning Electron Microscopy: Physics of Image Formation and Microanalysis*. Springer Series in Optical Sciences. Springer, 1998.

[132] R. Mallik, C. Stiewe, G. Karpinski, R. Hassdorf, and E. Mueller, E.ller. Thermoelectric properties of Co_4Sb_{12} skutterudite materials with partial in filling and excess in additions. *Journal of Electronic Materials*, 38(7):1337–1343, July 2009.

[133] A. Sesselmann, T. Dasgupta, K. Klemens, S. Perlt, S. Zastrow, and
      E. Mueller. Transport properties and microstructure of indium added
      cobalt-antimony based skutterudites. *J. Mater. Res.,Focus Issue: Ad-
      vances in Thermoelectric Materials*, 26(15):1820–1826, 2011.

[134] J. Fleurial, T. Caillat, and A. Borshchevsky. Skutterudites: A new class
      of promising thermoelectric materials. *XIII International Conference
      on Thermoelectrics (Kansas City, MO 1994)*, pages 40–44, 1994.

[135] J.R. Carvajal. Fullprof: A program for Rietveld refinement and pat-
      tern matching analysis. *Abstracts of the Satellite Meeting on Powder
      Diffraction of the XV Congress of the IUCr*, 1990.

[136] J. Rodriguez-Carvajal. Recent advances in magnetic structure deter-
      mination by neutron powder diffraction. *Physica B: Condensed Matter*,
      192(12):55 – 69, 1993.

[137] D. Sieboerger, H. Brehm, F. Wunderlich, D. Moeller, and U. Glatzel.
      Temperature dependence of lattice parameter, misfit and thermal ex-
      pansion coefficient of matrix, γ-phase and superalloy. *Zeitschrift fuer
      Metallkunde*, 92:58–61, 2001.

[138] B.C. Chakoumakos and B.C. Sales. Skutterudites: Their structural
      response to filling. *Journal of Alloys and Compounds*, 407(1-2):87 –
      93, 2006.

[139] K.N. Trueblood, H.B. Bürgi, H. Burzlaff, J.D. Dunitz, C.M. Gramac-
      cioli, H.H. Schulz, U. Shmueli, and S.C. Abrahams. Atomic dispace-
      ment parameter nomenclature. report of a subcommittee on atomic
      displacement parameter nomenclature. *Acta Crystallographica Section
      A*, 52(5):770–781, 1996.

[140] http://www.ill.eu/sites/fullprof/php/tutorials.html.

[141] Y. Okada and Y. Tokumaru. Precise determination of lattice parameter
      and thermal expansion coefficient of silicon between 300 and 1500 K.
      Journal of Applied Physics, 56(2):314–320, 1984.

[142] D. Platzek, G. G. Karpinski, C. Drasar, and E. Mueller. Seebeck scan-
      ning microprobe for thermoelectric FGM. In *8th International Sym-
      posium on Multifunctional and Functionally Graded Materials FGM,
      Leuven, Belgium*, pages 587–592, Leuven, Belgium, 2004.

[143] V.L. Kuznetsov, L.A . Kuznetsova, and D.M. Rowe. Effect of partial void filling on the transport properties of $Nd_xCo_4Sb_{12}$ skutterudites. *Journal of Physics: Condensed Matter*, 15(29):5035–5048, 2003.

[144] R.D. Shannon. Revised effective ionic radii and systematic studies of interatomic distances in halides and chalcogenides. *Acta Crystallographica Section A*, 32(5):751–767, 1976.

[145] D.T. Morelli, T. Caillat, J.P. Fleurial, A. Borshchevsky, J. Vandersande, B. Chen, and C. Uher. Low-temperature transport properties of p-type $CoSb_3$. *Phys. Rev. B*, 51(15):9622–9628, 1995.

[146] M. Cutler and N.F. Mott. Observation of anderson localization in an electron gas. *Phys. Rev.*, 181:1336–1340, 1969.

[147] N.F. Mott and E.A. Davis. *Electronic processes in non-crystalline materials*. International series of monographs on physics. Clarendon Press, 1971.

[148] M. Jonson and G. D. Mahan. Mott's formula for the thermopower and the Wiedemann-Franz law. *Phys. Rev. B*, 21:4223–4229, 1980.

[149] A. Leithe-Jasper, W. Schnelle, H. Rosner, M. Baenitz, A. Rabis, A. A. Gippius, E. N. Morozova, H. Borrmann, U. Burkhardt, R. Ramlau, U. Schwarz, J. A. Mydosh, Y. Grin, V. Ksenofontov, and S. Reiman. Weak itinerant ferromagnetism and electronic and crystal structures of alkali-metal iron antimonides:$NaFe_4Sb_{12}$ and KFe_4Sb_{12}. *Phys. Rev. B*, 70:214418, 2004.

[150] D. Mandrus, A. Migliori, T.W. Darling, M.F. Hundley, E.J. Peterson, and J.D. Thompson. Electronic transport in lightly doped $CoSb_3$. *Phys. Rev. B*, 52(7):4926–4931, 1995.

[151] D.T. Morelli, G.P. Meisner, B. Chen, S. Hu, and C. Uher. Cerium filling and doping of cobalt triantimonide. *Phys. Rev. B*, 56(12):7376–7383, 1997.

[152] R. Bowers and Y. Yafet. Magnetic susceptibility of InSb. *Phys. Rev.*, 115:1165–1172, 1959.

[153] D.L. Rode. Electron transport in InSb, InAs, and InP. *Phys. Rev. B*, 3:3287–3299, 1971.

[154] S. Yamaguchi, T. Matsumoto, J. Yamazaki, N. Kaiwa, and A. Yamamoto. Thermoelectric properties and figure of merit of a Te-doped InSb bulk single crystal. *Applied Physics Letters*, 87(20):201902, 2005.

[155] M. Greenblatt. State University of New Jersey. pers. comm.

[156] F. Galasso and W. Darby. Ordering of the octahedrally coordinated cation position in the perovskite structure. *The Journal of Physical Chemistry*, 66(1):131–132, 1962.

[157] T.K. Mandal, A.M. Abakumov, M.V. Lobanov, M. Croft, V.V. Poltavets, and M. Greenblatt. Synthesis, structure, and magnetic properties of $SrLaMnSbO_6$: A new B-site ordered double perovskite. *Chemistry of Materials*, 20(14):4653–4660, 2008.

[158] J. E. Huheey, E. A. Keiter, and R. L. Keiter. *Inorganic Chemistry: Principles Of Structure And Reactivity*. Prentice Hall, 4 edition, 1997.

[159] L. Bertini and C. Gatti. The impact of the actual geometrical structure of a thermoelectric material on its electronic transport properties: The case of doped skutterudite systems. *The Journal of Chemical Physics*, 121(18):8983–8989, 2004.

[160] V.F. Sears. Neutron scattering lengths and cross sections. *Neutron News*, 3(3):26–37, 1992.

[161] G. Rogl, L. Zhang, P. Rogl, A. Grytsiv, M. Falmbigl, D. Rajs, M. Kriegisch, H. Mueller, E. Bauer, J. Koppensteiner, W. Schranz, M. Zehetbauer, Z. Henkie, and M. B. Maple. Thermal expansion of skutterudites. *Journal of Applied Physics*, 107(4):043507, 2010.

[162] J.L. Mi, M. Christensen, E. Nishibori, and B.B. Iversen. Multitemperature crystal structures and physical properties of the partially filled thermoelectric skutterudites $M_{0.1}Co_4Sb_{12}$(m=La,Ce,Nd,Sm,Yb, and Eu). *Phys. Rev. B*, 84:064114, 2011.

[163] J.P. Fleurial, A. Borshchevsky, and T. Caillat. New thermoelectric materials and devices for terrestrial power generators. *Space technology*

and applications international forum (STAIF - 97), 387(1):293–298, 1997.

[164] P. Dorenbos. f $\rightarrow$ d transition energies of divalent lanthanides in inorganic compounds. *Journal of Physics: Condensed Matter*, 15(3):575, 2003.

[165] R. Liu, X. Chen, P. Qiu, Liu J., J. Yang, Huang X., and Chen L. Low thermal conductivity and enhanced thermoelectric performance of Gd-filled skutterudites. *Journal of Applied Physics*, 109(2):023719, 2011.

[166] G.S. Nolas, G.A. Slack, D.T. Morelli, T.M. Tritt, and A.C. Ehrlich. The effect of rare-earth filling on the lattice thermal conductivity of skutterudites. *Journal of Applied Physics*, 79(8):4002–4008, 1996.

[167] Z.G. Mei, W. Zhang, L.D. Chen, and J. Yang. Filling fraction limits for rare-earth atoms in $CoSb_3$: An ab-initio approach. *Phys. Rev. B*, 74(15):153202, 2006.

[168] R. Wang and H. Steinfink. The crystal chemistry of selected AB_2 rare earth compounds with selenium, tellurium, and antimony. *Inorganic Chemistry*, 6(9):1685–1692, 1967.

[169] K.A. Gschneidner, L.R. Eyring, and J.C.G. Bünzli. *Handbook on the Physics and Chemistry of Rare Earths*. Number 33 in Handbook on the Physics and Chemistry of Rare Earths. Elsevier, 2003.

[170] A. Sesselmann, T. Dasgupta, C. Stiewe, and E. Mueller. Transport properties and microstructure of indium and cerium added cobalt-antimony based skutterudites. *MRS Proceedings 2011*, 1329, 2011.

Acknowledgements

First and foremost I would like to thank my reviewers, Prof. S. Horn for the academic supervision and Prof. H. Voggenreiter for giving me the opportunity to work at the Institute of Materials Research at the German Aerospace Center (DLR). I would like to thank my research advisor, Dr. Eckhard Müller, for his excellent guidance and furthermore the cooperation partners from the Deutsche Forschungsgemeinschaft (DFG) Schwerpunktprogramm "Nanostrukturierte Thermoelektrika" (SPP 1386), Prof. R. Hermann (FZ Jülich), Prof. B. Paulus (Freie Universität Berlin) and Prof. S. Schlecht (University of Giessen) for the good collaboration and scientific advice.

I want to thank Dr. T. Dasgupta and Dr. K. Zabrocki for helpful discussions and comments on my thesis.

Moreover I want to thank the DLR group and alumni for their expertise and helpfulness: G. Bähr, P. Blaschkewitz, Dr. J. de Boor, L. Böttcher, Dr. J. Dadda, I. Druschke, Dr. R. Hassdorf, B. Henke, M. Janich, Dr. G. Karpinski, H. Kolb, G. Oppitz, Dr. D. Platzeck, M. Rossmeier, A. Schmitz, R. Sottong, M. Steines, Dr. C. Stiewe, W. Schönau, S. Zastrow, Dr. A. Zhou, and P. Ziolkowski.

I want to thank further cooperation partners and their indispensable scientific help: Dr. O. Gourdon (ORNL), Dr. B. Klobes (FZ Jülich) and S. Perlt (IOM Leipzig).

Furthermore I want to thank my former fellow students at the University of Augsburg: Dr. B. Ecker, J. Leese, J. Mayer, H. Middelhoff and P. Pontiller.

I would like to acknowledge the DFG for funding the Schwerpunktpro-

Since there is little German in this doctoral thesis, I want to append a final quote from Meister Eckhar*t*:

> Der Mensch soll auch nie ein Werk so gut beurteilen noch als so recht ausführen, dass er je so frei oder so selbstsicher in den Werken werde, dass seine Vernunft je müssig werde und einschlafe. Er soll sich ständig mit den beiden Kräften der Vernunft und des Willens erheben und darin sein Allerbestes im höchsten Grade ergreifen und sich äusserlich und innerlich gegen jeden Schaden besonnen vorsehen; dann versäumt er nie etwas in irgendwelchen Dingen, sondern er nimmt ohne Unterlass in hohem Grade zu.

Meister Eckhart (1260-1328), "Reden der Unterweisung"

Curriculum Vitae

Name:	Andreas John Sesselmann
Date of birth:	23. October 1982
Nationality:	German

Education

09/1993 - 06/2002	A-levels, Adalbert-Stifter Gymnasium in Passau/Germany
10/2003 - 01/2007	B.Sc., Materials Science, University of Augsburg/Germany
10/2006 - 02/2009	M.Sc., Materials Science, University of Augsburg/Germany
from 02/2009	German Aerospace Center (DLR)